Carnegie Mellon University

CARNEGIE INSTITUTE OF TECHNOLOGY

THESIS

SUBMITTED IN PARTIAL FULFILLMENT OF THE REQUIREMENTS

FOR THE DEGREE OF Doctor of Philosophy

TITLE **Development of Geostatistical Models to Estimate CO 2 Storage Resource in Sedimentary Geologic Formations**

PRESENTED BY **Olga Popova**

ACCEPTED BY THE DEPARTMENT OF

Engineering and Public Policy

Mitchell Small — February 13, 2014
ADVISOR, MAJOR PROFESSOR — DATE

M. Granger Morgan — February 13, 2014
DEPARTMENT HEAD — DATE

APPROVED BY THE COLLEGE COUNCIL

Vijayakumar Bhagavatula — March 4, 2014
DEAN — DATE

Development of Geostatistical Models to Estimate CO_2 Storage Resource in Sedimentary Geologic Formations

Submitted in partial fulfillment of the requirements for

the degree of

Doctor of Philosophy

in

Engineering & Public Policy

Olga H. Popova

B.S./M.S., Geology and Geophysics, Novosibirsk State University
M.S., Information Management, University of Washington

Carnegie Mellon University
Pittsburgh, PA

May, 2014

Acknowledgments

Support for this work was provided by the Doris Duke Foundation Grant (No. 2007117) to Carnegie Mellon University's Department of Engineering and Public Policy for the project 'Regulation of Capture and Deep Geological Sequestration of Carbon Dioxide', by the US Department of Energy, the National Energy Technology Laboratory Grant (Award no. FE0004000, CP-686, DOE/NETL) to Carnegie Mellon University, and by the Bertucci Fellowship.

Thanks to the many colleagues who offered technical advice and research-related support including Ed Rubin, Jay Apt, Bill Harbert, Peter Warwick, Kelly Rose, Jennifer Bauer, Corinne Disenhof, Thanasis Karamalidis, Inês Azevedo, Lauren Fleishman, Peter Versteeg, Kyle Siler-Evans, Aniela Burant, Vicki Finney, Barbara Bugosh, Patti Steranchak, and Adam Loucks.

I am also extremely appreciative for the research assistance of Bobby Karimi, who helped me with ArcGIS and Steve Rose, who helped me with Matlab coding.

I am deeply grateful for the guidance and support from my doctoral committee members: Granger Morgan, who put things in motion and backed me up; Kristin Carter, who provided data and advice on geology; Angela Goodman, who gave all possible NETL support; and Andrew Thomas, who advised me on statistics. I would most like to thank my co-advisors: Committee Chair Mitch Small (and my primary advisor for the last two and a half years) and Sean McCoy (my primary advisor for the first two years). Mitch and Sean, thanks for your constant support and guidance. This research would not have been possible without you; and I feel blessed to have had such dutiful advisors who inspired me, believed in me, and pushed me to accomplish more than I thought possible.

I would like to thank my Professors from Novosibirsk State University (Affiliation of the Siberian Branch of the Russian Academy of Science) Konstantin Bogolepov, Chermen Borukaev, and Konstantin Mikulenko, who trained me in Geology and Geophysics; as well as my Professors from the University of Washington: Michael Crandall, Cheryl Metoyer, Jochen Scholl, Karine Barzilai-Nahon, and Ricardo Gomez, who trained me in Information Management.

I am also grateful to my colleagues who encouraged and supported me since my first days in the US: Les Collins and Dave Finnel of Epoch Well Services/ Nabors Drilling, Earl Bone of Lee Engineers, Valery Kucheravy of Seattle Department of Transportation, Ward Crell and John North of Delta Environmental, Rick Powell and Chuck Couvrette of Cornerstone GeoEngineers, and Steve Mullen and Cindy Spiry of Snoqualmie Tribe.

Finally, I would like to thank my sister Alla and my friends and classmates, who have been by my side during these four and a half challenging and amazing years. Thanks to my grandparents Varya and Semen who brought me up.

Abstract

Carbon capture and sequestration (CCS) is a technology that provides a near-term solution to reduce anthropogenic CO_2 emissions to the atmosphere and reduce our impact on the climate system. Assessments of carbon sequestration resources that have been made for North America using existing methodologies likely underestimate uncertainty and variability in the reservoir parameters. This thesis describes a geostatistical model developed to estimate the CO_2 storage resource in sedimentary formations. The proposed stochastic model accounts for the spatial distribution of reservoir properties and is implemented to a case study of the Oriskany Formation of the Appalachian sedimentary basin. The developed model allows for estimation of the CO_2 sequestration resource of a storage formation with subsequent uncertainty analysis. Since the model is flexible with respect to changing input parameters and assumptions it can be parameterized to calculate the CO_2 storage resource of any porous subsurface unit.

The thesis continues with evaluation of the cost of CO_2 injection and storage for the Oriskany Formation utilizing storage resource estimates generated by our geostatistical model. Our results indicate that the cost of sequestering CO_2 has significant spatial variation due to heterogeneity of formation properties and site geology. We identify the low-cost areas within the Oriskany footprint. In general, these areas correspond to the deepest portions of the Appalachian basin and could be considered as potential CO_2 injection sites for CCS industrial scale projects.

Overall, we conclude that significant improvement can be made by integrating basin geology and spatial heterogeneity of formation petrophysical properties into CCS cost assessments, and that should be a focus of future research efforts. This will allow for more accurate cost estimates for the entire CCS system and identify areas of sedimentary basins with optimal conditions for CO_2 injection and storage. To mitigate the effects of climate change, the U.S. will need a widespread

deployment of low-carbon electricity generating technologies including natural gas and coal with CCS. More precise CO_2 storage resource and CCS cost estimates will provide better recommendations for government and industry leaders and inform their decisions on what greenhouse gas mitigation measures are the best fit for their regions.

Table of Contents

List of Figures

List of Tables

Abbreviations

C	Celsius
CCS	Carbon capture and sequestration
CDF	Cumulative distribution function
CGSS	CO_2 Geological Storage Solutions, Australia
GHG	Greenhouse gas
CO_2	Carbon dioxide
BEG	Bureau of Economic Geology, The University of Texas at Austin
BTGS	Bureau of Topographic and Geologic Survey
DOE	US Department of Energy
EPA	US Environmental Protection Agency
F	Fahrenheit
ft	Foot
Gt	Gigatonne
GWh	Gigawatt-hour
IPCC	Intergovernmental Panel on Climate Change
kg	Kilogram
kg/km^2	Kilogram per square kilometer
kWh	Kilowatt-hour
L	Liter
MPa	Megapascal
MW	Megawatt
MWh	Megawatt-hour
Mt	Megatonne
m	Meter
km	Kilometer
km^2	Square kilometer
K	Kelvin
NAS	National Academy of Sciences
NETL	National Energy Technology Laboratory
Pa	Pascal
PA DCNR	Pennsylvania Department of Conservation and Natural Resources
PDF	Probability distribution function
psi	Pound per square inch
SGS	Sequential Gaussian Simulation
USGS	United States Geological Survey

Chapter 1. Introduction

Fossil fuels are likely to remain the principle source of energy for society well into the 21st century. As a result, emissions from energy use will continue to drive atmospheric concentrations of carbon dioxide (CO_2) upwards unless energy conversion systems can be designed to otherwise dispose of CO_2 generated from combustion.

Electricity generation accounted for approximately 33 percent of United States (US) greenhouse gas emissions in 2011 (1). In recent years, electricity demand has grown at a rate of approximately 0.7 percent per year (2); and, at the same time, the US administration has set targets to reduce greenhouse gas (GHG) emissions significantly below current levels. With GHG mitigation becoming a stronger legislative priority and renewable generation technologies (e.g., wind and solar) still unable to provide dispatchable electric power, coal- and gas-fired power plants with carbon capture and sequestration (CCS) could serve much of the US electricity need in the near future. CCS is a technology that provides a near-term solution to reduce anthropogenic CO_2 emissions to the atmosphere and reduce our impact on the climate system. CCS involves a set of technologies for CO_2 capture, transport, and sequestration. The last step in this chain - geologic carbon sequestration - is defined as the placement of CO_2 into an appropriate geologic formation in such a way that it will remain permanently sequestered from the atmosphere. In the Fourth Assessment report of the Intergovernmental Panel on Climate Change (IPCC) , CCS technologies are referred to as the only way the continued use of fossil fuels could be "environmentally sustainable"(3).

Captured CO_2 can be stored in different types of underground geologic formations. To be suitable for carbon sequestration, geological media have to have space, injectivity, and a

structure that will preclude CO_2 return to the atmosphere for geologically long periods of time. Geologic media that could be used as a permanent repository for anthropogenic CO_2 include depleted/depleting oil and gas reservoirs, unminable coal beds, and deep saline formations (4). These types of formations are found in sedimentary basins. There are more than 800 sedimentary provinces in the world (5), and, thus many possible locations for geologic sequestration of CO_2.

This study addresses deep saline formations, which are believed to be the most promising class of CO_2 geologic repositories in the long-term (6, 7). Particularly, the goals of this Thesis are: 1) to perform a comparative analysis of the existing CO_2 storage resource assessment methodologies for sedimentary formations; 2) to develop a geostatistical model for carbon storage resource calculation, which accounts for the spatial distribution of formation parameters; and 3) using this model to probabilistically quantify the CO_2 sequestration resource and cost of CO_2 injection and storage for the Oriskany Formation of the Appalachian basin. A geologic framework of the model is based on data provided by the Pennsylvania State Department of Conservation and Natural Resources (DCNR) Bureau of Topographic & Geologic Survey.

This Thesis is divided into five chapters. First, this chapter provides a background information about CCS and briefly describes geologic media for CO_2 underground storage. The second chapter then presents the comparative study of three CO_2 storage assessment methodologies: the approach proposed by the U.S. Department of Energy (DOE) (6), the modified U.S. Geological Survey (USGS) methodology (7), and the CO_2 Geological Storage Solutions (CGSS) methodology (8). Chapter three describes a geostatistical model developed to estimate the CO_2 storage resource in sedimentary formations and implementation of this model to a case study of the Oriskany Formation of the Appalachian basin. Chapter four reports on cost estimates of CO_2

injection and storage for the Oriskany Formation. Finally, the fifth chapter summarizes results of our studies, briefly describes plans for future work, and concludes this Thesis.

References

(1) Environmental Protection Agency [EPA], (2012). National Greenhouse Gas Emissions Data, http://www.epa.gov/climatechange/ghgemissions/usinventoryreport.html (accessed June 24, 2012).

(2) Energy Information Administration [EIA], (2010). Annual Energy Outlook 2011 with Projections to 2035, http://www.epa.gov/climatechange/ghgemissions/usinventoryreport.html (accessed June 24, 2012).

(3) Allen Alley, R., T. N.L. Berntsen, Z. Bindoff, A. Chen, and A. Chidthaisong, 2007, Climate Change 2007: the physical science basis: Summary for policymakers, Working Group 1, Intergovernmental Panel on Climate Change., 18, http://www.ipcc.ch/pdf/assessment-report/ar4/wg1/ar4-wg1-spm.pdf (accessed June 24, 2012).

(4) Bachu, S., (2008). CO_2 storage in geological media: Role, means, status and barriers to deployment. Progress in Energy and Combustion Science, 34(2), 254-273.

(5) St John, B., Bally, A.W., Klemme, H.D., (1984). Sedimentary provinces of the world hydrocarbon productive and nonproductive, American Association of Petroleum Geologists, Tulsa, 378.

(6) National Energy Technology Lab [NETL], (2010). Carbon Sequestration Atlas of the United States and Canada. Pittsburgh, PA, US Department of Energy publication, Third Edition (Atlas III), Pittsburgh, PA, 159.

(7) Brennan, S.T., R.C. Burruss, M.D. Merrill, P.O. Freeman, and L.F. Ruppert, 2010, A probabilistic assessment methodology for the evaluation of geologic carbon dioxide storage: U.S. Geological Survey Open-File Report 2010–1127, 31, http://pubs.usgs.gov/of/2010/1127 (accessed June 24, 2012).

(8) Spencer, L.K., J. Bradshaw, B.E. Bradshaw, A. L. Lahtinen, and A. Chirinos, 2011, Regional storage capacity estimates: Prospectivity not statistics: Energy Procedia, v. 4, 4857-4864: http://www.sciencedirect.com/science/article/pii/S1876610211007326 (accessed June 24, 2012).

Chapter 2. Comparative Analysis of Carbon Dioxide Storage Resource Assessment Methodologies [1]

2.1. Introduction

Basin-scale CO_2 storage resource assessments in one form or another have been conducted for about two decades (1-14). Today, there is increased emphasis on the distribution, potential volume, and cost to develop CO_2 geologic sequestration resources (15-18). In the presence of climate change the need to make accurate and clearly understandable assessments of carbon sequestration potential that can be used by government and industry to plan for technology deployment has never been greater.

To implement CCS in industry applications, it is also essential to consider whether the removal of CO_2 from the atmosphere is best achieved through underground geological storage or use for other purposes. The former is referred to as carbon capture, utilization, and storage (CCUS), and this term is becoming increasingly interchangeable with CCS. The most common and well practiced options for CO_2 utilization are enhanced oil recovery (EOR) and enhanced gas recovery (EGR) petroleum production. Storage resource assessments related to EOR and EGR are not covered by this study.

The CO_2 sequestration capacity that can actually be used is a subset of the total resource, constrained by external factors, much as oil and gas reserves are a subset of the total resource (19). Capacity assessments must include economic, legal, and regulatory constraints on physical

[1] This Chapter was published in the Environmental Geosciences Journal. The full reference is as follows: Popova, O., Small, M.J., McCoy, S.T., Karimi, B., Thomas, A.C., Goodman, A., Carter, K., 2012. Comparative Analyses of Carbon Dioxide Storage Resource Assessment Methodologies, Environmental Geosciences, 23 (3), 105-124.

sequestration resource estimates. Under the most favorable geologic, economic, and regulatory scenarios, 100 percent of the estimated CO_2 sequestration resource may then be considered CO_2 storage capacity (20). These scenarios are unlikely, however, as such ideal conditions are rarely present.

This study compares three CO_2 storage resource assessment methodologies: the approach applied by the DOE in its Carbon Atlas III (7); the modified USGS methodology (13); and the CGSS methodology (9, 41).

Captured CO_2 can be stored in different types of subsurface geologic formations. To be suitable for carbon sequestration, geologic media must have both sufficient capacity and injectivity and a seal that will preclude the escape of CO_2 to the atmosphere over geologically long periods of time. Geologic environments that could potentially be used as permanent repositories for anthropogenic CO_2 include depleted/depleting oil and gas reservoirs, deep saline formations, unmineable coal beds, and shale and basalt formations. All three methodologies listed above address storage resources in porous geologic media in sedimentary basins, namely oil and gas reservoirs and saline formations. Methods to estimate the CO_2 storage potential of unmineable coal beds as well as shale and basalt formations are not considered in this Thesis.

2.2. Trapping Mechanisms

There are a number of studies that examine the mechanisms of CO_2 trapping in the subsurface (1, 21-23). Metz et al. (1) described four of these trapping mechanisms: structural and stratigraphic hydrodynamic trapping (physical), residual CO_2 trapping (physical), solubility trapping (geochemical) and mineral trapping (geochemical). The time scales associated with geochemical

trapping mechanisms are much larger than those of physical trapping mechanisms and become important when talking about very long-term retention, i.e., greater than thousands of years (1).

The ability of a formation to store CO_2 depends not only on its porosity and permeability characteristics but also its associated trapping mechanism(s). Reservoir traps are formed when a permeable reservoir rock is overlain or otherwise sealed by a low-permeability caprock. A structural trap is created by structural deformation (i.e., where folds and/or faults occur), and stratigraphic traps are created by facies changes, unconformities, or lateral and vertical changes in permeability. In all cases, there is a physical barrier to flow – the fluid cannot migrate out of the formation once it has been injected (22). The caprock serves as a barrier and prevents the CO_2 leakage to the surface. Bachu (24) demonstrated that, in residual trapping, gas bubbles are left behind a migrating CO_2 plume when water moves back into pore space during an imbibition cycle, after it was expelled from the pore space during a drainage cycle. These residual CO_2 bubbles are immobilized by capillary forces. In solubility trapping, CO_2 dissolves in the formation brine. Finally, in mineral trapping, dissolved CO_2 reacts with host rocks and ions in formation water to precipitate carbonate minerals (24).

2.3. Estimation of Sequestration Resource and Capacity

2.3.1. Concepts and Approaches

Methodical evaluation of geologic CO_2 sequestration resources at large scales dates back nearly two decades; thus there is a substantial body of literature examining sequestration potential at the national, regional or basin levels (2-8,10-14, 25-29). Studies on sequestration resource evaluation at a basin scale help us to understand how CCS technologies may work in theory; in other words, these studies provide a preliminary assessment of the prospective impact of CCS technology

deployment on CO_2 emission reduction at the national or regional level. The value of these studies is to inform decision makers as to whether CCS is a climate mitigation option worth pursuing in those regions (17, 26).

Some published studies examine analytical equations as a means of providing a quick spatial characterization of a CO_2 plume using minimal information for a given range of reservoir conditions. Nordbotten et al. (30) presented a solution for viscosity-dominated regimes. Denz and Tartakovsky (31) introduced an analytical expression and use a calculation technique to account for buoyancy-dominated regimes. Szulczewski and Juanes (32) presented a sharp-interface mathematical model of CO_2 migration in deep saline formations, which accounts for gravity override, capillary trapping, natural groundwater flow, and the shape of the plume during the injection period. The main outcome is an analytical equation that defines the ultimate footprint of the CO_2 plume and the time scale required for complete trapping. The model is suitable for storage resource estimates by capillary trapping at the basin scale.

Other models have been developed to examine the amount of CO_2 that can be sequestered given constraints on reservoir pressure (33, 34). Because these types of analytical models consider pressure, they also allow injectivity constraints on capacity to be considered - that is, the rate at which CO_2 can be injected into a specific geological formation is limited by pressure conditions.

Models considering injectivity or the spatial extent of injected CO_2 require a significant amount of information on reservoir properties and, as such, may only be applied in cases where reservoir parameters are well known, e.g., for screening candidate reservoirs for a specific CO_2 sequestration project. For the assessment of sequestration potential of deep saline formations on

a basin scale, implementation of analytical techniques is difficult because little is typically known about the formation(s)' subsurface structure and the reservoir properties.

There is also a body of work that examines issues relating to CCS regulation. The CCSReg project (35, 36) examined the technical capabilities, legal framework, regulatory rulemaking, and administrative procedures that must be developed to make deep geological sequestration of CO_2 a practical reality in the United States. Ghaderi and Keith (37), McCoy and Rubin (38), and Gresham et al. (39) considered issues such as safety, environmental quality, reliability, liability, cost-effectiveness, project financing and management, long-term stewardship, and political and social feasibility associated with the life-cycle of a CCS project. Such findings are necessary for storage capacity assessments, which include economic, legal, and regulatory constraints on physical sequestration resource estimates.

Ideally, CO_2 storage resource estimates should be made on the basis of detailed geological and geophysical analysis and modeling. However, high-level assessments are required to understand where public and private resources should be focused, as well as provide a regional understanding of the role that CCS can play in reducing emissions. While site assessments require detailed geological and reservoir simulation modeling to determine if the site has the capacity to contain the volumes proposed for injection, basin-scale estimates need a more general, aggregated approach to allow high-level assessment of the total potential resource. When a CO_2 sequestration industry emerges, storage resource and capacity estimates will be considered a commodity.

The relationship between resource and capacity is much like the relationship between "resources" and "reserves" in the National Oil and Gas Assessment (NOGA) classification (44),

but with the additional caveat that CO_2 storage capacity estimates must meet economic and regulatory requirements at the time of the storage assessment. Specifically, resources are estimated quantities of a commodity that exist at a given time within a given geographic area or jurisdiction. Resources are of two types - discovered (in-place) and undiscovered (inferred). Reserves are estimated quantities of a commodity that are known to exist and economically recoverable from known accumulations. Technology, economic, and regulatory cutoffs are used to define reserves as a subset of resources. similarly, a CO_2 resource estimate is defined as the volume of porous and permeable sedimentary rocks that is accessible to injected CO_2 via drilled and completed wellbores and includes estimates of geologic storage reflecting physical constraints, but does not include economic or regulatory constraints. A CO_2 capacity estimate includes economic and regulatory constraints, such as land use, minimum well spacing, maximum injection rate and pressure, number and type of wells, operating costs, and proximity to a CO_2 source.

The methodologies explored in this Chapter - DOE (7), USGS (13), and CGSS (41) - classify a CO_2 resource as a volume of porous sedimentary rocks available for CO_2 storage and accessible to injected CO_2 under current technologies. In other words, these methodologies address the technically accessible resource that may be available using present-day geological and engineering knowledge and technology for CO_2 injection into geologic formations. The investigated methodologies are not intended for CO_2 storage capacity assessment.

The DOE, USGS, and CGSS methodologies consider only physical CO_2 trapping mechanisms (i.e., structural, stratigraphic, and residual trapping), not geochemical trapping mechanisms (i.e., solubility and mineral trapping). Because time scales associated with geochemical trapping mechanisms are much larger than those of physical trapping mechanisms, the former play an

important role only when considering very long-term retention (i.e., hundreds to thousands of years) (1, 22, 23). Since these three methodologies are intended to assess CO_2 storage resource available for immediate use, dissolution in brine and mineral precipitation are not considered in the estimates presented herein.

Methods for estimating subsurface volumes in porous and permeable geologic formations used by these approaches are widely applied in the oil and gas industry, for underground natural gas storage, groundwater assessments, and the underground disposal of fluids. By and large, these methods can be divided into two categories: static and dynamic. While dynamic methods involve injection volumes and reservoir pressure calculations, static models require only rock and fluid properties. Static methods include volumetric models and compressibility; dynamic methods utilize decline curve analyses, mass (or volumetric) balance, and reservoir simulation results.

All three methodologies address two boundary condition assumptions: open and closed systems. Open boundary conditions imply that *in situ* formation fluids are displaced away from the injection well into other parts of the formation or into adjacent formations. Conversely, closed systems are fluid-filled formations where fluid movement is restricted within the formation boundaries by impermeable barriers. Storage volume in a closed system is constrained by the compressibility of the formation's native fluids and rock matrix. It is difficult to collect hydrodynamic data on a basin-scale level to characterize closed system boundary conditions. Expectedly, three methodologies evaluated in this Thesis base storage resource calculations on open systems in which *in situ* fluids are either displaced away from the injection zone into other parts of the formation or otherwise managed.

Since detailed site injectivity and pressure data are generally not available prior to CO_2 injection or collection of field measured injection rates and pressure dynamics, all three methods use static volumetric models based on commonly accepted assumptions about *in situ* fluid distribution in porous media and fluid displacement processes. The volumetric methods employ a relatively simple description of 1) formation topology that includes formation thickness and area, 2) formation porosity, and 3) some type of factor that reflects the pore volume that injected CO_2 can fill.

2.3.2. Applicability

Subsurface units suitable for geologic CO_2 sequestration are regarded as those located approximately 800 meters (m) [2,625 feet (ft)] or more below ground surface, such that the increased pressure and temperature at depth are in excess of the critical point of CO_2. This means that CO_2 injected at these temperatures and pressures will be in the supercritical condition. Fluids in the supercritical state, including CO_2, typically exhibit gas-like viscosity, reducing resistance to flow relative to a liquid, and liquid-like density, reducing the volume required to store a given mass of fluid. Carbon dioxide exists as a supercritical fluid at a temperature and a pressure above a critical point: 304 Kelvin (K) (87.53° Fahrenheit (F)) and 7.38 Megapascal (MPa) (73.8 bar), respectively. The 800-m (2,625-ft) criterion is only an approximation, and varies somewhat depending on the geothermal gradient and formation pressure at a given site (25).

While the CGSS approach does not recommend any specific screening criteria, the DOE and USGS methodologies clearly define requirements for the formation depth. DOE recommends taking into consideration only formations deeper than 800 m (2,625 ft) (or the depth needed to ensure that CO_2 is in a supercritical phase), but does not explicitly specify a lower depth limit. USGS recommends formation depth limits of 914 m (2,999 ft) and 3,962 m (13,999 ft). The

lower vertical limit of 3,962 m (13,999 ft) for a potential storage formation is based on the imputed CO_2 injection depth at pipeline pressures without additional compression at the surface (10). Additionally, both methodologies recommend excluding from CO_2 resource estimates those formations with water having a salinity less than 10,000 milligrams per liter (mg/l) (or parts per million (ppm)) total dissolved solids (TDS) regardless of depth, to ensure that potentially potable water-bearing units according to the Safe Drinking Water Act are not included or potentially affected by sequestration activities (42,43).

2.4. DOE Methodology

Over a number of years, a group of researchers led by Dr. Scott Frailey at the Illinois State Geological Survey has collaborated through DOE's Regional Sequestration Partnerships Initiative to develop the DOE approach. The methodology has been used in the three generations of the National Carbon Atlas (5-7), and the most recent version of the methodology is also presented in Goodman et al. (14). The DOE Carbon Atlas III (7, p. 23) specifies the targeted storage resource as follows: "Carbon dioxide storage resource estimates in Atlas III are defined as the fraction of pore volume of sedimentary rocks available for CO_2 storage and accessible to injected CO_2. Storage resource assessments do not include economic or regulatory constraints."

2.4.1. Oil and Gas Reservoirs

As a result of exploration and production, oil and gas reservoirs are among the most well-known and characterized resources associated with porous sedimentary formations. Oil and gas reservoirs are discrete and stochastically distributed over the host formation.

In the case of oil and gas reservoirs that are not in hydrodynamic contact with an aquifer, the pore space previously occupied by the produced hydrocarbons becomes, by and large, available

for injected CO_2. In reservoirs that are in hydrodynamic contact with an underlying aquifer, formation water enters the reservoir as the pressure decreases because of production, reducing the pore volume available for CO_2 storage. CO_2 injection can to some extent drive water out, thus making more pore space available for CO_2. However, not all of the pore space previously occupied by formation fluids will become available for CO_2 because some residual fluids may remain within the pore space due to capillary trapping.

The CO_2 storage resource is calculated according to:

$$\mathbf{G_{CO2} = A\ h_n\ \varphi_e\ (1\text{-}S_{wi})\ B\ \rho_{CO2std}\ E_{oil/gas}} \quad (1)$$

where

- G_{CO2} = mass estimate of oil and gas reservoir CO_2 storage resource (M)
- A = area of the oil or gas reservoir that is being assessed for CO_2 storage (L^2)
- h_n = net thickness (net oil and gas column height in the reservoir (L)
- φ_e = average effective porosity in volume defined by the net thickness (L^3/L^3)
- S_{wi} = average initial water saturation within the total area (A) and net thickness (h_n) (L^3/L^3)
- B = fluid formation volume factor; converts standard oil or gas volume to subsurface (L^3/L^3) volume at reservoir pressure and temperature (fraction)
- ρ_{CO2std} = standard density of CO_2 evaluated at standard pressure and temperature (M/ L^3)
- $E_{oil/gas}$ = CO_2 storage efficiency factor, the volume of CO_2 stored in an oil or gas reservoir per unit volume of original oil or gas in place (fraction)

The efficiency factor *per se* reflects the fraction of the total reservoir pore volume from which oil and/or gas has been produced and that can be filled by CO_2. The CO_2 storage efficiency factor E involves the original oil or gas in place and the recovery factor, and can be derived based on experience or reservoir simulations. Factors not taken into account include CO_2 miscibility into oil, dissolution of CO_2 into brine, and water flooding. An appropriate reservoir volume factor (B) should be utilized to scale oil or gas volume to subsurface volume at reservoir pressure and temperature. Since CO_2 storage resources for oil and gas reservoirs are reported at the field level, assessment on a basin level can be performed by summing up individual field estimates.

2.4.2. Saline Formations

By definition, a deep saline formation is a body of porous rock that meets the depth conditions for CO_2 storage and that contains water with TDS greater than 10,000 mg/l (ppm). This specific threshold is defined according to the Safe Drinking Water Act (42), stating that any groundwater with salinity less than 10,000 mg/l (ppm) TDS has the potential to be used as a water supply regardless of depth. Therefore, the potential storage resources for CO_2 in formations with salinities lower than 10,000 mg/l (ppm) are excluded from assessment. Generally, any given saline formation is a member of a sedimentary succession in a certain sedimentary basin or province.

DOE differentiates between physical and chemical CO_2 trapping mechanisms. Because chemical trapping mechanisms are time-dependent processes requiring hundreds to thousands of years to unfold, DOE does not consider these mechanisms in calculating CO_2 storage resources at the basin and regional scales. The DOE methodology focuses on buoyant (structural and stratigraphic) and residual trapping, since initially those are the leading trapping mechanisms.

$$G_{CO2} = A_t\, h_g\, \varphi_{tot}\, \rho_{CO2std}\, E_{saline} \quad (2)$$

where

- G_{CO2} = mass estimate of saline formation storage resource (M)
- A_t = total area that defines the basin or region being assessed for CO_2 storage (L^2)
- h_g = gross thickness of saline formation (L)
- φ_{tot} = total porosity that accounts for the total volume of pore space (L^3/L^3)
- ρ_{CO2} = density of CO_2 evaluated at pressure and temperature that represent storage conditions expected for a given formation averaged over h and A (M/L^3)
- E_{saline}= CO_2 storage efficiency factor that reflects a fraction of the total pore volume that is filled by CO_2. E_{saline} factors fall in between 0.40 and 5.5 percent over 10^{th} to 90^{th} percentile range.

2.4.3. Storage Efficiency Factor for Saline Formations

Efficiency factor, E_{saline}, is a scaling coefficient that incorporates the cumulative effects of formation heterogeneity (geologic layering), CO_2 buoyancy, and sweep efficiency. No distinction is made between CO_2 stored by various mechanisms. More specifically, for saline formations, the CO_2 storage efficiency factor is a function of uncertainty in input formation parameters such as area (A), gross thickness (h_g), and total porosity (φ_{tot}). Additionally, four displacement efficiency constituents - areal, vertical, gravity, and microscopic - incorporate different physical barriers that restrain CO_2 from occupying 100 percent of the formation pore volume. Since it is difficult to discriminate the areal, vertical, and gravity displacement terms for a heterogeneous geologic unit, these terms are integrated by DOE into a single volumetric displacement term, E_V, following the International Energy Agency Greenhouse Gas Programme report (44).

Efficiency estimates use statistical properties including mean values, standard deviation, ranges, and distributions that describe formation parameters. Little information is known regarding the statistical characteristics of saline formations because formation properties are not well characterized. Based on results of previous research, DOE assumes that saline formations do not differ essentially from oil and gas reservoirs (10, 27, 44-47). DOE uses values provided by IEAGHG (44) for the 10th and 90th percentiles of geologic and displacement parameters for clastics, dolomite, and limestone lithologies for saline formations.

Equation 3 defines the individual parameters needed to estimate the CO_2 storage efficiency factor E_{saline}, for saline formations:

$$\mathbf{E_{saline} = E_{An/At}\, E_{hn/hg}\, E_{\varphi e/\varphi tot}\, E_v\, E_d} \quad (3)$$

where

- $E_{An/At}$ = the net-to-total area ratio, the fraction of the total basin or region area that is suitable for CO_2 storage
- $E_{hn/hg}$ = the net-to-gross thickness ratio, the fraction of the total geologic unit that meets minimum porosity and permeability requirements for injection
- $E_{\varphi e/\varphi tot}$ = the effective-to-total porosity ratio, the fraction of total porosity that is interconnected
- E_v = the volumetric displacement efficiency, integrates the areal displacement efficiency (the fraction of planar area surrounding the injection well that CO_2 can contact), the vertical displacement efficiency (the fraction of vertical cross section or thickness with the volume defined by the area that can be contacted by the CO_2 plume from a single well), and the gravity displacement efficiency (the fraction of net thickness that is

contacted by CO_2 as a consequence of the density and mobility difference between CO_2 and *in situ* water

- E_d = the microscopic displacement efficiency, the fraction of water-filled pore volume that can be replaced by CO_2

In the DOE methodology, efficiency for saline formations, as estimated by Monte Carlo sampling, is established based on the P10 and P90 percentiles provided by IEAGHG (2009) as follows:

- $E_{hn/hg}$, fraction of total geologic unit that meets minimum porosity and permeability requirements for injection: 0.13 to 0.76
- $E_{\varphi e/\varphi tot}$, fraction of total porosity that is effective, i.e., interconnected: 0.53 to 0.77
- E_v, combined fraction of immediate volume surrounding an injection well that can be contacted by CO_2: 0.16 to 0.57
- E_d, fraction of pore space unavailable due to immobile *in situ* fluids: 0.27 to 0.76

Since no recorded data for the net-to-total area ratio are available (values will be very site-specific), it was assumed that CO_2 could be stored in between 20 and 80 percent of the formation for the purposes of these simulations (5,6). The area $E_{An/At,}$ thickness $E_{hn/hg}$, and porosity $E_{\varphi e/\varphi tot}$ components establish the fraction of the volume that is suitable for CO_2 sequestration. The volumetric displacement component (E_v) corrects for the effective CO_2 plume shape. The microscopic displacement component (E_d) accounts for the pore volume accessible by CO_2.

Efficiency (E_{saline}) is estimated from the individual efficiency coefficients in equation 3 by Monte Carlo simulation. Each individual factor in Equation 3 is specified by a fraction, *p*, ranging between 0 and 1. To represent this fraction in Monte-Carlo simulations the log-odds normal

distribution, also known as the logistics-normal distribution, is selected. This distribution for *p* is properly constrained to the range (0, 1), and the distribution parameters can be readily computed from the P10 and P90 ranges of geologic and displacement parameters presented by IEAGHG (44).

In the log-odds normal distribution the transformed variable $X = \ln\left(\frac{p}{1-p}\right)$ is normally distributed. The values of P10 and P90 determine X_{10} and X_{90}, which are then used to compute μ_x and δ. With parameters determined X_{QI} can be readily sampled with Monte Carlo techniques. Then, the simulated X value is converted back to the respective *p* value by the inverse equation: $p = \frac{1}{1+e^{-X}}$. In applications of the DOE methodology to date, the parameters are assumed and sampled independently (14). However, should data become available to estimate correlation among parameters, these could be incorporated in future studies.

The saline formation efficiency factors encompass a range from a 10th percentile of 0.40 percent to a 90th percentile of 5.5 percent for clastics, dolomite, and limestone lithologies. In comparison, the previous versions of the Carbon Sequestration Atlas of the United States and Canada reported the saline formation efficiency factors ranging from 1 to 4 percent over the P15 and P85 percentiles (5, 6). P10 and P90 present lower and upper bounds that define a likely range of efficiency factors. This range reflects various depositional environments and corresponding lithologies of saline formations that occur in North America.

2.5. USGS Methodology

The methodology proposed by USGS is consistent with the resource-reserve pyramid concept (14,16,20,44) and equivalent with the definition of a CO_2 resource estimate as defined by DOE.

The USGS approach is similar to probabilistic natural resource assessments in the USGS National Oil and Gas Assessment and treats the geological commodity of subsurface pore space as a resource that can be assessed much like other natural resources. The methodology developed by USGS uses the concept of the storage assessment unit (SAU), "a mappable volume of rock that consists of a porous flow storage unit and a bounding regional sealing formation. Within the SAU, the porous flow unit is defined as the storage formation (SF)" (13). Any part of the SF that is not beneath the seal formation is excluded from the SAU. A schematic cross section through a SAU is illustrated in Figure 2.1.

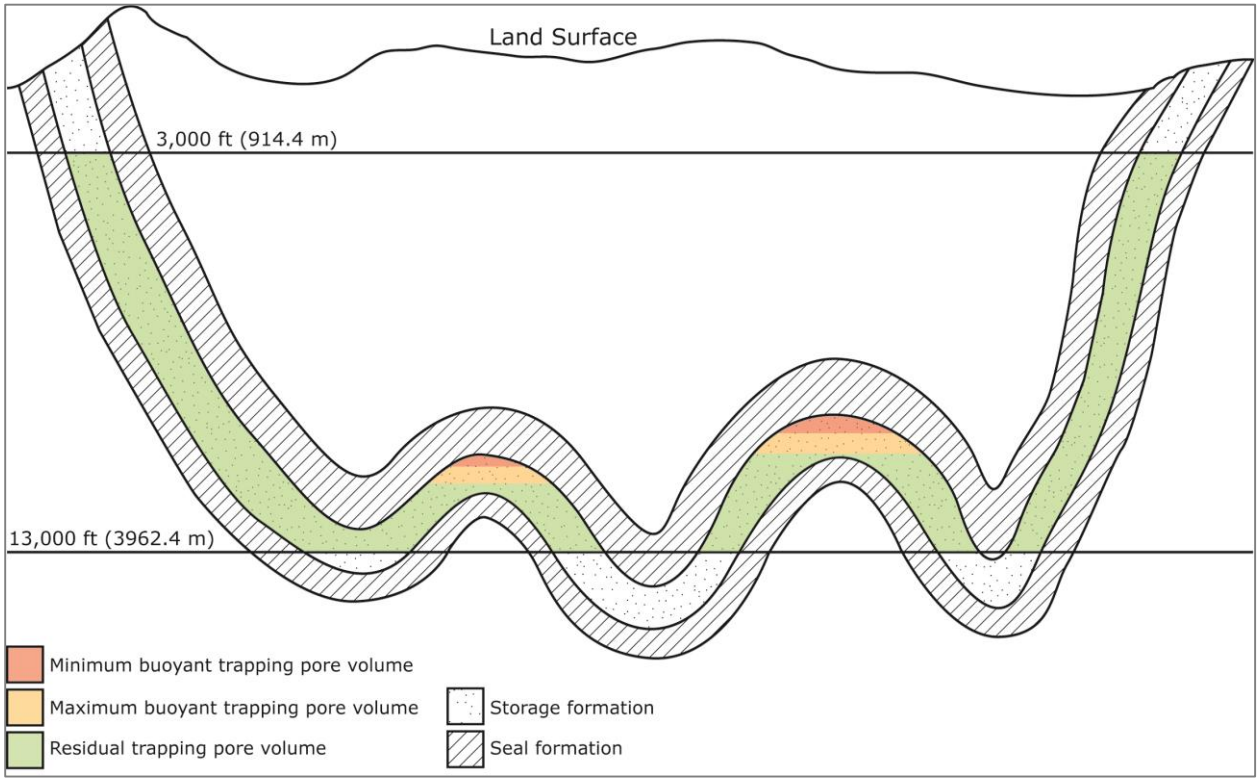

Figure 2.1. Schematic cross section through a storage assessment unit (SAU) (modified from Brennan et al. [13]).

In this conceptual framework, sedimentary basins are subdivided into a series of SAUs. The USGS methodology is based on two major calculations, that of 1) the buoyant trapping storage

resource and 2) the residual trapping storage resource. The technically accessible storage resource for the SF as a whole is a sum of the buoyant trapping storage resource and residual trapping storage resource.

2.5.1. Buoyant Trapping

Injected into the subsurface as a separate fluid, CO_2 displaces formation water and forms a buoyant plume migrating up-dip beneath a seal away from the injection site. When CO_2 encounters a trap enclosed by the seal, the buoyant fluid continues to displace the formation water, forming an accumulation in the same way that hydrocarbons accumulate. The USGS methodology defines the pore space within large geologic structures that retain CO_2 in this manner as buoyant trapping. Since many of these structures include petroleum reservoirs, and production data are available from the oil and gas industry, USGS bases their buoyant trapping storage resource estimates (B_{SR}) on data from petroleum reservoirs that have more than 500,000 barrels of oil equivalent (B_{OE}).

The USGS methodology is applied in two steps. First, the buoyant trapping pore volume (B_{PV}), "a geologically determined, probabilistic distribution of the volume of the SF that can store CO_2 by buoyant trapping" (13), is calculated. USGS proposes some default values to generate the B_{PV} distribution:

a) The minimum B_{PV} input is determined as the volume of known recovery of petroleum, scaled to subsurface volumes.

$$\mathbf{B_{PV\_MIN} = KR_{RES} = [((KR_{OIL} + KR_{NGL} +) FVF_{OIL}) + (KR_{GAS} FVF_{GAS})]} \quad (4)$$

where

- KR_{RES} = volume estimate corrected to reservoir conditions (L^3)
- KR_{OIL} = the known recovery of oil (L^3)

- KR_{NGL} = the known recovery of natural gas liquids (L^3)
- FVF_{OIL} = the formation volume factor for oil and natural gas liquids (fraction)
- KR_{GAS} = the known recovery of gas (L^3)
- FVF_{GAS} = the formation volume factor for gas (fraction)

b) To evaluate a median B_{PV} an intermediate or 'best guess' estimate of buoyant trapping, USGS uses the reported mean values for USGS NOGA undiscovered petroleum resource volumes. These mean resource volumes allocated to the SF are scaled to reservoir conditions using $quation 4. The corrected undiscovered NOGA volumes are then added to the KR_{RES} value to estimate the median B_{PV}.

c) The USGS methodology does not specify how to estimate maximum B_{PV}. They suggest, however, the maximum B_{PV} input should include some estimate of the volume of the total pore space that is within large enclosures. It is likely that a number of 'dry traps' exists within the SF, and it is desirable to incorporate their volume into KR_{RES}. However, because there are no known available datasets on 'dry trap' attributes, evaluating any volume relevant to USGS NOGA or KR_{RES} values will be difficult.

A range of B_{PV} values reflects the variety of basin-specific conditions and can be evaluated in a number of ways. The USGS methodology suggests that the assessment geologist should estimate the buoyant trapping pore volume using the best engineering judgment and all available geologic data.

Second, the buoyant trapping storage resource (B_{SR}) is calculated. The buoyant trapping storage efficiency (B_{SE}) is generally assumed to be lower than reservoir hydrocarbon saturation because it is impossible for a relatively low-viscosity supercritical CO_2 fluid to displace 100 percent of a

high-viscosity fluid, whether oil or water. The buoyant trapping storage efficiencies used by USGS are based on experimentally derived relative permeability curves (22, 23). These values will likely change, however, when more research or field data become available. A probabilistic distribution of the density of CO_2 is computed by the assessment geologist based on an equation of state for CO_2, the upper and lower depth boundaries of the SF and geothermal and pressure gradients relevant for the region. The buoyant trapping storage resource (B_{SR}) is obtained according to:

$$\mathbf{B_{SR} = B_{PV}\, B_{SE}\, \rho_{CO2}} \qquad (5)$$

where

- B_{SR} = mass estimate of the buoyant trapping storage resource (M)
- B_{PV} = pore volume available for buoyant trapping (L^3)
- B_{SE} = storage efficiency of buoyant CO_2 storage (fraction)
- ρ_{CO2} = density of CO_2 evaluated at pressure and temperature that represent storage conditions expected for a given SF (M/L^3)

2.5.2. Residual Trapping

The methodology used by USGS to estimate the residual trapping storage resource is based on a multistep procedure. The first step of the assessment process is to define the storage formation pore volume. The proposed relationship for calculating pore volume in the storage formation is a probabilistic product as follows:

$$\mathbf{SF_{PV} = A_{SV}\, T_{PI}\, \varphi_{PI}} \qquad (6)$$

where

- SF_{PV} = pore volume of the storage formation (L^3)
- A_{SV} = the mean area of the storage formation (L^2)

- T_{PI} = the mean thickness of the porous interval (ft), where the porous interval is defined as the stratigraphic thickness of the storage formation with a porosity of 8 percent or higher (L)
- φ_{PI} = the mean porosity of the porous interval (fraction)

The pore volume available for the residual trapping is defined as the remaining SF_{PV} that is not accounted for the buoyant storage resource. A single value is selected from the simulated B_{PV} distribution, and then this value is subtracted from the SF_{PV} chosen in the same Monte Carlo iteration:

$$\mathbf{R_{PV} = SF_{PV} - B_{PV}} \quad (7);$$

where

- R_{PV} = residual trapping pore volume (L^3)
- SF_{PV} = pore volume of the storage formation (L^3)
- B_{PV} = pore volume of the storage formation (L^3)

Next, USGS breaks up the residual pore volume into three rock classes or "injectivity category allotments" depending on permeability, as presented in Table 2.1.

This approach assumes that the assessment geologist will obtain permeability values from databases, existing literature, and any other available sources. Based on these permeability values, the percentages of the SF that comprise each class are estimated. Little is known about reservoir properties for these parts of the SF due to limited field observations.

Table 2.1. Rock classes or injectivity category allotments within a storage formation (after Brennan et al. [13]).

Rock Class	Permeability	Storage Efficiency (based on Gorecki et al., 2009 [a,b,c])
Class 1	High, greater than 1 Darcy	Storage efficiency values for these rocks are generally lower than Class 2 rocks as a result of high mobility of a CO_2 plume and lack of pore-scale residual trapping
Class 2	Moderate, between 1 milliDarcy and 1 Darcy	Highest storage efficiency values as a result of the presence of full range of potential residual trapping types
Class 3	Low, less than 1 milliDarcy	Low storage efficiency values, with minimum and mode values approaching or equal to zero, given that little CO_2 will enter these rocks without artificially fracturing the rock. However, maximum values for different lithologies are taken into account covering the possibility that some mass of CO_2 could enter and be stored within this part of the SF.

Since the storage efficiency values are not well constrained, USGS proposes to use a standard set of minimum, mode, and maximum values based on modeled values from Gorecki et al. (45). Using permeability data from the SF, the R_{PV} is then allocated between these three classes ($R1_{PV}$, $R2_{PV}$, and $R3_{PV}$).

The proposed relationship for calculating the residual storage resource for each rock class is:

$$\mathbf{R_{SR} = R_{PV}\, R_{SE}\, \rho_{CO2}} \qquad (8);$$

where

- R_{SR} = the residual trapping storage resource as a probabilistic product (M)

- R_{PV} = the residual trapping pore volume ((L^3))
- R_{SE} = the residual trapping storage efficiency, sampled from the predetermined probability distributions. The suggested storage efficiency ranges are provided in Table 2. 2 (fraction)
- ρ_{CO2} = the density of CO_2; a probabilistic distribution of the density of CO_2 is calculated by the assessment team based on the upper and lower depth boundaries of the storage formation, temperature and pressure gradients appropriate for the area, and an equation of state for CO_2 (M/L^3).

Table 2.2. Suggested storage efficiency ranges, based on the set modeled by Gorecki et al. [45].

Rock Class	Suggested Storage Efficiency Values
Class 1	minimum 1% mode 5% maximum 7%
Class 2	minimum 1% mode 7% maximum 15%
Class 3	minimum 0% mode 0% maximum 7%

2.5.3. Technically Accessible Storage Resource

The technically accessible storage resource (TA_{SR}) for the entire SF is determined by an iterative summation of buoyant and residual trapping storage resources as follows:

$$\mathbf{TA_{SR} = B_{SR} + R1_{SR} + R2_{SR} + R3_{SR}} \quad (9);$$

where

- TA_{SR} = the technically accessible storage resource (M)
- B_{SR} = the buoyant trapping storage resource (M)
- $R1_{SR}$ = the residual trapping class 1 storage resource (M)
- $R1_{SR}$ = the residual trapping class 2 storage resource (M)
- $R1_{SR}$ = the residual trapping class 3 storage resource (M)

Storage in Oil and Gas Reservoirs

Since storage in oil and gas reservoirs is a special case of buoyant trapping, it can be estimated by using the KR_{RES} values determined in the buoyant trapping section. The volumetric relationship used in the USGS methodology is:

$$\mathbf{KRR_{SR} = KR_{RES}\, B_{SE}\, \rho_{CO2}} \quad (10);$$

where

- KRR_{SR} = oil and gas reservoir storage resource, the known recovery replacement storage resource (M)
- KR_{RES} = the known recovery corrected to a volume at subsurface conditions calculated in equation 4 (L^3)
- B_{SE} = the buoyant storage efficiency (fraction)
- ρ_{CO2} = the density of CO_2; a probabilistic distribution of the density of CO_2 is calculated by the assessment team based on the upper and lower depth boundaries of the storage formation, temperature and pressure gradients appropriate for the area, and an equation of state for CO_2 (M/L^3).

The storage efficiency distribution for the oil and gas reservoirs used for this resource estimation is the same as the buoyant storage efficiency values described above.

2.6. CGSS Methodology

The CGSS methodology was developed for the 2009 Queensland CO_2 Geological Storage Atlas through the Queensland Carbon Geostorage Initiative (9, 41). The CGSS methodology includes the following key steps and assumptions: (1) examine regional seal and reservoir distributions, their quality and characteristics and identifying defined storage fairways, (2) determine CO_2 density curves for each geological province and use these to better estimate *in situ* CO_2 density in vertical layers of 100 m (328 ft) or more in the subsurface, (3) use migration-assisted storage (MAS) trapping as a major mechanism for subsurface CO_2 storage at the industrial scale, and (4) include in the assessments only the volume of rock that is likely to be permeated by a migrating CO_2 plume.

2.6.1. Migration-assisted storage (MAS) Trapping

According to the CGSS methodology, in the process of residual trapping only a thin layer beneath the base of the seal will be affected by the migrating plume, and the residual gas saturation (RGS) associated with the immobilized portion of the plume will represent only a small percentage of the reservoir's available pore volume. In the absence of a reservoir simulation model, a regional volumetric assessment should attempt to account for these limiting factors.

The CGSS methodology uses the following assumptions:

- the reservoir is considered homogeneous;
- initial injection occurs in a single well over the entire thickness of the reservoir;

- formation water is displaced radially and uniformly away from the well bore during injection (the pressure-driven phase of a storage project); and
- the injected-affected-cylinder of CO_2 that develops around the wellbore only extends out to a radius of 2.5 km (1.55 mi) (beyond this, gravity-driven forces begin to override the pressure-driven forces).

The CGSS methodology considers the CO_2 storage within the injection-affected-cylinder around the well to be ideally only a function of reservoir gas saturation: $Sg = 1\text{-}Sw_{(irr)}$, where$Sw_{(irr)}$ is the irreducible water saturation of the pore space. When injection ceases, formation water moves by imbibition (gravity-driven phase) back into the original injection-affected-cylinder and the ultimate storage within it is now a function of the RGS. Figure 2.2 is a representation of a siliciclastic pore environment, illustrating how residual gas and formation water may occupy the pore space post-injection. The remaining mass of gas ($1\text{-}Sw_{(irr)} - Sg_{r,}$ where Sg_r is RGS), needs to be stored outside of the original injection-affected cylinder. This mass rises to the top of the reservoir and migrates underneath its seal. The total lateral distance that the CO_2 plume can migrate away from the injection well is a function of Sg_r and the thickness of the migrating plume.

The CGSS approach uses simulation models that suggest that migration plumes will rarely be thicker than 25 m (82 ft) in most homogeneous reservoirs, and are often much thinner. More specifically, the Queensland Atlas assumes a generic migrating plume thickness of 15 m (49 ft); $Sw_{(irr)}$ is set consistent with known basin values of 35 percent; and a MAS reservoir efficiency factor is calculated for each reservoir (9, 41).

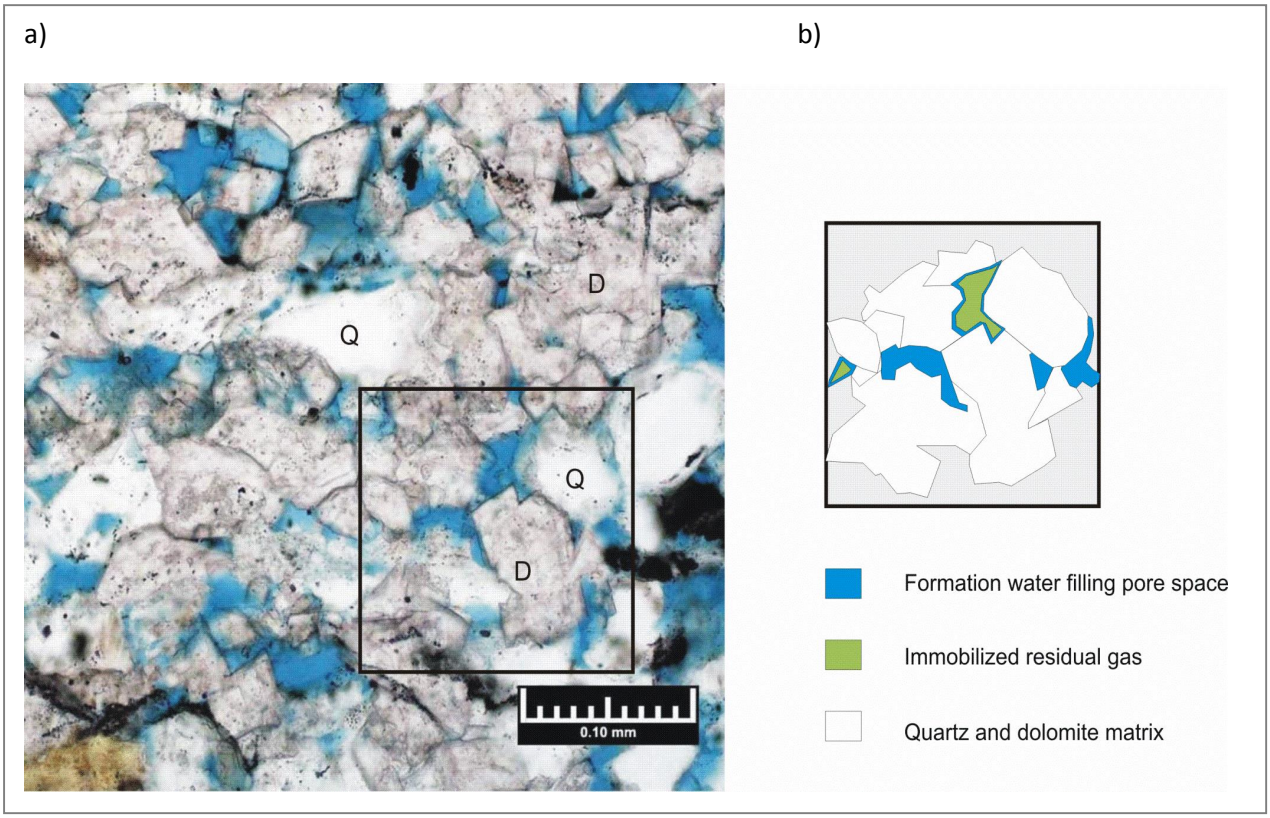

Figure 2.2. (a) Thin section photomicrograph of the Oriskany Formation from Ohio Core 3583, 1,269 m (4,164 ft), illustrating detrital quartz grains (Q) and dolomite (D) fabric in this sample; (b) Cartoon illustration based on photomicrograph, showing how formation water and residual gas may occur in the pore space of a reservoir rock. (Source: The Pennsylvania Bureau of Topographic and Geologic Survey).

The thicker the reservoir, the smaller the efficiency factor will be. For example, at 15 m (49 ft), it is 100%; at 50 m (164 ft), it is approximately 30%; and at thicknesses greater than 150 m (492 ft), the efficiency factor is less than 10%. The MAS reservoir efficiency factor provides only an approximation for any given site, but it serves to reduce unrealistic regional maximum volumetric estimates.

By and large, in porous rocks RGS increases with: (1) decreasing porosity, sorting, and grain size and (2) increasing cementation and clay content. It is difficult to estimate RGS without rock core

samples, and for regional assessments, available estimation methods are limited. Various authors quote ranges of 0.05 to 0.95 for RGS (48, 49). Using an empirical method published by Holtz (48) and using the 10% cut-off porosity, the CGSS approach calculates RGS values between 0.2 to 0.6. However, the conservative value of $Sg_r = 0.1$ is applied when calculating final regional CO_2 potential storage volumes. The discounted volumetric relationship proposed by the CGSS methodology is:

$$\mathbf{M_{CO2} = RV\ Ø\ Sg\ \rho_{CO2}\ E} \qquad (11);$$

where

- M_{CO2} = mass of CO_2 (M)
- RV = total reservoir rock volume, discounted for the average CO_2 plume thickness (L^3)
- Ø = porosity as an average total effective pore space of RV (fraction)
- Sg = the gas saturation within the above pore space as a fraction of the total pore space, either as Sg_r for residual gas saturation trapping or $1\text{-}Sw_{(irr)}$ for conventional trapping, where Sg_r = residual gas (CO_2) saturation and $Sw_{(irr)}$ = irreducible water saturation (fraction)
- ρ_{CO2} = the density of CO_2 at the temperature and pressure at the given reservoir depth (M/L^3)
- E= MAS reservoir storage efficiency factor, calculated for each reservoir assuming a migrating plume thickness of 15 m (49 ft)

2.6.2. Storage Efficiency Factor

The CGSS methodology considers that only a thin layer beneath the seal will be affected by the migrating plume (Figure 2.2). In the Queensland Atlas, a generic migrating plume thickness of

15 m (49 ft) is assumed (9, 41). MAS reservoir efficiency factors are calculated for each reservoir - the thicker the reservoir, the smaller this number will be. Storage efficiency factors are back-calculated for three sedimentary basins assessed in the Queensland Atlas using the CGSS methodology (9, 41). The results of that comparison are presented in Table 2.3.

Table 2.3. CO_2 storage resource estimates for three basins from the Queensland CO_2 Geological Storage Atlas using the CGSS methodology, comparing application of a 4% storage efficiency factor and a "back-calculated" storage efficiency factor [41].

Basin	Area (Km^2)	CO_2 storage resource		Back-calculated Storage Efficiency (%)
		CGSS Methodology (Mt CO_2)	Methodologies using E=4% (Mt CO_2)	
Galilee	147,000 *56,757*[1]	3,430	122,250	0.11
Bowen	180,000 *69,498*	340	13,100	0.10
Surat	327,000 *126,255*	2,300	61,800	0.15

[1] *square miles (mi^2)*

Each of the gross rock pore volumes of the assessed reservoir/seal pairs for the three basins are multiplied by 4% with an assumed generic CO_2 density of 700 kilograms per cubic meter (kg/m^3) [43.7 pound per cubic foot (lb/ft^3)]. As shown, these CO_2 resource estimates are orders of magnitude greater than the CGSS methodology estimates. The back-calculated storage efficiency factors for the three basins using the CGSS approach are derived to be 0.1 to 0.15% - more than an order of magnitude lower than values calculated employing other volumetric methodologies.

2.7. Findings

In this section we present the results of our comparative study of the three CO_2 storage assessment methodologies used by DOE, USGS, and CGSS, respectively. Tables 2.4-2.8 provide side-by-side comparisons across methodologies in terms of physical setting, physical processes, key equations/input parameters, and storage efficiencies.

With respect to physical setting (Table 2.4), the investigated methodologies are designed to assess permeable formations occurring in sedimentary basins. Even so, these entities use different language to define an assessment unit/formation. The DOE methodology discriminates oil and gas fields and saline formations; the USGS methodology defines storage formations within storage assessment units; and the CGSS methodology identifies basin-scale reservoirs as permeable formations. The DOE and USGS methodologies are consistent with a resource-reserve pyramid concept, while the authors of the CGSS methodology do not structure their approach in terms of this framework.

Table 2.4. Physical setting of potential CO_2 storage formations.

	DOE	USGS	CGSS
Regional setting	Sedimentary basins	Sedimentary basins subdivided into storage assessment units (SAUs)	Sedimentary basins
Assessment unit/ formation	Oil and gas fields Deep saline formations	Storage Formations (SFs)	Reservoirs as permeable formations

Regarding physical processes (Table 2.5), the DOE methodology references structural and stratigraphic hydrodynamic trapping as the dominant mechanism for retaining CO_2 in oil and gas fields, and structural and stratigraphic hydrodynamic and residual trapping as the dominant mechanism in saline formations. The USGS methodology differentiates buoyant (structural and stratigraphic hydrodynamic) trapping and residual trapping within storage formations. In the USGS method, any pore space that is not found in a known dry structural or stratigraphic trap is treated as residual pore space (whether or not the principle trapping mechanism is residual phase trapping). Thus, USGS is using different storage efficiencies to account for a lack of knowledge about the subsurface rather than making a judgment about what mechanism is at play in trapping CO_2. Unlike these two approaches, the CGSS methodology considers only residual trapping.

All three methodologies discuss the boundary condition assumptions: the two endpoints defined for potential CO_2 storage reservoirs are open and closed. However, it is difficult or impossible to collect hydrodynamic data on a basin-scale level to characterize closed system boundary conditions. Hence, the authors of the proposed methodologies base their storage resource calculations on open systems in which *in situ* fluids are either displaced away from the injection zone into other parts of formation or managed.

In terms of dealing with uncertainty, the DOE and USGS methodologies are probabilistic approaches, meaning that both methodologies use Monte Carlo simulation for estimating formation parameters. Conversely, the CGSS approach relies on a geological prospectivity of sedimentary basins and detailed geological data and applies geological, geophysical, and chemical constraints; in other words, the CGSS methodology is deterministic.

The methodologies proposed by DOE for oil and gas fields and USGS for buoyant trapping in storage formations use static volumetric methods for estimating the subsurface CO_2 storage

resource (Table 2.6.a). These methods rely on parameters that are related to the geologic description of an assessment formation (e.g. thickness, porosity, temperature, and pressure). The DOE equation for calculation of CO_2 storage resource is based on the geometry of the reservoirs (reservoir area and thickness) and water saturation as given in reserve databases. The CO_2 storage efficiency factor involves the original oil and gas in-place and recovery factor and can be derived based on experience, especially in the cases where good production records are available. The alternate USGS volumetric equation is a production-based formula where CO_2 storage resource is calculated on the basis of reservoir properties such as original oil and gas in-place, recovery factor, and *in situ* CO_2 density defined by reservoir temperature and pressure. It also requires reliable production records - the volume of known recovery of petroleum, scaled to subsurface volume, particularly when cumulative production is greater than original oil and gas in place. In addition, according to the USGS methodology, buoyant trapping storage resource in storage formations includes the mass of CO_2 that can be stored in dry traps. Comparing the two methodologies, we have identified several analogies and distinctions:

- Static volumetric storage of CO_2 in free phase is considered by both methodologies.
- Methods for CO_2 storage resource calculation are production-based for both approaches, although the DOE equation is based on reservoir geometry and properties, as well as oil and gas production data. Unlike the DOE formula, the USGS equation does not require reservoir area and thickness; it utilizes known recovery of oil and gas and reservoir properties.
- The DOE methodology does not explicitly include the volume of dry traps (without petroleum production) in CO_2 storage resource estimates for oil and gas fields. On the

other hand, the USGS approach incorporates the volume of dry traps into the CO_2 storage resource for buoyant trapping in storage formations, where data are available.

- As for storage efficiency, both methodologies use the buoyant trapping (oil and gas fields under the DOE classification) storage efficiency based on known production data.

CO_2 storage resource assessment methodologies developed by DOE for saline formations, USGS for residual trapping in storage formations, and CGSS for migration assisted storage trapping in basin-scale porous reservoirs are computationally equivalent and use volumetric-based CO_2 storage estimates (Table 2.6.b). The volumetric models rely on parameters that are directly related to the geologic description of the sedimentary basin and formation properties: area, thickness, porosity, temperature, and pressure, where the last two parameters define CO_2 density at *in situ* conditions. Nonetheless, the following high-level differences remain:

- The DOE methodology considers an assessment formation as an undivided unit and provides storage resource calculations for the formation as a whole, while the USGS methodology subdivides a storage formation into three rock classes or 'injectivity category allotments' on the basis of permeability. CO_2 storage resource is determined for each class; consequently, the computed values are summed iteratively to calculate the total residual trapping storage resource. Unlike the DOE and USGS approaches, the CGSS methodology assumes that in the process of the MAS trapping only 15 m (49 ft) of formation thickness is affected by the migrating CO_2 plume.
- Storage efficiency: the proposed methodologies introduce storage efficiency factors in calculations. The DOE methodology provides a range of values of storage efficiency for saline formations, which are between 0.40 and 5.5%. On the other hand, the USGS

methodology suggests that for calculation of residual trapping CO_2 storage resource, a specific range of storage efficiency values should be applied for each rock class (Tables 2.2 and 2.7).

- Unlike the DOE and USGS approaches, the CGSS methodology assumes that only a thin layer beneath the seal will be affected by the migrating plume. A generic thickness migrating plume used in the Queensland Atlas is 15 m (49 ft). MAS reservoir efficiency factors are calculated for each assessment unit: the thicker the reservoir the smaller this number will be, so the derived storage efficiency factors are typically more than an order of magnitude less than what the DOE and USGS methodologies suggest (Tables 2.3 and 2.7). For these reasons, the CGSS approach would produce the most conservative storage estimates if applied for the same assessment formation.

Table 2.5. Physical processes involved in CO_2 underground trapping.

	DOE	USGS	CGSS
Trapping mechanism	Structural and stratigraphic hydrodynamic trapping for oil and gas fields Structural and stratigraphic hydrodynamic and residual trapping for saline formations	Buoyant trapping (structural and stratigraphic hydrodynamic) within SFs Residual trapping within SFs	Residual trapping through migration assisted storage (MAS) trapping
Operating time frames	Months to thousands of years	Months to thousands of years	Months to thousands of years
Boundary conditions	Open system	Open system	Open system

Table 2.6. a. Key equations and input parameters for Oil and gas fields/buoyant trapping and b) Saline formations/residual trapping.

DOE	USGS	CGSS
Oil and gas fields	**SF Buoyant trapping**	**NA**
$G_{CO2} = A\ h_n \varphi_e\ (1\text{-}S_{wi}) B\ \rho_{CO2std}\ E_{oil/gas}$	*Two steps* 1) Pore volume available for buoyant trapping a) The minimum BPV $B_{PV\_MIN} = KR_{RES} = [((KR_{OIL} + KR_{NGL} +)\ FVF_{OIL}) + (KR_{GAS}\ FVF_{GAS})]$	-
G_{CO2} = mass estimate of oil and gas reservoir CO_2 storage resource (M) A = area of the oil or gas reservoir (L^2) h_n = net thickness (L) φ_e = average effective porosity (L^3/L^3) S_{wi} = average initial water saturation (L^3/L^3) B = fluid formation volume factor (fraction)	KR_{RES} = volume estimate corrected to reservoir conditions (L^3) KR_{OIL} = the known recovery of oil (L^3) KR_{NGL} = the known recovery of natural gas liquids (L^3) FVF_{OIL} = the formation volume factor for oil and natural gas liquids (fraction) KR_{GAS} = the known recovery of gas (L^3) FVF_{GAS} = the formation volume factor for gas (fraction) b) median B_{PV}	

DOE	USGS	CGSS
Oil and gas fields	**SF Buoyant trapping**	**NA**
ρ_{CO2std} = density of CO_2 evaluated at reservoir pressure and temperature (M/ L^3) $E_{oil/gas}$ = CO_2 storage efficiency factor (fraction)	undiscovered NOGA petroleum resource volumes scaled to subsurface condition for the given SF are added to the BPV_MIN value to estimate a median BPV c) maximum B_{PV} B_{PV_MAX} should include some estimate of the volume of the total pore space that is within large enclosures. No specific way to estimate BPV_{MAX} is suggested	
	2) Buoyant trapping storage resource $B_{SR} = B_{PV} B_{SE} \rho_{CO2}$ B_{SR} = mass estimate of the buoyant trapping storage resource (M) B_{PV} = pore volume available for buoyant trapping (L^3) B_{SE} = storage efficiency of buoyant CO_2 storage (fraction) ρ_{CO2std} = density of CO_2 evaluated at formation pressure and temperature (M/ L^3)	

Table 2.6. b. Key equations and input parameters for Saline formations/residual trapping.

DOE	USGS	CGSS
Saline formations	**Storage Formation Residual Trapping**	**Permeable Formation Residual Trapping**
$G_{CO2} = A\ h_n\ \varphi_{tot}\ \rho_{CO2std}\ E_{saline}$ G_{CO2} = mass estimate of saline formation storage resource (M) A_t = total area (L^2) h_g = gross thickness of saline formation (L) φ_{tot} = total porosity that accounts for the total volume of pore space (L^3/L^3) ρ_{CO2} = density of CO_2 evaluated at formation pressure and temperature (M/L^3) E_{saline}= CO_2 storage efficiency factor that reflects a fraction of the total pore volume that is filled by CO_2	*Four steps* 1) Pore volume of the storage formation $SF_{PV} = A_{SV}\ T_{PI}\ \varphi_{PI}$ SF_{PV} = pore volume of the storage formation (L^3) A_{SV} = the mean area of the storage formation (L^2) T_{PI} = the mean thickness of the porous interval (L) φ_{PI} = average effective porosity (L^3/L^3) 2) residual trapping pore volume $R_{PV} = SF_{PV} - B_{PV}$ R_{PV} = residual trapping pore volume (L^3)	$M_{CO2} = RV\ Ø\ Sg\ \rho_{CO2}\ E$ M_{CO2} = mass of CO_2 (M) RV = total reservoir rock volume, discounted for the average CO_2 plume thickness (L^3) Ø = porosity as an average total effective pore space of RV (fraction) Sg = the gas saturation within the above pore space as a fraction of the total pore space ρ_{CO2} = the density of CO_2 at the temperature and pressure at the given reservoir depth (M/L^3) E= MAS reservoir storage efficiency factor, calculated for each reservoir

DOE	USGS	CGSS
Saline formations	**Storage Formation Residual Trapping**	**Permeable Formation Residual Trapping**
	SF_{PV} = pore volume of the storage formation (L^3) B_{PV} = pore volume of the storage formation (L^3)	assuming a generic migrating plume thickness = 15 meters
	3) Three rock classes or 'injectivity category allotments', $R1_{PV}$, $R2_{PV}$, and $R3_{PV}$, depending on permeability (as presented in Table X) are defined 4) Residual storage resource for each rock class $R_{SR} = R_{PV} R_{SE} \rho_{CO2}$ R_{SR} = the residual trapping storage resource (M) R_{PV} = the residual trapping pore volume ((L^3)	

DOE	USGS	CGSS
Saline formations	**Storage Formation Residual Trapping**	**Permeable Formation Residual Trapping**
	R_{SE} = the residual trapping storage efficiency (fraction) ρ_{CO2std} = density of CO_2 evaluated at formation pressure and temperature (M/L^3)	

Table 2.7. Comparison of storage efficiency factors applied by the DOE, USGS, and CCGS methodologies.

	DOE	USGS	CGSS
Storage efficiency	**Oil and gas fields**	**Storage Formation Buoyant trapping**	**NA**
	formation specific efficiency for the given field	10-60% formation specific efficiency, based on oil recovery factor for the given field	-
Storage efficiency	**Saline formations**	**Storage Formation Residual trapping**	**Permeable Formation Residual trapping**
	0.4-5.5 %	1 - 7% for Rock class I 1 - 15% for Rock class II 0 - 7% for Rock class III	0.10 - 0.15%

2.8. Conclusions

Prior efforts to assess CO_2 storage resource used an array of approaches and methodologies, employing data sets of variable size and quality and resulting in a broad range of estimates with a high degree of uncertainty. Through its Regional Carbon Sequestration Partnership Program, the DOE developed standards for CO_2 storage resource estimation in oil and gas fields and deep saline formations for producing a Carbon Sequestration Atlas of the United States and Canada. In parallel, the USGS generated a report that provides a coherent set of methods for estimating CO_2 sequestration resource in storage formations including buoyant and residual trapping. In addition, the CGSS recommended a methodology for assessing CO_2 storage resource in basin-scale porous reservoirs, which was utilized in the 2009 Queensland CO_2 Geological Storage Atlas. A concise comparison of these methodologies is provided in Table 2.8.

Based on our analyses, these methodologies are similar in terms of computational formulation. Specifically, the explored methodologies use static volumetric methods to calculate CO_2 storage resource in open systems and are applicable at either regional or basin-scale levels. The methodologies, however, are not intended for site screening and selection. Siting of specific CCS facilities requires estimates of storage resource capacity for candidate formations, based on numerical modeling that takes into consideration the site-specific CO_2 injection rates, reservoir properties, and dynamics of the CO_2 plume.

We find that each of the proposed methodologies is science- and engineering-based. As such, they are important in identifying the geographical distribution of CO_2 storage resource and regional carbon sequestration potential at the national and basin-scale levels for use in energy-related government policy and business decisions. Policy makers need these high level estimates

Table 2. 8. Comparison at a glance: side-by-side appraisal of the DOE, USGS, and CCGS methodologies in terms of regional setting, trapping mechanisms, equations/methods, consistency with the resource-reserve pyramid concept, and uncertainty.

	DOE	USGS	CGSS
Regional setting	Sedimentary basins	Sedimentary basins subdivided into storage assessment units (SAUs) that contain storage formations (SFs)	Sedimentary basins
Trapping mechanism	Structural and stratigraphic trapping for oil and gas fields Residual trapping for saline formations	Buoyant trapping (structural and stratigraphic) within SFs Residual trapping within SFs	Residual trapping through migration assisted storage (MAS) trapping
Equations/ methods	Volumetric	Volumetric	Volumetric
Resource-reserve pyramid concept	Consistent	Consistent	Not specified
Dealing with uncertainty	Probabilistic in terms of storage efficiency	Probabilistic	Deterministic

to evaluate the prospective role that CCS technologies can play in reducing nation's or region's CO_2 emissions over long term. The value of these high level assessments of CO_2 storage resource is to help inform decision makers in governments and industry as to whether CCS is a climate mitigation option worth pursuing in particular regions.

References

(1) Metz, B., O. Davidson, H. De Coninck, M. Loos, and L. Meyer (eds), 2005, IPCC Special Report on Carbon Dioxide Capture and Storage, p. 431: http://www.ipcc.ch/pdf/special-reports/srccs/srccs_wholereport.pdf (accessed June 24, 2011).

(2) van der Meer, L.G.H., 1992, Investigation regarding the storage of carbon dioxide in aquifers in the Netherlands: Energy Conversion and Management, v. 33, no. 5-8, p. 611-618.

(3) Bergman, P.D., and E. M. Winter, 1995, Disposal of carbon dioxide in aquifers in the US: Energy - Conversion and Management, v. 36, no. 6-9, p. 523-526.

(4) Dilmore, R., D. E. Allen, R. J. Jones, W. Sheila, S. Hedges, and Y. Soong, 2008, Sequestration of dissolved CO_2 in the Oriskany formation: Environmental Science & Technology, v. 42, no. 8, p. 2760-2766.

(5) National Energy Technology Laboratory (NETL), 2006, Carbon Sequestration Atlas of the United States and Canada, US Department of Energy (DOE) publication: Pittsburgh, PA, 136 p.

(6) NETL, 2008, Carbon Sequestration Atlas of the United States and Canada, Second edition, US DOE publication: Pittsburgh, PA, 140 p.

(7) NETL, 2010, Carbon Sequestration Atlas of the United States and Canada., Third Edition, US DOE publication: Pittsburgh, PA, 159 p.: http://www.netl.doe.gov/technologies/carbon_seq/refshelf/atlas/ (accessed June 24, 2011).

(8) Bradshaw, J., G. Allinson, B. E. Bradshaw, V. Nguyen, A. J. Rigg, L. Spencer, and P. Wilson, 2004, Australia's CO_2 geological storage potential and matching of emissions sinks: Energy, v. 29, no. 9-10, p. 1623-1631.

(9) Bradshaw, B.E., L.K. Spencer, A.C. Lahtinen, K. Khider, D.J. Ryan, J.B. Colwell, A. Chirinos, and J. Bradshaw, 2009, Queensland carbon dioxide geological storage atlas. Compiled by Greenhouse Gas Storage Solutions on behalf of Queensland Department of Employment, Economic Development and Innovation: http://mines.industry.qld.gov.au/geoscience/carbon-dioxide-storage-atlas.htm (accessed June 24, 2011).

(10) Burruss, R.C., S.T. Brennan, L.F. Ruppert, M.D. Merrill, and P.O. Freeman, 2009, Development of a probabilistic assessment methodology for evaluation of carbon dioxide storage: U.S. Geological Survey Open-File Report 2009–1035, 81 p.: http://pubs.usgs.gov/of/2009/1035/ (accessed June 24, 2011).

(11) Michael, K., M. Arnot, P. Cook, J. Ennis-King, R. Funnel, J. Kaldi, D. Kirste, and L. Paterson, 2009[a], CO_2 storage in saline aquifers I: Current state of scientific knowledge: Energy Procedia, v. 1, no. 1, p. 3197-3204.

(12) Michael, K., G. Allinson, A. Golab, S Sharma, and V. Shulakova, 2009 [b], CO_2 storage in saline aquifers II: Experience from existing storage operations. Energy Procedia, v. 1, no. 1, p. 1973-1980.

(13) Brennan, S.T., R.C. Burruss, M.D. Merrill, P.O. Freeman, and L.F. Ruppert, 2010, A probabilistic assessment methodology for the evaluation of geologic carbon dioxide storage: U.S. Geological Survey Open-File Report 2010–1127, 31 p., http://pubs.usgs.gov/of/2010/1127 (accessed June 24, 2011).

(14) Goodman, A., A. Hakala, G. Bromhal, D. Deel , T. Rodosta, S. Frailey , M. J. Small, D. Allen, V. Romanov, J. Fazio, N. Huerta, D. McIntyre, B. Kutchko, and G. Guthrie, 2011, U.S. DOE methodology for development of geologic storage potential for carbon dioxide at the national and regional scale: International Journal of Greenhouse Gas Control, v. 5, no. 4, p. 952–965: http://www.sciencedirect.com/science/article/pii/S1750583611000405 (accessed June 24, 2011).

(15) Alley, R., T. N.L. Berntsen, Z. Bindoff, A. Chen, and A. Chidthaisong, 2007, Climate Change 2007: the physical science basis: Summary for policymakers, Working Group 1, Intergovernmental Panel on Climate Change., 18 p.: http://www.ipcc.ch/pdf/assessment-report/ar4/wg1/ar4-wg1-spm.pdf (accessed June 24, 2011).

(16) van der Meer, L.G.H., and P.J.P. Egberts, 2008, A general method for calculating subsurface CO_2 storage capacity: Offshore Technology Conference, Houston, Texas, p. 887–895.

(17) Dooley, J. J., 2010, Valuing national and basin level geologic CO_2 storage capacity assessments in a broader context: International Journal of Greenhouse Gas Control, v. 5, no. 1, p. 177-178.

(18) Szulczewski, M. L., C. W. MacMinn, H. J. Herzog, and R. Juanes, 2012, Lifetime of carbon capture and storage as a climate-change mitigation technology: Proceedings of the National Academy of Sciences of the U.S.A., v. 109, no. 14, p. 5185-5189.

(19) McKelvey, V. E., 1972, Mineral resource estimates and public policy, American Scientist, v. 60, no. 1, p. 32-39.

(20) Bradshaw, J., and S. Bachu, 2007, CO_2 storage capacity estimation: Issues and development of standards: International Journal of Greenhouse Gas Control, v. 1, no. 1, p. 62-68.

(21) Dullien, F.A.L., 1992, Porous media: fluid transport and pore structure: San Diego, Academic Press Inc., 351 p.

(22) Bennion, D.B., and S. Bachu, 2006, Supercritical CO_2 and H_2S–brine drainage and imbibition relative permeability relationships for intergranular sandstone and carbonate formations: Proceedings of Society of Petroleum Engineers, European Association of Geoscientists & Engineers Annual Conference and Exhibition, p. 1-13, doi: 10.2523/99326-MS.

(23) Burton, M., N. Kumar, and S.L. Bryant, 2009, CO_2 injectivity into brine aquifers: Why relative permeability matters as much as absolute permeability: Energy Procedia, v.1, no. 1, p. 3091-3098.

(24) Bachu, S., 2008, CO_2 storage in geological media: Role, means, status and barriers to deployment: Progress in Energy and Combustion Science, v. 34. no. 2, p. 254-273.

(25) Bachu, S., 2003, Screening and ranking of sedimentary basins for sequestration of CO_2 in geological media in response to climate change: Environmental Geology, v. 44, p. 277-289.

(26) Bachu, S., D. Bonijoly, J. Bradshaw, R. Burruss, S. Holloway, N. P. Christensen, and O.M. Mathiassen, 2007, CO_2 storage capacity estimation: methodology and gaps: International Journal of Greenhouse Gas Control, v.1, no. 4, p. 430-443.

(27) Frailey, S. M., 2009, Methods for Estimating CO_2 Storage in Saline Reservoirs: Energy Procedia, v. 1, no.1, p. 2769-2776: http://www.sciencedirect.com/science/article/pii/S1876610209006912 (accessed June 24, 2011).

(28) Frailey, S. M., and R. J. Finley, 2009, Classification of CO_2 geologic storage: Resource and capacity: Energy Procedia, v. 1, no.1, p. 2623-2630.

(29) Dahowski, R., Li, X., Davidson, C., Wei, N., Dooley, J., 2009, Regional Opportunities for Carbon Dioxide Capture and Storage in China: A Comprehensive CO2 Storage Cost Curve and Analysis of the Potential for Large Scale Carbon Dioxide Capture and Storage in the People's Republic of China: Pacific Northwest National Laboratory, Richland, WA, 85 p.: http://energyenvironment.pnnl.gov/pdf/roccs_china_pnnl_19091.pdf (accessed June 24, 2011).

(30) Nordbotten J. M., M. A. Celia, and S. Bachu, 2005, Injection and storage of CO_2 in deep saline aquifers: Analytical solution for CO_2 plume evolution during injection: Transport in Porous Media, v. 58, no. 3, p. 339-360.

(31) Dentz, M., and D. M. Tartakovsky, 2009, Abrupt-interface solution for carbon dioxide injection into porous media: Transport in Porous Media, v. 79, no. 1, p. 15-27: http://www.springerlink.com/content/t336247w7p2462q2/fulltext.pdf (accessed June 24, 2011).

(32) Szulczewski, M. L., and R. Juanes, 2009, A simple but rigorous model for calculating CO_2 storage capacity in deep saline aquifers at the basin scale: Energy Procedia, v. 1, no.1, p. 3307-3314.

(33) Zhou, J. T. Birkholzer, C. Tsang, and J. Rutqvist, 2008, A method for quick assessment of CO_2 storage capacity in closed and semi-closed saline formations: International Journal of Greenhouse Gas Control, v. 2, no. 4, p. 626-639.

(34) Mathias, S. A., and P. E. Hardisty, 2009, Screening and selection of sites for CO_2 sequestration based on pressure buildup: International Journal of Greenhouse Gas Control, v. 3, no. 5, p. 577-585.

(35) CCSReg Project, Carnegie Mellon University, 2009, Carbon Capture and Sequestration: Framing the issues for regulation, 162 p.: http://www.ccsreg.org/pdf/CCSReg_3_9.pdf (accessed June 24, 2011).

(36) CCSReg Project, Carnegie Mellon University, 2010, Policy brief: Carbon dioxide accounting in Carbon Capture and Sequestration, 17 p.: http://www.ccsreg.org/pdf/GHG%20Accounting%20Policy%20Brief_01042010.pdf (accessed June 24, 2011).

(37) Ghaderi, S. M., and D. W. Keith, 2009, Feasibility of Injecting Large Volumes of CO_2 into Aquifers: Energy Procedia, v. 1, no.1, p. 3113-3120.

(38) McCoy, S. T., and E. S. Rubin, 2009, Variability and uncertainty in the cost of saline formation storage: Energy Procedia, v. 1, no. 1, p. 4151-4158.

(39) Gresham, R.L., S.T. McCoy, J. Apt, and M.G. Morgan, 2010, Implications of Compensating Property-Owners for Geologic Sequestration of CO_2: Environmental Science & Technology, v. 44, no.8, p. 2897-2903.

(40) Department of Interior (DOI), 2008, Inventory of onshore federal oil and natural gas resources and restrictions to their development, Phase III Inventory – Onshore United States: http://www.blm.gov/wo/st/en/prog/energy/oil_and_gas/EPCA_III.html (accessed June 24, 2011).

(41) Spencer, L.K., J. Bradshaw, B.E. Bradshaw, A. L. Lahtinen, and A. Chirinos, 2011, Regional storage capacity estimates: Prospectivity not statistics: Energy Procedia, v. 4, p. 4857-4864: http://www.sciencedirect.com/science/article/pii/S1876610211007326 (accessed June 24, 2011).

(42) Environmental Protection Agency (EPA), 2009, Safe Drinking Water Act (SDWA): http://www.epa.gov/ogwdw/sdwa/index.html (accessed June 24, 2011).

(43) EPA, 2011, Draft underground injection control (UIC) program class VI primacy application and implementation manual: http://water.epa.gov/type/groundwater/uic/class6/upload/primacy_application_and_impl_manual_508_compliant.pdf (accessed June 24, 2011).

(44) International Energy Agency Greenhouse Gas R&D Programme (IEAGHG), 2009, Development of storage coefficients for CO_2 storage in deep saline formations, IEAGHG publication 2009/13: Cheltenham, UK, 38 p.

(45) Gorecki, C.D, J.A. Sorensen, J.M. Bremer, D.J. Knudsen, S.A. Smith, E.N. Steadman, and J.A. Harju, 2009, Development of storage coefficients for determining the effective CO_2 storage resource in deep saline formations: Society of Petroleum Engineers (SPE) International Conference on CO_2 Capture, Storage, and Utilization , San Diego, CA Proceedings: SPA no. 126444, 12 p.

(46) Kopp, A., H. Class, and R. Helmig, 2009[a], Investigations on CO_2 storage capacity in saline aquifers Part 1: Dimensional analysis of flow processes and reservoir characteristics: International Journal of Greenhouse Gas Control, v. 3, p. 263–276.

(47) Kopp, A., H. Class, and R. Helmig, 2009[b], Investigations on CO_2 storage capacity in saline aquifers Part 2: Estimation of storage capacity coefficient: International Journal of Greenhouse Gas Control, v. 3, p. 277–287.

(48) Holtz, M.H., 2003, Optimization of CO_2 sequestered as a residual phase in brine-saturated formations: Second Annual Conference on Carbon Sequestration: developing & validating the technology base to reduce carbon intensity, Gulf Cost Carbon Center (GCCC) Digital Publication Series: Alexandria, Virginia: http://www.beg.utexas.edu/gccc/bookshelf/Final%20Papers/03-03-Final.pdf (accessed June 24, 2011).

(49) Juanes, R., E. J. Spiteri, F. M. Orr Jr., and M. J. Blunt, 2006, Impact of relative permeability hysteresis on geological CO_2 storage: Water Resource Research, v. 42, p.1-13: http://webpages.fc.ul.pt/~fbarriga/ZeroEm/Bibliografia_files/Juanes%2Bal_2006_WaterResourcesRes_7479721.pdf (accessed June 24, 2011).

Chapter 3. Spatial Stochastic Modeling of Sedimentary Formations to Assess CO_2 Storage Potential. A Case Study for the Oriskany Formation of the Appalachian Basin.[2]

3.1 Introduction

With greenhouse gas mitigation expected to become a higher priority and a rapid widespread adoption of alternative generation technologies such as renewables (e.g., wind, solar) and nuclear being costly and difficult, coal- and gas-fired power plants with CCS could play an important role in satisfying U.S. electricity demand in the coming decades. In particular, natural gas fired-power generation equipped with CCS may play an important role in a future where production from shale gas resources keeps gas prices relatively low. This Thesis focuses on storage resources in deep saline formations that are found in sedimentary basins worldwide and believed to offer the largest CO_2 storage capacity (1-3). If CCS is to be used widely, accurate and clearly understandable assessments of carbon storage potential are needed to help governments and industry plan for its deployment (4-7).

Estimating the CO_2 storage resource at a basin-scale level is commonly performed using a geologic model (geomodel) of the prospective storage formation (8-12). However, the data needed to produce a detailed geomodel are usually lacking. Instead, generalized geomodels are constructed in which a storage formation is assumed homogeneous without consideration of natural facial change or depositional zone distribution. As such, the inherent heterogeneity of geophysical properties is not explicitly characterized in basin-scale models (13, 14). A sufficient

[2] Much of this text is accepted for publication in the Environmental Science and Technology journal. The full reference is as follows: Popova, O., Small, M.J., McCoy, S.T., Thomas, A.C., Rose, S., Karimi, B., Carter, K., Goodman, A., Spatial stochastic modeling of sedimentary formations to assess CO_2 storage potential: Case study for the Appalachian basin, 2014. Environmental Science and Technology Journal (accepted for publication pending revision).

representation of a formation as a complex natural system, using available data and geomodels helps increase the accuracy of storage estimates and informs a cost-effective strategy for further data collection. It is essential to characterize not only reservoir properties that are highly formation specific and depend on the geology, stratigraphy, and tectonics of a sedimentary basin, but also to understand the adequacy of such models for representing the spatial distribution of natural system parameters. Computational methods for sequestration resource assessment should take into account the full range of parameter values and their joint distribution across the targeted formations.

Estimates of the carbon sequestration resources that have been made for North America using existing methodologies likely underestimate the uncertainty and variability in formation parameters. These methodologies use average values of formation parameters (e.g., the DOE method, with the exception of storage efficiency), or probability distributions of formation parameters based on minimum and maximum values established for a given sedimentary basin (15-19). However, these approaches do not account for the spatial variability in reservoir parameters.

In this Thesis, a spatial stochastic approach is used to assess CO_2 residual trapping storage resources on a regional level. This method characterizes the uncertainty distribution of the storage resource over the formation area, while other methods typically provide only a single value (e.g., mean or mode) or in some cases upper and lower bounds for the estimates (15-19). For modeling spatial variability in input parameters and the resulting uncertainty in predictions we employ the Sequential Gaussian Simulation technique. The spatial stochastic model is an extension of ordinary kriging where, instead of a single best estimate for system variables in each grid cell, multiple spatial realizations are simulated. This approach allows for estimation of the

CO_2 sequestration resource of a storage formation with subsequent parameter sensitivity and prediction uncertainty analysis. The model integrates basin-specific data with a probabilistic approach, is computationally efficient, and suitable for the uncertainty analysis in settings where data are limited. Since the model is flexible with respect to changing input parameters and assumptions it can be parameterized to calculate the CO_2 storage resource of any porous subsurface unit.

The model is applied here to a regional case study of the Oriskany Formation of the Appalachian sedimentary basin. The Appalachian region, a major producer of both conventional and unconventional petroleum hydrocarbons, includes Pennsylvania, Ohio, West Virginia, and Eastern Kentucky, which together generate approximately 764 Mt CO_2 /year from fossil fuel combustion (20). More than a half of the annual CO_2 emissions in the region, or about 431Mt CO_2/year, are linked to stationary sources, such as fossil - fuel power plants, steel mills, refineries, cement plants, chemical plants, and gas processing plants (15, 16). Gas- and coal-fired power plants account for the 84% of the region's CO_2 stationary source emissions (15, 16). The Appalachian basin contains a number of permeable formations, including the Oriskany Formation, capable of sequestrating CO_2 (See Appendix A, Figure 1). This combination of large stationary sources and potential CO_2 geological sinks makes this region particularly attractive for CCS technology deployment. For this reason, we need reliable estimates of the size of the available CO_2 underground storage in the area. This application of the model shows the effects of the variability of input parameters on the carbon storage resource. Additionally, this study identifies ways to reduce uncertainty in storage estimates.

In the remainder of this chapter, the proposed model is introduced, followed by the results of its application, discussions, and conclusions. Appendices A and B contain information on the

Oriskany Formation geological setting and details of CO_2 storage resource simulations using the efficiency factor, respectively.

3.2. Materials and Methods

A geostatistical model for the Oriskany Formation is constructed using four separate datasets provided by BTGS. These datasets contain records from wells installed in the Appalachian basin by different industry operators, including depth and thickness measurements from 4,810 development wells in the study area; neutron porosity log readings from 194 wells; and bottom-hole temperature and shut-in pressure measurements from 3,970 and 5,744 wells, correspondingly. The well locations are shown in Figure 3.1. The formation geostatistical model is created based on the Stratigraphic Schema of the Central part of the Appalachian Basin developed in previous studies (21-24). A schematic cross section though the Appalachian Basin is presented in Appendix A, Figure 2).

The Appalachian basin bounded by the Allegheny front to the southeast and the Cincinnati arch to the northwest was formed in response to the Alleghanian orogenic event (25, 26). A map showing the paleogeography of the Appalachian basin area during the Middle Devonian period is provided in Appendix A, Figure 1. Major causes of subsidence during the Paleozoic era were related to tectonic flexure of the lithosphere and sediment loading associated with the rejuvenation of the Appalachian foreland basin (27, 28).

The well-studied Lower Devonian Oriskany Formation of the Appalachian Basin is an eastward and southeastward thickening wedge of shallow marine sandstone and is exposed in Northeast-trending folds in the Valley and Ridge province of the central Appalachians (29-32). The

Oriskany typically unconformably overlies the Helderberg Limestone or analogous strata, and is overlain by Bois Blanc Formation, Onondaga Limestone, Huntersville Chert, or Needmore Shale (23, 29, 33). Further details on the Oriskany depositional history and stratigraphy, including a regional geological cross-section are provided in Appendix A.

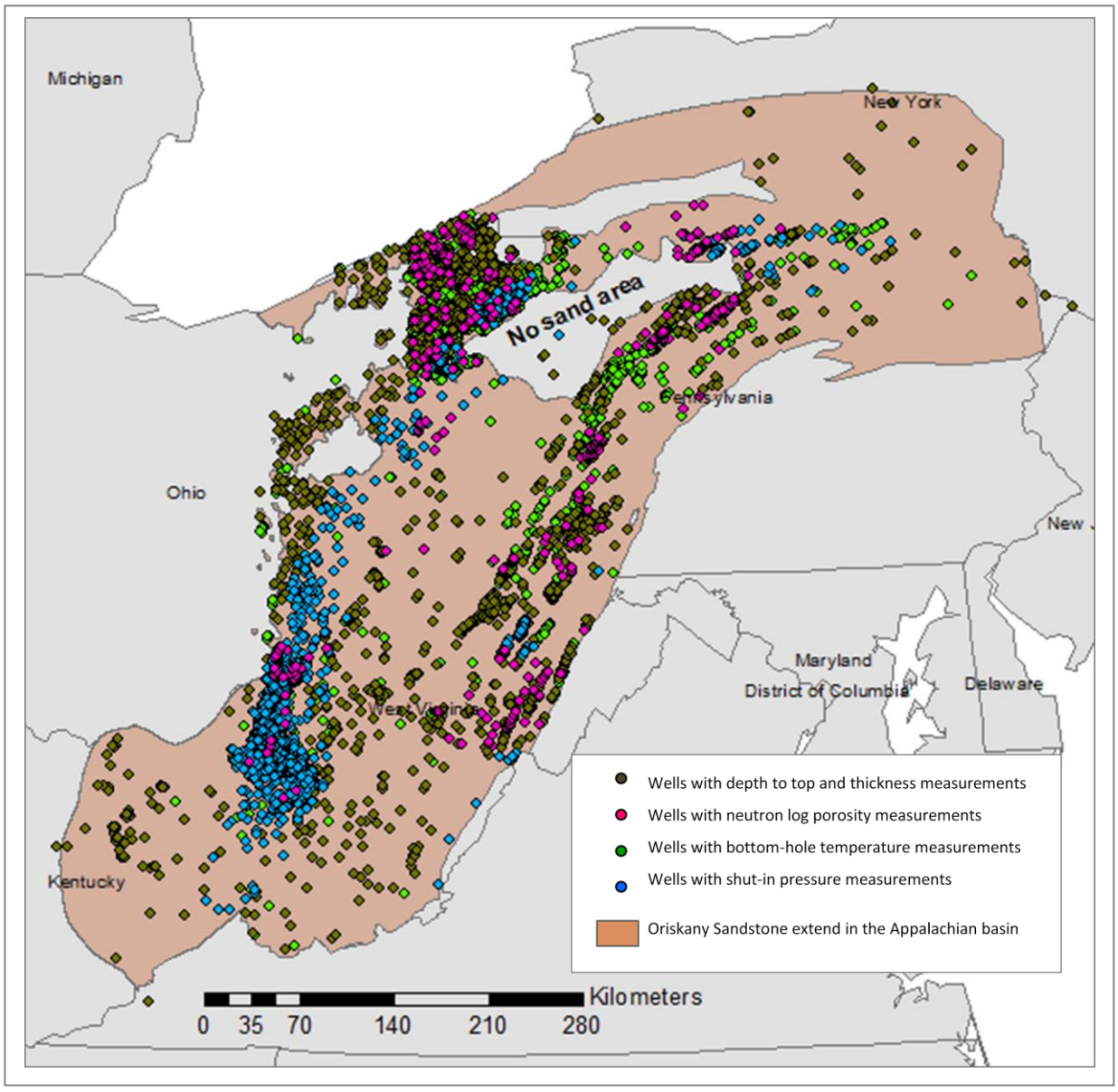

Figure 3.1. Well locations and area underlain by the Oriskany Formation extend in the Appalachian basin.

For CO_2 residual trapping storage resource calculation we use the volumetric method. This method is based on methods applied in the petroleum industry and similar to that used by the DOE (15, 16). The equation for the mass of CO_2 which can be stored in the formation is:

$$\boldsymbol{M = A\, h\, \varphi(d)\rho[T(d), P(d)]E} \qquad (1)$$

where M is the mass estimate of the formation CO_2 resource (M), A is the formation gross area (L^2), h is the formation gross thickness (L), φ is the formation porosity (unitless), which varies as a function of depth, ρ is the CO_2 density (M/L^3) at reservoir temperature [T(Θ)] and pressure [$P(M/LT^2)$], which are both functions of depth, and E is the storage efficiency factor (unitless) that reflects the fact that only a fraction of the total (potential) pore space volume could be filled by CO_2. In effect, E scales the total pore volume of the reservoir to the volume of CO_2 that can be trapped for long-term storage. For saline formations, the efficiency factor depends on (1) geologic parameters such as formation area, thickness, and total porosity and (2) on displacement efficiency components that reflect different physical barriers that impede CO_2 from filling 100 percent of the formation pore volume. A consensus has not yet emerged on the best and most complete methods for estimating E (8, 34-39). Since 100 percent displacement of formation fluid by CO_2 is not technically feasible due to the presence of an immobile *in situ* fluid residual and other physical constraints (8, 34-39), the storage resource estimates with the efficiency factor of 100% serve as an upper bound that establishes a plausible maximum. This total storage resource is defined as a Theoretical Storage Capacity, assuming the system‘s entire pore space is 100 percent accessible and utilized to its full capacity (40). Preliminary estimates that attempt to consider the high degree of uncertainty in the efficiency and its spatial variation are provided in Appendix B.

Worldwide saline formations meeting CCS requirements can be found at a variety of depths. By and large, in any given sedimentary basin, formation depth varies significantly due to regional tectonics and structural and/or depositional peculiarities. To estimate formation depth and thickness we use data from 4810 wells where depth to the top and bottom of the Oriskany are identified and extend these estimates using the geostatistical kriging interpolation methods described below.

To estimate rock petrophysical properties we develop a set of regression models with depth as a predictor variable. Response variables include reservoir porosity, temperature, and pressure and are predicted by linear regression using the estimates for depth from the kriging model for each well location where the dependent variables are measured. To characterize the spatial distribution of error terms for each regression model we perform kriging on the regression residuals determined for the observation wells.

As is appropriate for a dependent variable with values constrained between zero and one, we implement a variable transformation, here a logit transform (LT) for porosity:

$$\mathbf{F} = \boldsymbol{ln}\left[\frac{\boldsymbol{\varphi}}{\mathbf{1}-\boldsymbol{\varphi}}\right] \qquad (3)$$

When the LT transform variable, F, is normally distributed, the porosity, φ, is said to follow a logistic (or log-odds) normal distribution. Once the fitted value of F is predicted from its regression equation on depth, it is transformed back to the corresponding value of φ using the inversion of equation (3):

$$\boldsymbol{\varphi} = \frac{\mathbf{1}}{\mathbf{1}+\boldsymbol{e}^{-Y}} \qquad (4)$$

The density of CO_2 is calculated as a function of the formation temperature and pressure based on a cubic Equation of State (EOS) with Peng-Robinson coefficients (41). Based on a

comparative analysis of seven EOS developed by different researchers, McCoy demonstrated that the coefficients proposed by Peng and Robinson generate estimates of physical properties for pure CO_2 with the lowest relative error across a range of conditions similar to those encountered in geologic storage (42). The Peng and Robison EOS is implemented in a Matlab application employing an algorithm developed by Serna (43).

3.2.1. Kriging Analysis and Sequential Gaussian Simulation

For modeling spatial variability in input parameters including depth, thickness, and respective residuals for LT porosity, temperature, and pressure regression models we employ the method of kriging with Sequential Gaussian Simulation (SGS). The SGS is routinely used by the petroleum industry as a part of off-the-shelf software packages for reservoir modeling[44, 45]. SGS is a means for generating multiple equally probable realizations of a variable, rather than simply estimating the mean. The underlying algorithm of SGS is ordinary kriging. Since kriging is based on a local average, the predictions it produces are smoothed and averaged. SGS identifies the underlying variability and uncertainty still present, given the data used, to predict the multiple kriging results. Multiple realizations produce a more complete representation of the formation heterogeneity and allows for a fully-informed quantification of uncertainty.

Since SGS assumes a Gaussian random field, the conditional cumulative density function is completely characterized by its mean and variance-covariance matrix (46). In the SGS process, simulation is performed upon the Gaussian transformation of the observed data and each realization is conditional on the observed data and all previous realizations (47-51). The value at one location is simulated from the normal distribution function defined by the kriging mean and the variance-covariance matrix based on neighborhood values. In addition to the conditioning data, SGS characterizes the spatial covariance structure in terms of a variogram. In our analysis

variograms are fitted to the observed depth and thickness, and to the respective residuals of the LT porosity, temperature, and pressure vs. depth relationships. Finally, the simulated normal values are transformed back into their original units. This process is repeated for multiple realizations (e.g., n=1000), yielding many interpolated surfaces, all of which are consistent with the spatial characteristics found in the observed data. Aggregation of these surfaces provides a joint distribution of model inputs (and computed model outputs) for each location in the study area. This joint distribution is the basis for the uncertainty and risk analysis.

The key steps for calculating the CO_2 residual trapping storage resource in a saline formation are summarized as follows:

1) Input well data into Matlab and generate a grid

2) Fit variograms for depth and thickness

3) Simulate depth in each grid cell (Use SGS for realization i=1, … n on depth kriging; the grid cell size is 5 by 5 km)[3]

4) Simulate thickness in each grid cell (SGS on thickness kriging)

5) Regress LT Porosity, T, and P vs. depth and calculate regression residuals at each observation point

6) Fit variograms for residuals of LT Porosity, T, and P

[3] Although the fitted pressure gradient yields *in situ* pressure below the supercritical threshold at a depth of 800 m (the typical cutoff value chosen to assure preinjection pressures above the supercritical threshold when a formation exhibits a standard hydrostatic pressure gradient), it is assumed that the CO_2 injection in combination with the preinjection pressure field maintains a total pressure above the supercritical threshold at the depth of 800 m and below. Cells with estimated depth less than 800 m are thus excluded from the consequent storage resource calculations.

7) Generate LT Porosity, T, and P residuals in each grid cell (SGS on residual kriging)

8) Calculate LT Porosity, T, and Pressure in each grid cell using estimated depth in the respective regression equations

9) Compute porosity (inverse equation (4) for logit transform) for each grid cell

10) Compute the CO_2 density in each cell based on estimated T and P using the Peng-Robinson EOS

11) Compute the CO_2 mass (equation 1) for each grid cell

12) Sum over the grid cells in the formation

3.3. Results

3.3.1. Regression Models

Three separate linear regression equations were fit to LT porosity, bottom-hole temperature (BHT)[4] and final shut-in pressure as a function of depth, with the following form and parameters:

$$\mathbf{Y = a + b \cdot d + \varepsilon} \qquad (5)$$

where *Y* is the dependent variable (LT porosity, dimensionless; temperature, Kelvin; and pressure, Mega Pascal), *d* is the depth to the top of a formation (meters), and ε *is* a residual error. The error is assumed to be a normally distributed random variable with mean zero and a fitted

[4] This is a common practice in the petroleum industry to obtain temperature measurements only from a few control points, usually at the bottom of a well, from which to estimate the temperature profile of the entire sedimentary section. Bottom-hole temperature measured at the well bore may not reflect a true equilibrium temperature owing to differences between the temperature of the rock and that of the circulating fluid. Since data on recorded temperature derived from formation testing are unavailable (equilibrium temperature and fluid temperature), we do not apply an equilibrium correction to bottom-hole temperature [51]. The geothermal gradient is calculated from the observed BHT data applying surface temperature constraint [52].

variance that is independent of value of *Y*. In the case of temperature, the intercept is assigned a value of 282.47 K, consistent with the average annual surface temperature for the Appalachian Region (54), and only the slope is determined in the regression analysis.

The estimated values of the regression parameters are summarized in Table 3.1, and the fitted relationships are compared to the observed data in Figure 3.2. While the fitted parameters are all statistically significant at a high level of confidence (95% confidence interval does not include zero), the residual error terms exhibit high standard deviations, indicating a high degree of spatial variability in formation properties at a given depth. As described below, to account for the spatial correlation in the relationship residuals, the residuals are fitted using kriging methods in a geostatistical model, simulated over multiple realizations, and added to the respective predicted property values using the appropriate regression equation evaluated at the simulated values of depth in each spatial grid cell.

Table 3. 1. Estimated intercepts, slope coefficients, and residual errors for LT of porosity, Temperature, and Pressure (as a function of depth), respective regression models for the Oriskany Formation.

Formation Parameter		Overall Model Fit R-squared (number of observations)	Parameter Estimate Intercept (Standard Error)	 Slope (Standard Error)	Residual Error
Logit transform of Porosity	$L_{g\phi}$	**$R^2_{Lg\phi}$ = 0.180 (n = 194)**	**$a_{Lg\phi}$ = -2.4814 (.12909)**	**$b_{Lg\phi}$ = -0.00049 (.000077)**	**$\sigma_{\varepsilon Lg\phi}$ = 0.721**
Temperature	T	**R^2_T = 0.970 (n = 3970)**	**$a_T \equiv$ 282.47 (--)**	**b_T= 0.0206 (.000055)**	**σ_{ε_T} = 4.985**
Pressure[5]	P	**R^2_P = 0.6983 (n = 5744)**	**a_P = 2.03 0.0404)**	**b_P = 0.0033 (.000029)**	**σ_{ε_P} = 1.023**

[5] The regression analysis for pressure vs. depth was repeated with a) the intercept set to zero; and (b) the intercept set to 0.101325MPa (the standard absolute pressure). The maximum difference in predicted pressure for the observed data points (over the range of depth form 300 m to 3000 m) using these alternative regressions vs. the one indicated in Table 1 was 6 percent. This is much lower that the observed scatter of measured pressure around any of these fitted regression lines (the average percent error was 35 percent).

As indicated by the values of $b_{Lg\phi}$ (= -0.00049), b_T (= 0.0206) and b_P (= 0.0033), the porosity decreases with depth, while the temperature and pressure increase with depth. The results for temperature can be expressed in terms of T in degrees Fahrenheit and depth in feet, as follows: *T= 44.85 + 0.0121d,* which is slightly different from a geothermal gradient formula produced by the University of Texas at Austin, Bureau of Economic Geology (BEG) (55, 56) and based on data of Opritza (31) and Harper (32): *T=63+0.0092d*. Our results suggest that the geothermal gradient in the Appalachian basin ranges from 16 to 32 K/km, with a mean of 22.0±1.5 K/km.

a)

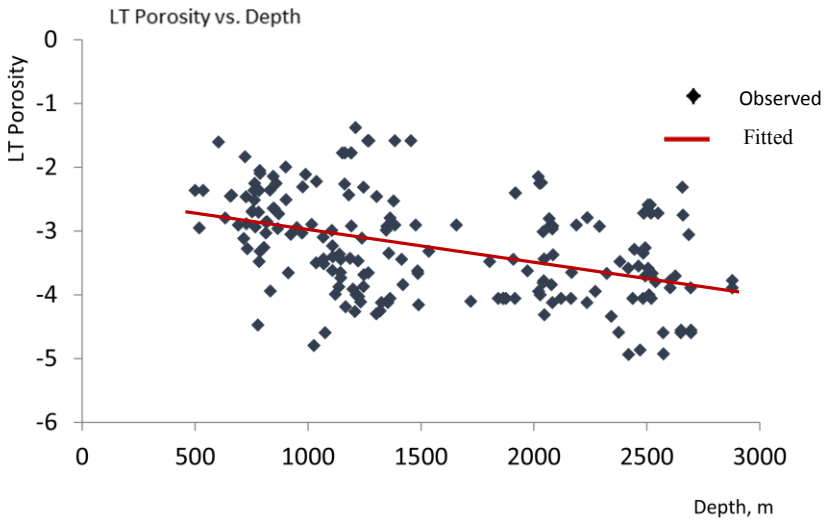

b)

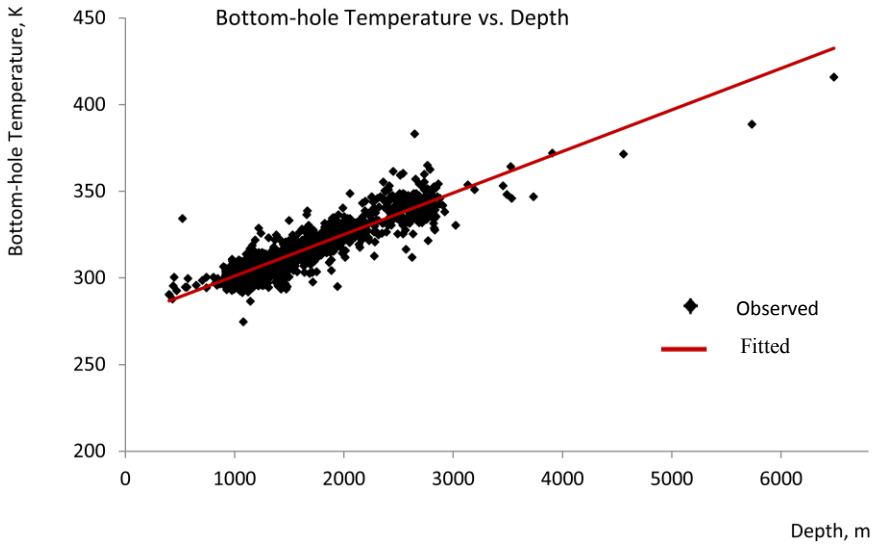

c)

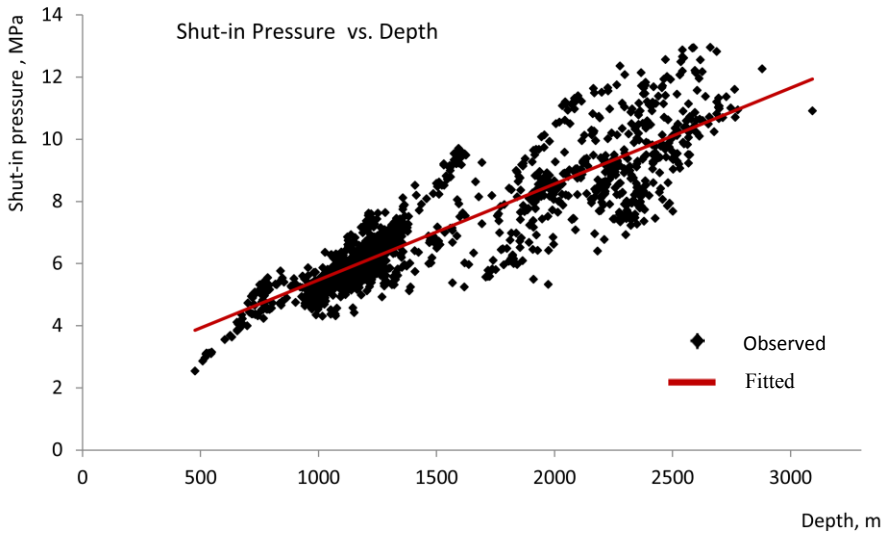

Figure 3. 2. Property - depth relationships: a) Observed and fitted Logit transform of porosity (unitless) – depth (m) relationship; b) Observed and fitted bottom-hole Temperature (K) – depth (m) relationship; and c) Observed and fitted shut-in Pressure (MPa) – depth (m) relationship for the Oriskany Formation.

The results for pressure are also consistent with expected trends and physical principles. The equation for pressure can be defined in terms of P in pounds per square inch and depth in feet (the intercept set to zero), as follows: $P = 0.21d$. Using data of Harper (32) for reservoir pressure in the Oriskany Formation, BEG determined a hydrostatic gradient as follows: $P=0.44\ d$, where P is the pressure in pounds per square inch and d is depth in feet (55, 56). Generally, formation pressures less than hydrostatic (referenced to the weight of a water column) are defined as underpressure. Considering that hydrostatic pressure gradients for freshwater and for brine with dissolved solids 100,000 mg/L (ppm) are approximately 0.00979 MPa/m (0.443 psi/ft) and 0.0105 MPa (0.465 psi/ft) respectively, the regression results indicate that the Oriskany Formation is underpressured. Our results indicate that the pressure gradient of the Oriskany Formation ranges from 3.5 to 5.9 MPa/km, with a mean of 4.7±1.2 MPa/km.

3.3.2. Variography

Experimental variograms were calculated for formation parameters including depth, thickness, and corresponding residuals for LT porosity, temperature, and pressure[6]. A relatively consistent set of best-fit model with minimum Root MSE (mean square error) values were generated by least squares model fitting of these variograms. Fitting a model equation to an experimental variogram is a trial and error process. In theory, the model selected to represent the semivariogram should begin near the origin (displaced upward by the amount of the nugget), rise smoothly to some upper limit defined as a sill, and then continue at a permanent level. The *exponential model* has these properties, though it never quite reaches the constraining value of the sill, but approaches asymptotically. Exponential models are the best-fit models for depth,

[6] LT porosity residuals, Temperature residuals, and Pressure residuals are derived from the corresponding regression models.

thickness, and respective residuals for LT porosity, temperature, and pressure with the following equation:

$$\gamma_h = (s\text{-}n)(1 - e^{-h/a}) \quad (6)$$

where γ_h is the semivariogram, h is the distance, s is the sill (variance (σ_0^2)), n is the nugget, (s-n) is the partial sill, and a is a range. Table 3.2 provides a summary of fitted model parameters for depth, thickness, and respective residuals for LT porosity, temperature, and pressure.

Table 3.2. Fitted variogram model parameters for depth, thickness, and respective residuals of LT porosity, temperature, and pressure.

Parameter	Nugget effect (unit)	Sill (unit)	Partial sill (unit)	Range (unit)
Depth	**0** (m)	**694,770** (m)	**694,766** (m)	**441,420** (m)
Thickness	**5.70** (m)	**13.72** (m)	**8.02** (m)	**15,820** (m)
LT porosity residuals	**0.3567** (unitless)	**0.5094** (unitless)	**0.1526** (unitless)	**209,250** (m)
Temperature residuals	**0.1259** (K)	**0.2076** (K)	**0.0816** (K)	**104,680** (m)
Pressure residuals	**0.0079** (Mpa)	**0.3174** (Mpa)	**0.3095** (Mpa)	**63,760** (m)

3.3.3. Storage Estimate Results

Using the regression models and the spatial stochastic tool implemented in Matlab with n=1000 SGS realizations, we calculate the CO_2 residual trapping storage resource of the Oriskany

Formation over 5 by 5 km grid with an effective efficiency factor, E ≅ 5%. Details on storage efficiency factor computation for the Oriskany Formation are provided in Appendix B.

Table 3.3. Summary statistics for the simulated CO_2 storage resource of the Oriskany Formation (over 7930 grid cells, 5 by 5 km) with efficiency factor, E ≅ 5%, using SGS, n=1000.

Statistics	Mean	St. deviation	Median	10% Percentile	90% Percentile	Min	Max	Range width
Mass of CO_2, Gt	**4.08**	**0.80**	**4.06**	**3.05**	**5.10**	**1.08**	**7.30**	**6.22**

This yields a storage estimate of 4.08 gigatonnes of CO_2. In this scenario the mass of CO_2 varies from a 10th percentile value of 3.05 gigatonnes to a 90th percentile value of 5.1 gigatonnes. Figure 3.3 shows the probability distribution function (PDF) and cumulative distribution function (CDF) of the Oriskany Formation storage resource, expressed in Gt of CO_2 with the effective efficiency factor, E ≅ 5%. This chart demonstrates that in the presence of uncertainty in formation structure and reservoir properties, the estimate of storage resource varies greatly. Not surprisingly, from the resulting distribution it is clear that the point estimate of storage resource using the mean values of the model empirical parameters is different from the mean value calculated using SGS.

As shown in Figure 3.3 the mean of the distribution (4.08 Gt) is higher than that of the storage resource determined using the mean of the input parameters (3.06 Gt). This outcome shows the importance of having better information about the values of formation geologic parameters, and that the average value of input parameters may not be sufficient to provide a precise estimate of the storage resource.

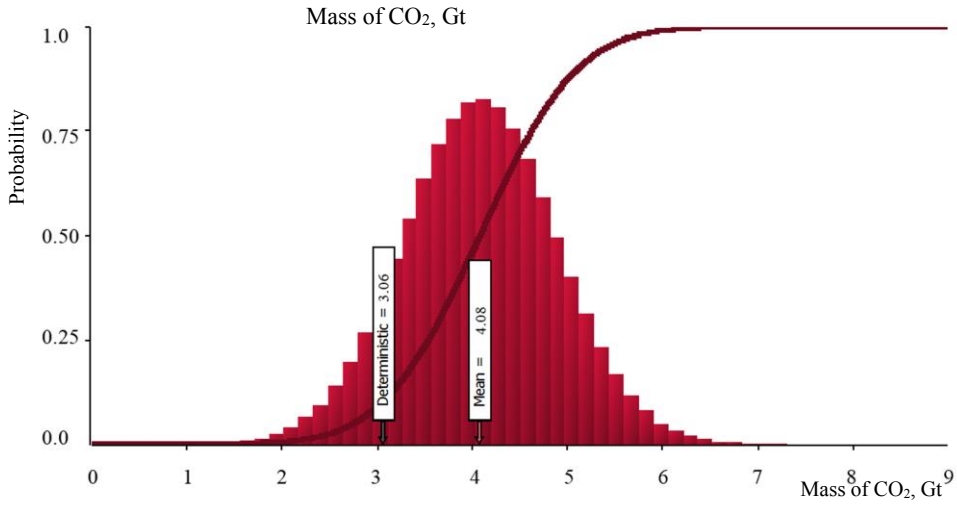

Figure 3.3 Simulated PDF (bars) and CDF (line) of the Oriskany Formation CO_2 potential storage resource (over 7930 grid cells, 5 by 5 km) with efficiency factor, E=5%, using SGS, n=1000.

The estimated spatial distribution of the potential CO_2 storage resource (E ≅ 5%) for the Oriskany Formation expressed in Kilotonnes per square kilometer and the storage resource coefficient of variation are presented in Figure 3. 4. As expected, the grid cells with the highest storage (Kt/km^2) estimates are located in the areas with the deepest occurrence of the Oriskany Formation (Figure 3.4a). The greatest relative uncertainty in the local storage resource (Figure 3.4b) occurs where the observation wells are sparse (See Figure 3.1).

a)

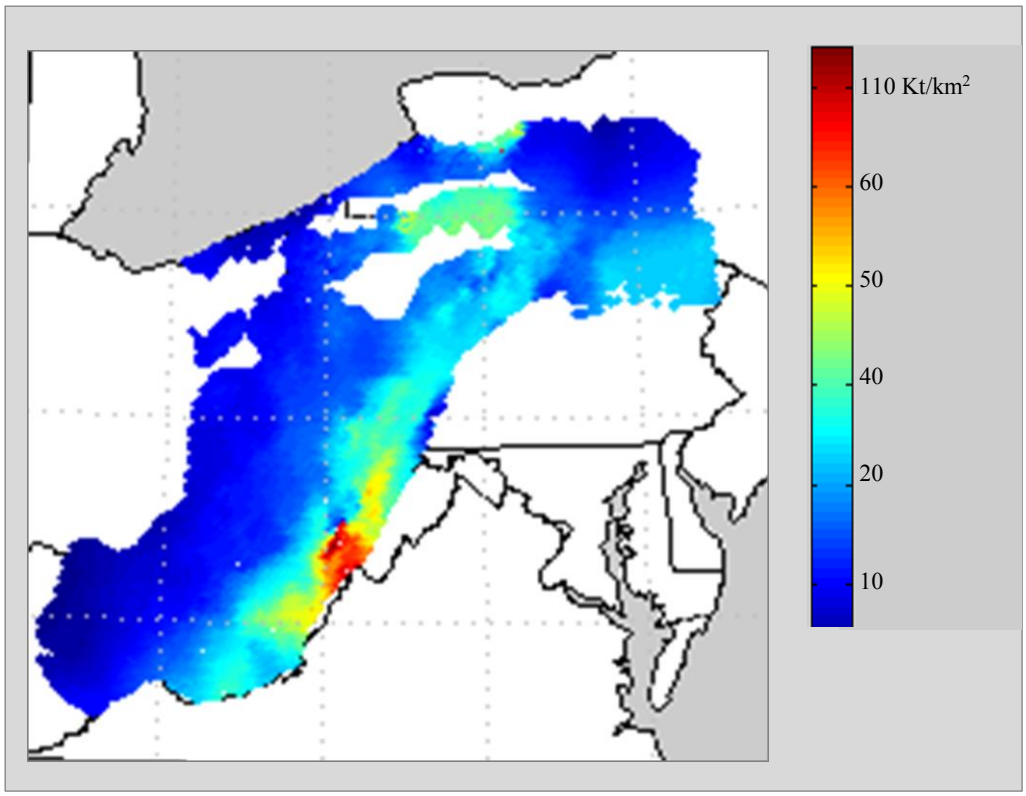

b)

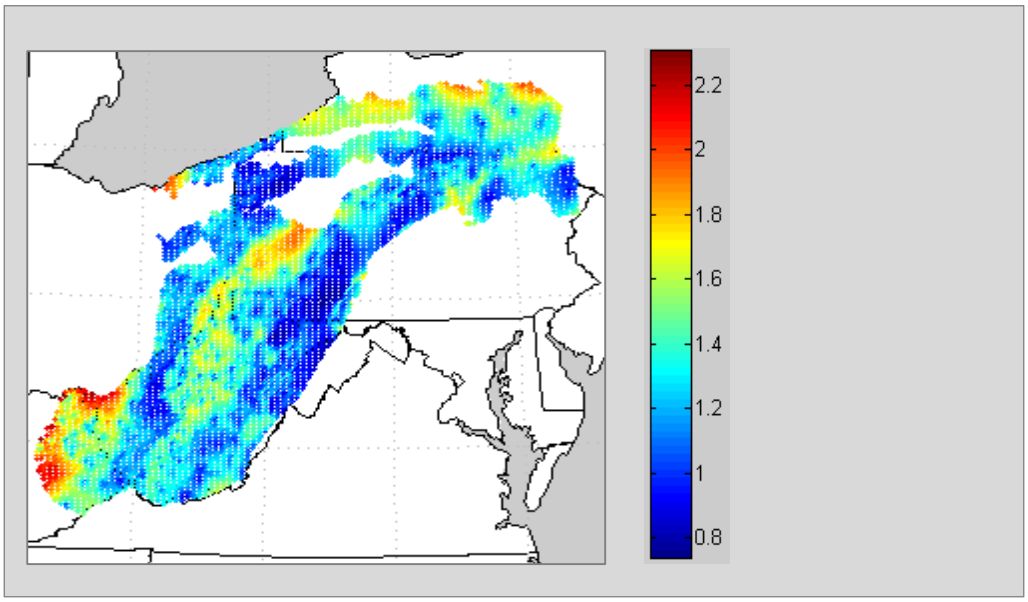

Figure 3.4. a) Estimated CO_2 storage resource (E=5%) for the Oriskany Formation expressed in Kilotonnes per square kilometer and b) Estimated CO_2 storage resource Coefficient of variation.

3.4. Discussion

The estimation variances can be useful in the selection of optimum locations for additional exploratory wells to support the estimation of the CO_2 storage resource. This method is explained in detailed in Journel and Huijbregts (48), where it is referred to as the "fictitious point method". Istok and colleagues applied this approach to reduce the estimation variance for an organic groundwater contaminant and design a cost-effective monitoring well network (57). In this method the grid point with the maximum estimation variance is identified first. This location can be regarded as the optimum location for a single additional exploratory well because, if a well was located there, the largest possible reduction in estimation variance would take place. The optimum locations of additional exploratory wells can be identified sequentially by substituting previously determined well locations into the interpolation equations, calculating new estimation variances, and identifying the grid location with the highest estimation variance (48). Thus, the information return is measured by the reduction in CO_2 storage resource uncertainty achieved. In other words, since a reduction in the uncertainty about the sequestration resource is desired, this analysis will suggest where reductions in uncertainty could be most valuable and what future studies and data collection (e.g. additional characterization wells) should be undertaken.

In this analysis we implement SGS to a geostatistical dataset to calculate the storage resource of the Oriskany Formation using effective efficiency of 5%, as the first step in estimating storage capacity. The results presented above suggest that the Oriskany Formation can hold 4.08 gigatonnes of CO_2 ($E \cong 5\%$).In that case the mass of CO_2 varies from a 10th percentile value of 3.05 gigatonnes to a 90th percentile value of 5.1 gigatonnes.

Assuming that the average CO_2 emissions of a 1 GW power plant is approximately 8 Mt per year, the Oriskany Formation can accommodate about 500 years of CO_2 emissions generated by the 1 GW power plant. However, these estimates are not actual, realizable capacity estimates, and once other constraints are taken into account, the actual storage capacity that could be realized will most likely be much lower. Thus policies promoting CCS deployment must take this uncertainty into consideration. Additionally, there are other issues that may impose further limitations, such as regulatory and economical concerns, long-term safety and security of storage sites, and public perception of the technology.

References

(1) Bachu, S., Screening and ranking of sedimentary basins for sequestration of CO_2 in geological media in response to climate change. Environmental Geology, 2003, 44, 277-289.

(2) St John, B.; Bally, A.W.; Lemma H.D., Sedimentary provinces of the world hydrocarbon productive and nonproductive. Tulsa, American Association of Petroleum Geologists Map Series, 1984.

(3) Department of Interior (DOI), Inventory of onshore federal oil and natural gas resources and restrictions to their development, Phase III Inventory – Onshore United State, 2008; http://www.blm.gov/wo/st/en/prog/energy/oil_and_gas/EPCA_III.html.

(4) Alley, R.; Berntsen, T. N.L.; Bindoff, Z.; Chen, A.; Chidthaisong, A., Climate Change 2007: the physical science basis: Summary for policymakers. Working Group 1, Intergovernmental Panel on Climate Change, 2007; http://www.ipcc.ch/pdf/assessment-report/ar4/wg1/ar4-wg1-spm.pdf.

(5) Edmonds, J.; Dooley, J. J.; Kim, S.; Friedman, S.; Wise, M., Technology in an Integrated Assessment Model: The Potential Regional Deployment of Carbon Capture and Storage in the Context of Global CO_2 Stabilization. In: Schlesinger, M. (Ed.), Human-induced Climate Change: An Interdisciplinary Assessment, Cambridge University Press, 2007, 181-197.

(6) Dooley, J. J., Valuing national and basin level geologic CO_2 storage capacity assessments in a broader context. International Journal of Greenhouse Gas Control, 2010, 5 (1), 177-178.

(7) Metz, B.; Davidson, O.; De Coninck, H.; Loos, M.; Meyer, L., Eds., IPCC Special Report on Carbon Dioxide Capture and Storage, 2005; http://www.ipcc.ch/pdf/special-reports/srccs/srccs_wholereport.pdf.

(8) Bachu, S., CO_2 storage in geological media: Role, means, status and barriers to deployment. Progress in Energy and Combustion Science, 2008, 34 (2), 254-273.

(9) Michael, K.; Arnot, M.; Cook, P.; Ennis-King J.; Funnel, R.; Kaldi, J.; Kirste, D., CO_2 storage in saline aquifers I: Current state of scientific knowledge. Energy Procedia, 2009, 1 (1), 3197-3204.

(10) Michael, K., Allinson, G.; Golab, A.; Sharma, S.; Shulakova, V., CO_2 storage in saline aquifers II: Experience from existing storage operations. Energy Procedia, 2009, 1 (1), 1973-1980.

(11) Bachu, S.; Bonijoly, D.; Bradshaw, J.; Burruss, R.; Holloway, S.; Christensen, N. P.; Mathiassen, O.M., CO_2 storage capacity estimation: methodology and gaps. International Journal of Greenhouse Gas Control, 2007, 1 (4), 430-443.

(12) Frailey, S. M.; Finley, R. J., Classification of CO_2 geologic storage: Resource and capacity. Energy Procedia, 2009, 1 (1), 2623-2630.

(13) Frailey, S. M., Methods for Estimating CO_2 Storage in Saline Reservoirs. Energy Procedia, 2009, 1 (1), 2769-2776.

(14) Popova, O.; Small, M.J.; McCoy, S.T.; Thomas, A.C.; Karimi, B.; Goodman, A.; Carter, K.M., Comparative analysis of CO_2 storage assessment methodologies, Environmental Geosciences Journal, 2012, 23 (3), 105-124.

(15) National Energy Technology Laboratory (NETL), Carbon Sequestration Atlas of the United States and Canada, Third Edition. Pittsburgh, PA, US DOE publication, 2010; http://www.netl.doe.gov/technologies/carbon_seq/refshelf/atlasIII/2010atlasIII.pdf.

(16) NETL, Carbon Utilization and Storage Atlas of the United States, Fourth Edition. Pittsburgh, PA, US DOE publication, 2012; http://www.netl.doe.gov/technologies/carbon_seq/refshelf/atlasIV/.

(17) Brennan, S.T.; Burruss, R.C.; Merrill, M.D.; Freeman, P.O.; Ruppert, L.F., A probabilistic assessment methodology for the evaluation of geologic carbon dioxide storage. U.S. Geological Survey Open-File Report 2010–1127, 2010; http://pubs.usgs.gov/of/2010/1127.

(18) Spencer, L.K.; Bradshaw, J., Regional storage capacity estimates: Prospectivity not statistics. Energy Procedia, 2011, 4 (1), 4857-4864.

(19) Szulczewski, M. L.; Juanes, R., A simple but rigorous model for calculating CO2 storage capacity in deep saline aquifers at the basin scale: Energy Procedia, 2009, 1 (1), 3307-3314.

(20) EPA (Environmental Protection Agency), Inventory of U.S. Greenhouse Gas Emissions and Sinks: 1990-2010, EPA 430-R-12-001, 2012; http://www.epa.gov/climatechange/ghgemissions/usinventoryreport.html.

(21) Vanuxem, L., Third annual report of the Geological Survey of the third district. New York, NY, New York State Geological Survey publication, 1839.

(22) Stowe, M. H., Conditions of sedimentation and sources of the Oriskany Sandstone as indicated by petrology. AAPG Bulletin, 1938, 22, 541–564.

(23) Abel, K. D.; Heyman, L., The Oriskany Sandstone in the subsurface of Pennsylvania. In Mineral Resources Report, Harrisburg, PA, Pennsylvania Geological Survey publication 4th ser., 1981, 3-9.

(24) Diecchio, R. J., Regional controls of gas accumulation in the Oriskany Sandstone, central Appalachian Basin. AAPG Bulletin, 1985, 69, 722–732.

(25) Quinlan, G.M.; Beaumont, C., Appalachian thrusting, lithospheric flexure, and the Paleozoic stratigraphy of the Eastern Interior of North America. Canadian Journal of Earth Sciences, 1984, 21 (9), 973-996.

(26) Castle, J. W., Appalachian basin stratigraphic response to convergent-margin structural evolution. Basin Research, 2001, 13 (4), 397–418.

(27) Filer, J. K., Stratigraphic evidence for a Late Devonian possible back-bulge basin in the Appalachian basin, United States. Basin Research, 2003, 15 (3), 417-429.

(28) Schultz, C.H., Ed., The Geology of Pennsylvania; Pennsylvania Geologic Survey and Pittsburgh Geological Society special publication: Pittsburgh, PA, 2002.

(29) Roen, J. B.; Walker, B. J., Eds., The atlas of major Appalachian gas plays; West Virginia Geological and Economic Survey Publication 25: Morgantown, WV, 1996.

(30) Patchen, D. G., and J. A. Harper, The Lower Devonian Oriskany combination traps play. In Atlas of major Appalachian gas plays; J. B. Roen, and B. J. Walker, Eds.; West Virginia Geological and Economic Survey Publication 25: Morgantown, WV, 1996; pp 118-126

(31) Opritza, S. T., Play Dop: the Lower Devonian Oriskany Sandstone updip permeability pinchout. In Atlas of major Appalachian gas plays; J. B. Roen, and B. J. Walker, Eds.; West Virginia Geological and Economic Survey Publication 25: Morgantown, WV, 1996; pp 126–129.

(32) Harper, I.A.; Laughrey, C.D., Geology of oil and gas fields of southwestern Pennsylvania. In Mineral Resource Report, Harrisburg, PA, Pennsylvania Geological Survey publication, 4th ser., 1987; pp 148-166.

(33) Kostelnik, J.; Carter, K. M., Unraveling the stratigraphy of the Oriskany Sandstone: A necessity in assessing its site-specific carbon sequestration potential. Environmental Geosciences Journal, 2009, 16 (4), 187-200.

(34) International Energy Agency Greenhouse Gas R&D Programme (IEAGHG), Development of storage coefficients for CO_2 storage in deep saline formations. Cheltenham, UK, IEAGHG publication, 2009.

(35) Gorecki, C.D.; Sorensen, J.A.; Bremer, J.M.; Knudsen, D.J.; Smith, S.A.; Steadman, E.N.; Harju, J.A., Development of storage coefficients for determining the effective CO_2 Storage Resource in deep saline formations. Proceedings SPE International Conference on CO_2 Capture, Storage, and Utilization, 2009, 1-12.

(36) Kopp, A.; Class, H.; Helmig, R., Investigations on CO_2 storage capacity in saline aquifers Part 1: Dimensional analysis of flow processes and reservoir characteristics. International Journal of Greenhouse Gas Control, 2009, 3, 263–276.

(37) Kopp, A.; Class, H.; Helmig, R., Investigations on CO_2 storage capacity in saline aquifers Part 2: Estimation of storage capacity coefficient. International Journal of Greenhouse Gas Control, 2009, 3, 277–287.

(38) IEA GHG (International Energy Agency Greenhouse Gas R&D Programme), Development of Storage Coefficients for CO_2 Storage in Deep Saline Formations 2009/13, 2009; http://www.ieaghg.org/.

(39) Goodman, A.; Hakala, A.; Bromhal, G.; Deel, D.; Rodosta, T.; Frailey, S.; Small, M. J.; Allen, D.; Romanov, V.; Fazio, J.; Huerta, N.; McIntyre, D.; Kutchko, B.; Guthrie, G., U.S. DOE methodology for development of geologic storage potential for carbon dioxide at the national and regional scale. International Journal of Greenhouse Gas Control, 2011, 5 (4), 952–965, http://www.sciencedirect.com/science/article/pii/S1750583611000405.

(40) Bachu, S., Comparison between Methodologies Recommended for Estimation of CO_2 Storage Capacity in Geological Media by the CSLF Task Force on CO_2 Storage Capacity Estimation and the USDOE Capacity and Fairways Subgroup of the Regional Carbon Sequestration Partnerships Program, Phase III Report, Carbon Sequestration Leadership Forum (CSLF) publication, 2008; http://www.cslforum.org/publications/documents/PhaseIIIReportStorageCapacityEstimationTaskForce0408.pdf.

(41) Peng, D. Y.; Robinson, D. B., A new two-constant equation of state. Industrial and Engineering Chemistry: Fundamentals, 1976, 15, 59–64.

(42) McCoy, S. T., The economics of carbon dioxide transport by pipeline and storage in saline aquifers and oil reservoirs. PhD Dissertation, ProQuest Dissertations and Theses, Carnegie Mellon University, Pittsburgh, PA, 2008; http://search.proquest.com/docview/304665440?accountid=9902.

(43) Serna, J.G., Peng-Robinson EoS: Calculates the compressibility factor, fugacity coefficient and density of a pure component. Mathworks online publication; http://www.mathworks.com/matlabcentral/fileexchange/4519-peng-robinson-eos/content/PengRobinson.m.

(44) Deutsch, C. V., Geostatistical Reservoir Modeling. Oxford University Press: New York, NY, 2002.

(45) Boisvert, J.B., Deutsch, C. V., Programs for kriging and sequential Gaussian simulation with locally varying anisotropy using non-Euclidean distances. Computers & Geosciences, 2011, 37 (4), 495–510.

(46) McClamroch, N.H., Simulation Methods for large scale system. The University of Michigan publication, 1980.

(47) Journel, A. G., Geostatistics for conditional simulation of ore bodies. Economic Geology, 1974, 69, 673–687.

(48) Journel, A.G.; Huijbregts, C.J., Mining Geostatistics. Academic Press Inc.: London, UK, 1978.

(49) Dietrich, C. R.; Newsam, G. N., A fast and exact method for multidimensional Gaussian stochastic simulations. Water Resources Research, 1993, 29 (8), 2861–2869.

(50) Deutsch, C. V.; Journel, A. G., GSLIB Geostatistical Software Library and User's Guide, 2nd edition. Oxford University Press: New York, NY, 1998.

(51) Leuangthong, O.; McLennan, J. A.; Deutsch, C. V., Minimum acceptance criteria for geostatistical realizations. Natural Resources Research, 2004, 13 (3), 131–141.

(52) Feng, C.; Liu, S.; Wang, L.; Li, C., Present-day geothermal regime in Tarim basin, northwest China. Chinese Journal Geophysics, 2009, 52 (11), 2752-2762.

(53) Förster, A.; D. F. Merriam eds., Geothermics in Basin Analysis. Kluwer Academic: New York, NY, 1999.

(54) NOAA (National Oceanic and Atmospheric Administration) online publication; http://www.esrl.noaa.gov/psd/data/usclimate/tmp.state.19712000.climo.

(55) Bureau of Economic Geology (BEG), University of Texas at Austin, Oriskany Formation, Appalachian Basin (Western Pennsylvania, Eastern OH, and Eastern KY); http://www.beg.utexas.edu/environqlty/co2seq/co2data/0oriskany.htm.

(56) Dilmore, R.; Allen, D. E.; Jones, R. J.; Sheila, W.; Hedges, S.; Soong, Y., Sequestration of dissolved CO_2 in the Oriskany formation. Environmental Science & Technology, 2008, 42 (8), 2760-2766.

(57) Istok, J. D.; Smyth, J. D.; Flint, A. L., Multivariate geostatistical analysis of ground-water contamination: a case history. Ground Water, 1993, 31, 63–74

Chapter 4. Geostatistical Scoping Analysis of CO_2 Injection and Storage Cost in the Oriskany Formation [7]

4.1. Introduction

The cost of CO_2 geologic sequestration in the Oriskany Formation of the Appalachian basin is assessed here using the carbon sequestration resource computed for the formation (see Chapter 3). Results of the analysis presented in this chapter allow us to identify the low-cost areas within the Oriskany Formation which might be considered as potential injection sites. Note that the reported cost estimates are calculated for CO_2 injection and storage in a geologic formation and do not include carbon capture at a power plant and transport to an injection site.

The cost of geologic carbon sequestration in saline formations has been the subject of previous research (1- 4). CCS cost estimates in saline formations for the continental United States, Canada, Australia, and Europe are highly variable ranging from $0.5-304/tonne (5-9). Authors of prior studies admit that the uncertainty and variability of formation properties could cause the range in storage cost estimates to vary over several orders of magnitude (3, 10, 11). By and large, formation heterogeneity is not reflected in the existing cost analyses, primarily due to insufficient data and lack of appropriate methods. Various authors have developed transport optimization models as a part of the overall cost assessment of CCS systems. They use average values or summary statistics of reservoir properties in their cost computations (3, 10, 12-16). Since a majority of previous CCS cost analyses do not satisfactorily embrace the geologic

[7] This Chapter will be submitted for publication in the Economic Geology journal.

heterogeneity of sedimentary formations, variations in reported cost projections are mainly due to varying transport distances between the power plants and injection sites.

In a recent study Rubin at al. attempted to unify methods of estimating CCS cost and improve the communication of cost assumptions (17). They identified major deficiencies in existing CCS costing methods and developed a set of guidelines for a consistent costing methodology including cost reporting.

As shown in Chapter 2, the storage resource of any regional geological unit cannot be adequately characterized by deterministic calculations. Saline formations, as natural sedimentary geologic units, are large and heterogeneous with distinctive spatial variations in their reservoir properties, which result in substantial variations in storage costs. Using average estimates does not give us understanding of the spatial distribution of the storage resource and sequestration cost and, therefore, does not help identify areas within a formation where sequestration of CO_2 can be implemented in a cost-efficient manner.

In 2010 EPA developed a final rule that tailored the existing Underground Injection Control (UIC) regulatory framework to address the unique nature of CO_2 injection for Geologic Sequestration (GS) for the purposes of protecting underground sources of drinking water (USDW) (18). This Thesis builds on the studies performed by EPA (19, 20) to support their cost analysis for the federal requirements under the UIC Program for Carbon Dioxide Geologic Sequestration Wells (Final GS Rule) (18). The final GS rule establishes minimum Federal requirements under the Safe Drinking Water Act (SDWA) for injection of CO_2 for the purposes of long-term storage. The final rule creates a new class of injection well, Class VI, and sets minimum technical criteria for the purposes of protecting USDWs. The elements of the GS Rule are based ‘on the existing UIC regulatory framework with modifications to address the unique

nature of GS in the anticipation of its eventual use to reduce CO_2 emissions to the atmosphere'. (18, p.1-1).

4.2. Methods

To quantify the cost of CO_2 injection and storage we use EPA (19, 20) cost breakdowns for the individual cost components (project phases) categorized as follows:

- Site Characterization
- Area of Review and Corrective Action
- Injection Well Construction and Site Preparation
- Mechanical Integrity Tests
- Monitoring
- Injection Well Operation
- Well Plugging and Post-Injection Site Care

In our cost calculation model we combined the Site Characterization phase with the Area of Review and Corrective Action phase. Primary data sources for costs and tables summarizing individual cost units developed by EPA for the final rule and applied to the case study of the Oriskany formation are provided in Appendix C.

4.2.1. Assumptions

In our analysis we use the following assumptions:

- The study covers the six above-listed individual cost components
- Two injection wells are used per grid cell (25 km^2)
- CO_2 is injected at a rate of 1 million tonnes per year in each grid cell
- One stratigraphic well is drilled per grid cell

- One monitoring well reaching the injection zone per grid cell
- The monitoring period for the post-injection phase is 50 years based on the EPA final rule
- Using discount rates of 10%, 15%, and 20%

4.2.2. Cost model

The model for total cost of CO_2 storage in this saline formation incorporates six elements, including unit costs for each phase: (1) Site Characterization, Area of Review and Corrective Action, (2) Injection Well Construction, (3) Mechanical Integrity Tests, (4) Monitoring, (5) Injection Well Operation, and (6) Well Plugging and Post-Injection Site Care. The cost model comprises the following components: capital costs and operation and maintenance costs (O&M). Each of these elements consist of '**fixed costs** ' that are the same for all grid cells in the Oriskany Formation and *'***variable costs***'* that depend on the depth of the Oriskany Formation and are calculated individually for each cell . For example, the equipment cost represents a fixed cost component while drilling cost represents a cost-on-depth component in the capital cost of well installation. By the same token, the sampling cost does not depend on well depth and is a fixed component of monitoring O&M costs, while certain portions of monitoring O&M costs are depth-dependent.

The cost model is based on the following algorithm: (1) calculation of the capital and O&M costs for each project phase in nondiscounted value, including fixed cost and variable (cost-on-depth) component; (2) summation of these costs by project phase and by cost type (capital and O&M

expenditures); (3) conversion of these costs into discounted dollars[8]; and (4) calculation of cost (in terms of the net present value) for CO_2 injection and storage for each grid cell.

Table 4.1 provides a summary of undiscounted cost values by project phase and cost component. The cost reported in this analysis represent the price levels in 2008, inflated to 2012 using the Consumer Price Index inflationary factor of 7 percent. Some activities occur once, such as the initial site characterization, while other activities, such as injectate analysis reports and mechanical integrity tests occur annually during a project's lifetime. To simplify calculation, we include costs of one-time activities in the respective capital cost category and annual activities – in the corresponding O&M cost category.

Table 4.1. Cost breakdowns (undiscounted values) by project phase and cost component (2012 $) based on EPA (2010) projections implemented to the Oriskany Formation case study.

Phase	Capital		O&M	
	Fixed cost Million $	Cost-on depth $/meter	Fixed cost Million $	Cost-on depth $/meter
Site Characterization, Area of Review and Corrective Action	**1.75**	**274**	-	-
Injection Well Construction and site Preparation	**3.19**	**2,019**	-	-
Monitoring	**0.98**	**643**	**0.25**	**11**
Injection Well Operation	-	-	**0.70**	**22**
Mechanical Integrity Tests	-	-	**0.04**	**87**
Post-Injection Site Care	**1.5**	**32**	**0.14**	-

[8] $NPV(i, n) = \sum_{n=0}^{N} \frac{R_n}{(1+i)^n}$, where R_n is cash flow at time *n*, *i* is the discount rate, and *n* is a time period in years.

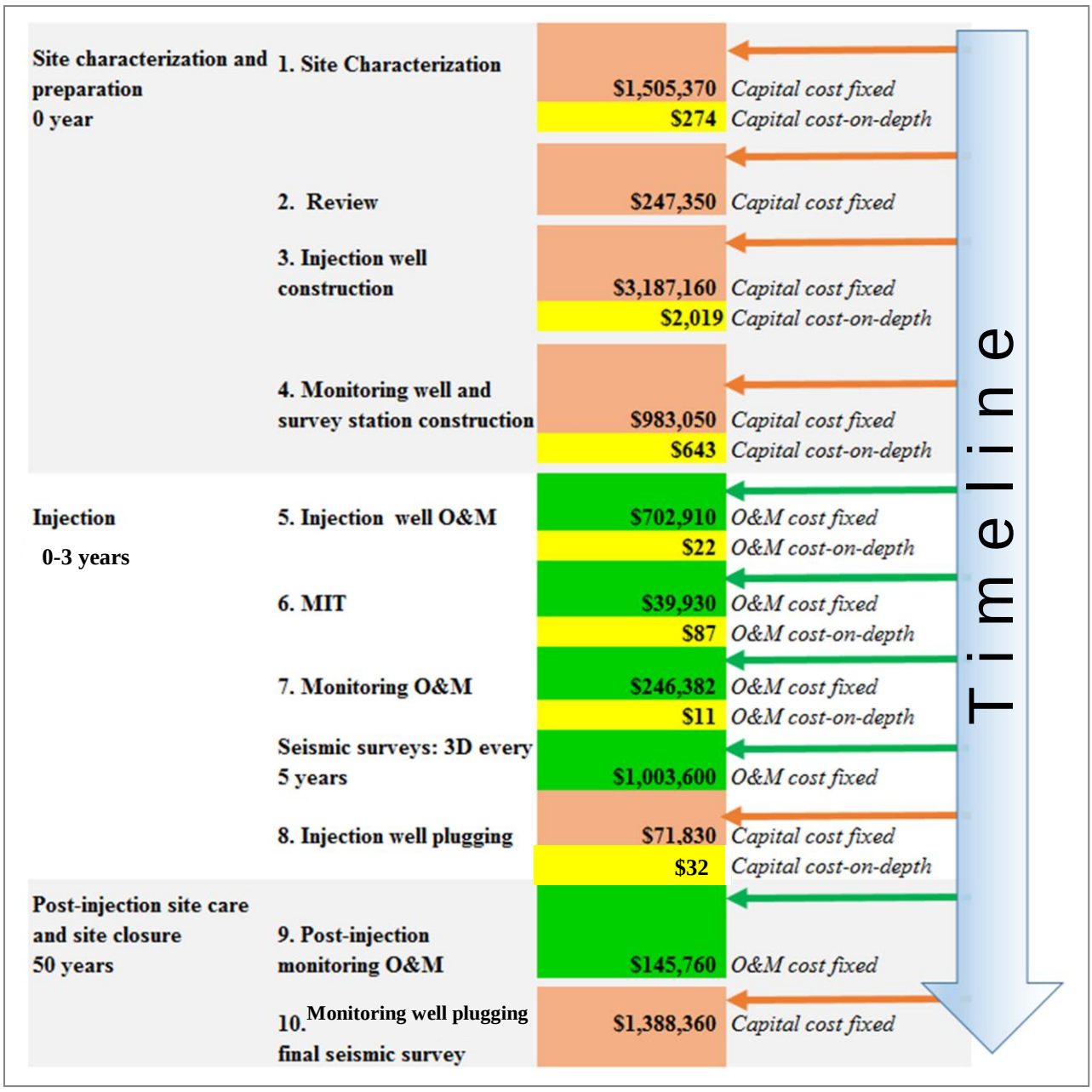

Figure 4.1. A timeline representing capital and O&M expenditures including fixed and cost-on depth components over the CO_2 sequestration project lifetime. Injection time for 5 by 5 km cells ranges from 0 to 3 years across the Oriskany formation based on the estimated storage resource and an injection rate of 1 Mt per year.

As with any technology and cost projections, there are many sources of uncertainty in cost estimates. This analysis does not cover uncertainties related to the unit cost of the technology, estimates of labor burden and hourly wage rate, and changes in costs over time. A timeline

representing capital and O&M expenditures including fixed and cost-on depth components over the CO_2 sequestration project lifetime is shown in Figure 4.1.

4.3. Results

Using sequestration resource estimates (computed with the effective efficiency factor of 5%) for residual trapping produced by our model implemented in Matlab with n=1000 SGS realizations over a 5 by 5 km grid system (as described in Chapter 3) we calculate the cost for CO_2 injections and storage (in terms of the present value with discount rate of 10%, 15%, and 20% in the Oriskany Formation of the Appalachian basin. The results are presented in Table 4.2. The net present value of CO_2 sequestration cost for each individual cell is calculated based on the estimated storage resource, formation depth, and period of injection. The injection period for each individual cell is computed as a quotient of the estimated CO_2 mass and an injection rate of 1 Mt/year. The injection period for 5 by 5 km cells ranges from 0 to 3 years across the Oriskany formation. Detailed calculations of the net present value of CO_2 sequestration cost in the Oriskany formation using 10%, 15%, and 20% discount rates are included in Appendix D.

Table 4.2. Summary statistics for the estimated cost (in terms of the net present value with discount rates of 10%, 15%, and 20%) of CO_2 injections and storage ($/tonne) in the Oriskany Formation of the Appalachian basin (over 7930 grid cells, 5 by 5 km, based on storage resource estimate using n=1000 SGS realizations, with injection at a rate of 1Mt/year).

Statistics	Mean	St. deviation	Median	10% Percentile	90% Percentile	Min	Max
Cost of CO_2, ***i=10%*** $/tonne	**30.56**	**42.30**	**30.44**	**9.90**	**114.83**	**1.84**	**235.14**

Statistics	Mean	St. deviation	Median	10% Percentile	90% Percentile	Min	Max
Cost of CO_2, ***i=15%*** $/tonne	**29.45**	**41.58**	**29.15**	**8.97**	**111.62**	**1.59**	**230.78**
Cost of CO_2, ***i=20%*** $/tonne	**28.80**	**41.07**	**28.01**	**8.44**	**106.24**	**1.47**	**227.29**

Figure 4.1. presents the PDF (probability distribution function) and CDF (cumulative distribution function) for the estimated costs (in terms of the net present value using a discount rate of 10%) of CO_2 injections and storage ($/tonne) in the Oriskany Formation across the 7930 5 by 5 km grid cells. This chart reveals that in the presence of uncertainty and variability in reservoir properties, cost estimates vary significantly across the Oriskany Formation.

As Figure 4.2. demonstrates, the deterministic calculation of the cost using the average values of empirical observations (27.17 $/tonne) is different from the mean value calculated using SGS (30.56 $/tonne). This outcome shows the importance of taking formation heterogeneity into account, and that the average values of input parameters may not produce an adequate estimate of cost of CO_2 sequestration in sedimentary geologic formations.

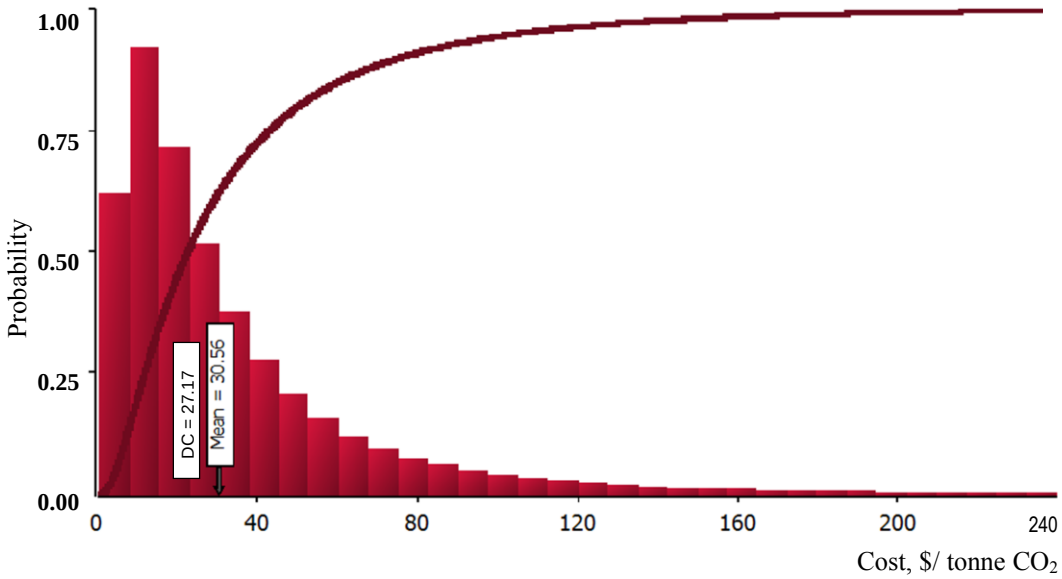

Figure 4.2. Simulated PDF (bars) and CDF (line) of estimated cost of CO_2 injections and storage ($/tonne, in terms of the net present value using a discount rate of 10%) in the Oriskany Formation of the Appalachian basin (over 7930 grid cells, 5 by 5 km, based on storage resource estimate using n=1000 SGS realizations, with injection at a rate of 1Mt/year).

The spatial distribution of the estimated cost of CO_2 injection and storage (in terms of the present value using a discount rate of 10%) in the Oriskany Formation expressed in US dollars per tonne for the mean, 10th percentile value, and 90th percentile values is presented in Figure 4.3. a), b), and c) respectively. Note that not all areas within the Oriskany Formation are appropriate for sequestering CO_2 in a supercritical state. The cells with estimated depth less than 800 meters are excluded from further computations.

a)

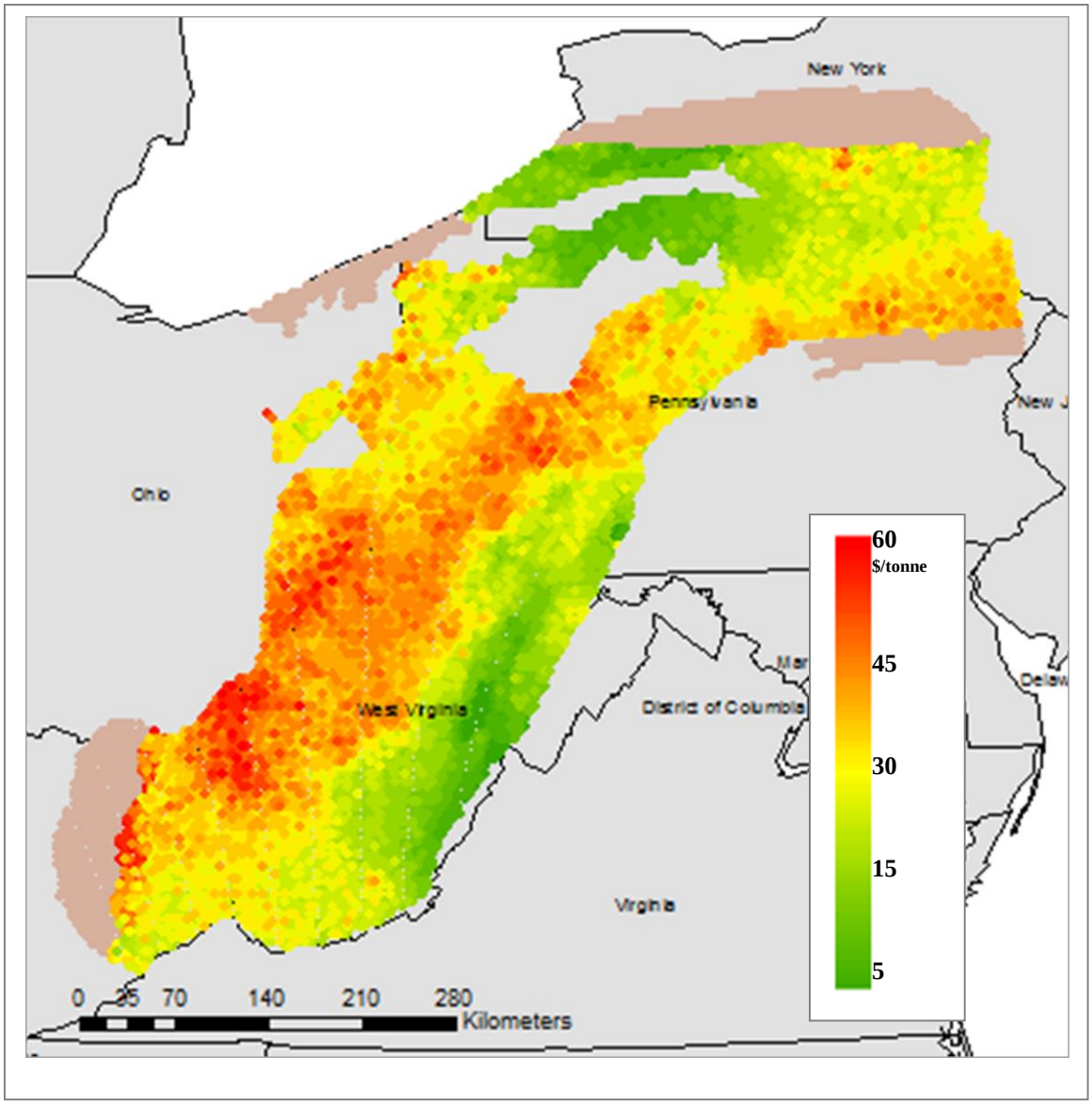

Figure 4.3. a) The spatial distribution of the mean of estimated cost ($/tonne, in terms of the present value using a discount rate of 10%) of CO_2 injections and storage in the Oriskany footprint (over 7930 grid cells, 5 by 5 km, based on storage resource estimate using n=1000 SGS realizations, with injection at a rate of 1Mt/year). The brown portions of the formation are the grid cells where estimated depth is less than 800 meters.

b)

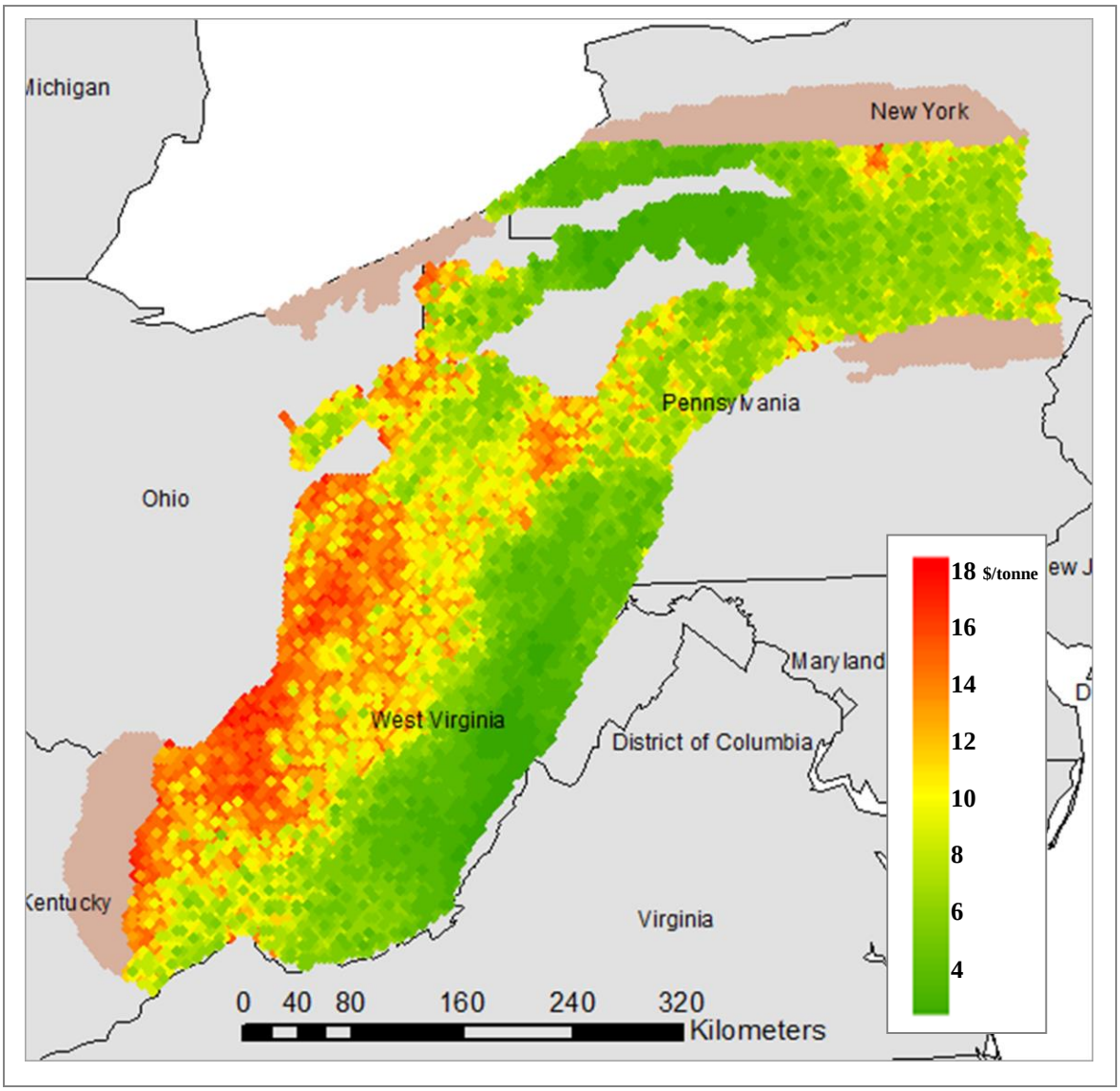

Figure 4.3. b) The spatial distribution of the 10th percentile of estimated cost of CO_2 injections and storage ($/tonne, in terms of the net present value using a discount rate of 10%) in the Oriskany footprint (over 7930 grid cells, 5 by 5 km, based on storage resource estimate using n=1000 SGS realizations, with injection at a rate of 1 Mt/year). The brown portions of the formation are the grid cells where estimated depth is less than 800 meters.

c)

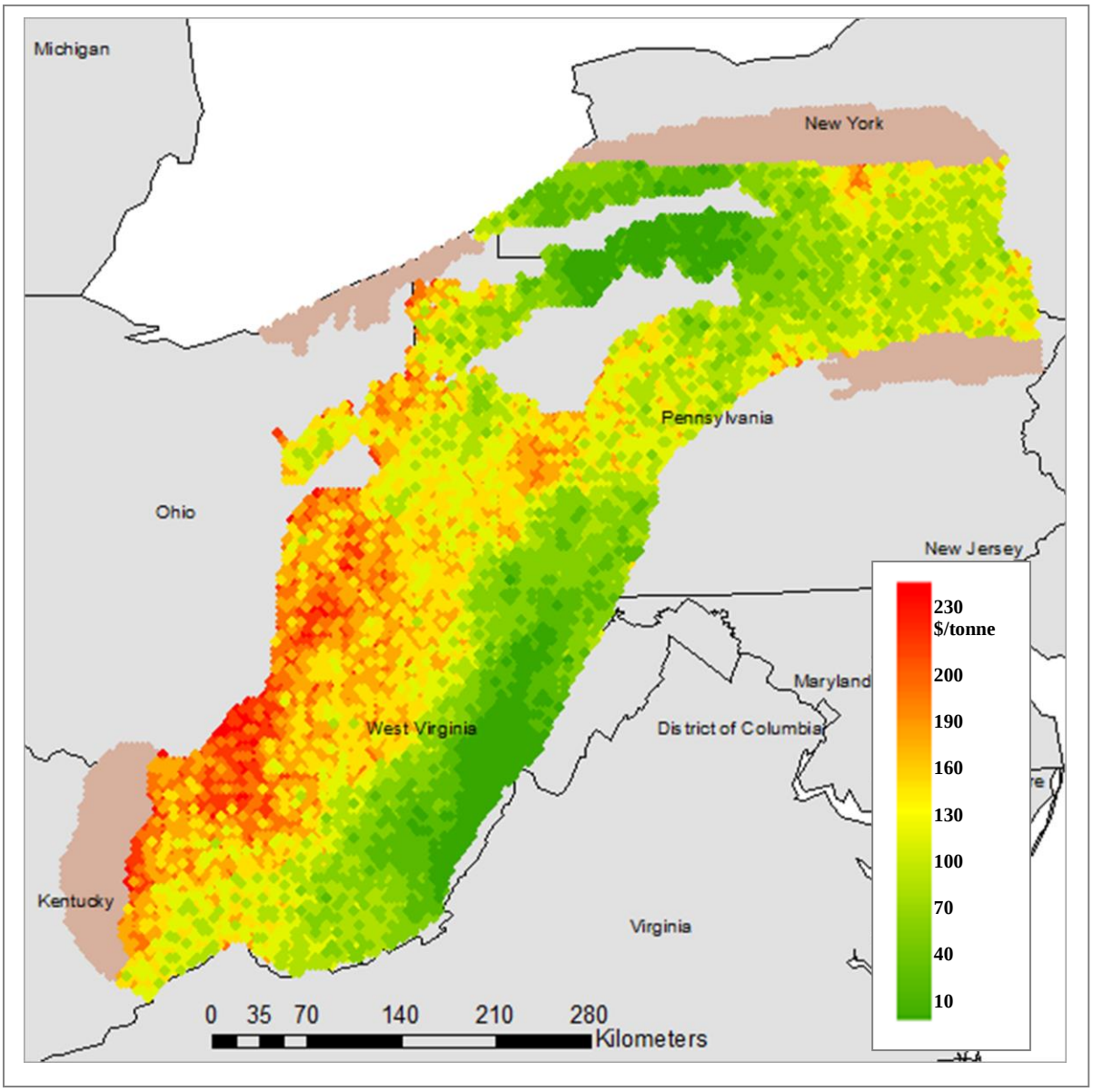

Figure 4.3. c) The spatial distribution of the 90th percentile of estimated cost of CO_2 injections and storage ($/tonne, in terms of the net present value using a discount rate of 10%) in the Oriskany footprint (over 7930 grid cells, 5 by 5 km, based on storage resource estimate using n=1000 SGS realizations, with injection at a rate of 1Mt/year). The brown portions of the formation are the grid cells where estimated depth is less than 800 meters.

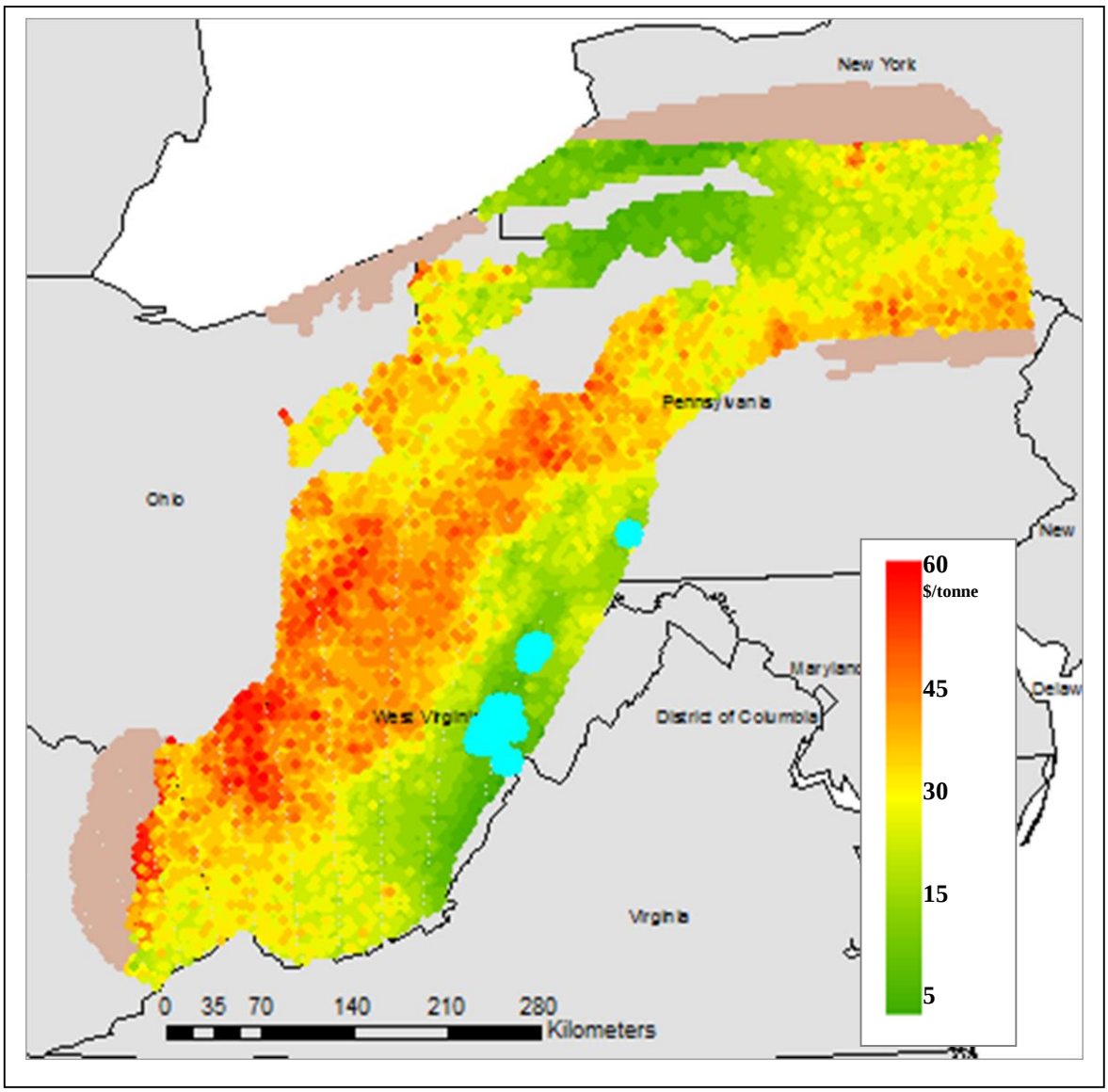

Figure 4.4. The spatial distribution of the estimated cost of CO_2 injections and storage ($/tonne, in terms of the net present value using a discount rate of 10%) in the Oriskany footprint for the mean values (over 7930 grid cells, 5 by 5 km, based on storage resource estimate using n=1000 SGS realizations) with highlighted areas (blue) with the lowest cost which can be filled during first 50 consecutive years (injection at a rate of 1 Mt/year). The highlighted areas can hold 51.4 Million tonnes at the average cost of 5.50 $/tonne.

The locations with insufficient estimated depth are depicted in Figures 4.3 (a - c) and 4.4 as light brown areas within the Oriskany Formation. As expected, the distributions of estimated cost and

storage resource (Figure 4.3 and Figure 3.2.a) exhibit a negative correlation with one another. Locations with high storage estimates generally have low cost estimates.

Figure 4.4 illustrates that the areas within the Oriskany footprint with the lowest cost, which can be filled during first 50 consecutive years (highlighted with blue color) are located in the southeastern part of the Oriskany where cells with the highest storage resource are found. The highlighted areas correspond to the deepest region of the Appalachian basin and can hold 51.5 Million tonnes at an average cost of 5.45 $/tonne (min= 1.84 $/tonne and max=6.98 $/tonne). These areas, subject to further assessment, could be considered as potential CO_2 injection sites for initial CCS industrial scale projects.

Estimated cumulative costs (in terms of the present value with a discount rate of 10%) for the entire Oriskany Formation and for the area of the Oriskany play that can be filled during first 50 years (shown in Figure 4.4 in blue color) with injection at a rate of 1Mt/year are plotted vs. storage resource and vs. time in years in Figure 4.5 a), b), c), and d) respectively.

a)

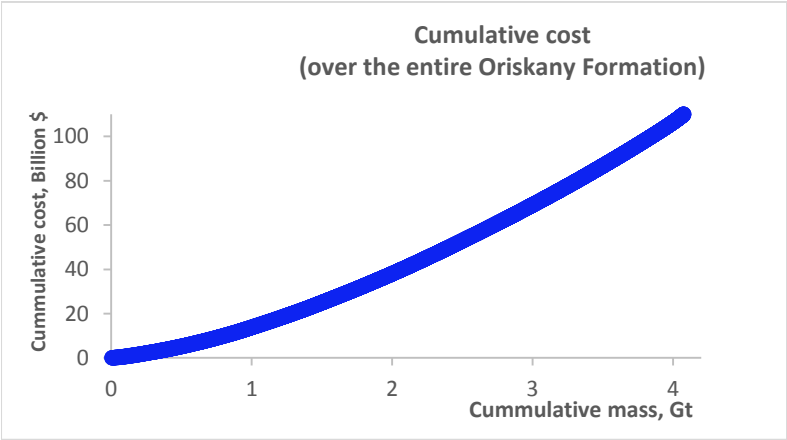

b)

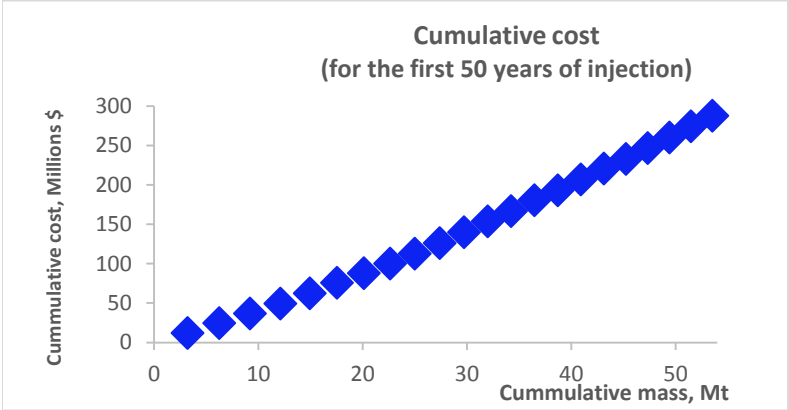

c)

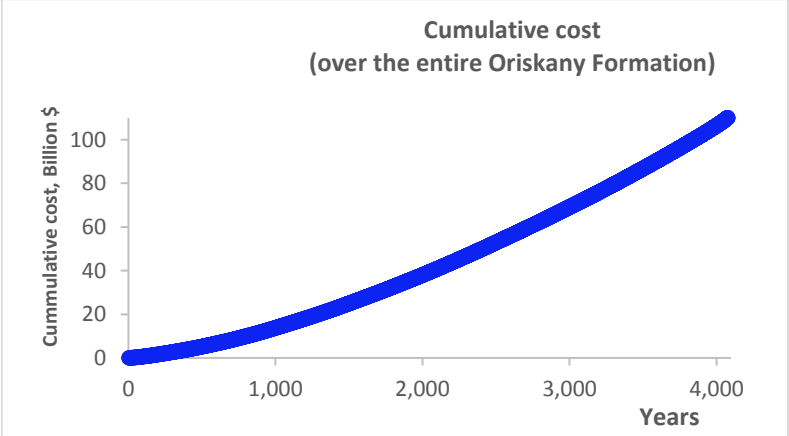

d)

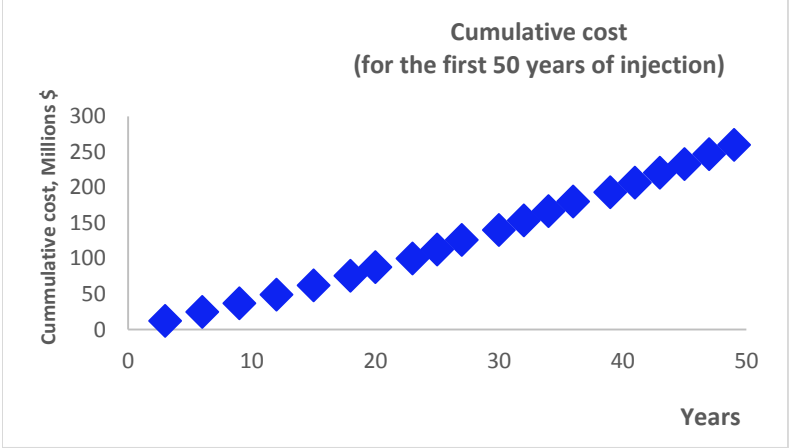

Figure 4.5. The estimated cumulative cost (in terms of the present value using a discount rate of 10%) plotted a) vs. storage resource for the entire Oriskany Formation; b) vs. storage recourse for the area of the Oriskany play that can be filled during first 50 years (shown in Figure 4.4 in blue color); c) vs. time in years for the entire Oriskany formation; and d) vs. time in years for the area of the Oriskany play that can be filed during first 50 years. In all cases CO_2 is injected at a rate of 1Mt/year.

We assume that injection starts in the cell with the lowest cost, and when the cell is 'filled' injection moves to another cell with the next lowest cost and so on. In this way the cell with the highest cost will be filled last. At a rate of 1 Mt of CO_2 per year, it would take 4,080 years to fill all grid cells one by one starting with the lowest cost locations.

4.4. Discussion

We show that the cost of sequestering CO_2 has significant spatial variation due to heterogeneity of formation properties and site geology. We model spatial variation of the storage resource to identify the areas of the Oriskany Formation where CO_2 can be sequestered at minimum cost.

Our results indicate that assessments that do not account for the spatial distribution of the reservoir parameters and use average values likely misrepresent the storage resource and, subsequently, the cost of CO_2 sequestration in geologic formations. Since the CO_2 storage resource and cost are not evenly distributed they need to be estimated in a spatial framework.

We find that areas of the Oriskany play with the largest storage resource have the lowest sequestration cost. Eccles at al. presented similar results for 15 sedimentary basins in the United States (11). The underlying reason that high-storage resource areas are also low-cost areas is derived from the geology of the Appalachian basin. Tectonics and the structure of the Appalachian region define the spatial shape and structural configuration of sedimentary formations in the basin. The depth and thickness of the Oriskany Formation, which are controlled by regional tectonics of the basin, are positively correlated, so the deepest parts of the Oriskany are also the thickest parts. The mass of CO_2 that can be stored increases with thickness, because the available volume is larger, and with depth, because the density of CO_2 (for a given depth range) increases with depth. Thus the thick, deep areas hold the majority of the potential

formation sequestration resource. Sequestration costs are lowest for these areas of the formation because the high fixed costs of sequestration are spread over larger masses of sequestered CO_2. Note that the increasing depth of these areas (which represent the largest portion of the variable sequestration costs) do not reverse this effect.

Until now, Eccles at al. have done the most to incorporate geologic variability and formation heterogeneity in modeling the cost of CO_2 sequestration (11). Though our storage resource model is similar to that of Eccles at al. (11) our modeling produces storage cost estimates for the Oriskany Formation (mean values of 30.56 $/tonne and median values of 30.44 $/tonne with a range between 1.84 and 235.14 $/tonne) that are different from those reported by Eccles at al. (11) (mean values of 180.87 $/tonne and median values of 32.39 $/tonne with a range between 4.88 and 1000 $/tonne). This notable discrepancy in cost estimates is explained by two main reasons: first, Eccles et al. (11) use reservoir data from the BEG to construct a formation geomodel (21). These data are generalizations of well observations and contain multiple data gaps. We base our geomodel on measurements of formation parameters from thousands wells in the Oriskany Formation (provided by the BTGS). Second, Eccles et al. (11) employed an injection-based cost model, where annual injection rate is defined as a function of reservoir permeability, thickness, porosity, temperature, and pressure and is calculated using the radial integration of Darcy's law, known as the Theis solution. We assume a constant annual injection rate of 1 Mt/year for each 5 by 5 km cell. In fact, a straight comparison of these two cost projections is not valid considering differences in cost assessment methodologies and distinctions in sets of geological properties between studies.

Since our analysis does not cover cost uncertainties due to variations in materials and labor costs, or the cost of land, our estimates most likely do not represent an upper bound on storage costs.

Also, our model does not account for the optimum injection rate; instead, we use a constant injection rate of 1 Mt/year across the entire formation. This simplifying assumption affects accuracy of results generated by our model. Undoubtedly, coupling the dynamic injection approach with a detailed formation geomodel will improve accuracy of the cost projections.

A number of CCS engineering-economic models include the costs of transporting CO_2 from each stationary point source to a potential carbon sequestration site (9, 12-16). However, the cost projections in these studies are reported as mean values accompanied in some cases by summary statistics, which can be misleading. Basin geology and variations in storage resource should be included in pipeline transport optimization algorithms, otherwise the pipeline optimal configuration is not 'optimal'.

We believe significant improvement can be made by integrating basin geology and spatial heterogeneity of formation parameters into CCS cost assessments; and that this should be a focus of future research efforts. This will allow for more accurate cost estimates for the entire CCS system and identify areas of sedimentary basins with optimal conditions for CO_2 injection and storage. Furthermore, more precise CCS cost estimates will provide better recommendations for government and industry leaders and inform their decisions on what greenhouse gas mitigation measures are the best fit for their regions.

References

1. Allinson, W.G., Nguyen, D.N., Bradshaw, J., 2003. The economics of geological storage of CO_2 in Australia. APPEA J. 623.

2. Hendriks, C., Graus, W., van Bergen, F., 2004. Global carbon dioxide storage potential and costs (No. EEP-02001). Ecofys, Utrecht.

3. Dooley, J.J., Dahowski, R.T., Davidson, C.L., Bachu, S., Gupta, N., Gale, J., 2004. A CO_2 - storage supply curve for North America and its implications for the deployment of carbon

dioxide capture and storage systems. Proceedings of the Seventh Inter-national Conference on Greenhouse Gas Control Technologies. Presented at the Seventh International Conference on Greenhouse Gas Control Technologies. Elsevier, Amsterdam, Netherlands.

5. IPCC, 2005. Carbon Capture and Storage. Cambridge University Press.

6. Friedmann, S.J., Dooley, J.J., Held, H., Edenhofer, O., 2006. The low cost of geological assessment for underground CO_2 storage: policy and economic implications. Energy Convers. Manage. 47, 1894–1901.

7. Nicot, J.-P., 2008. Evaluation of large-scale CO_2 storage on fresh-water sections of aquifers: an example from the Texas Gulf Coast Basin. Int. J. Greenhouse Gas Control 2, 582–593.

8. McKinsey Climate Change Initiative, 2008. Carbon Capture & Storage: Assessing the Economics. McKinsey & Company.

9. Dooley, J.J., Dahowski, R.T., Davidson, C.L., 2008. On the Long-Term Average Cost of CO_2 Transport and Storage (No. PNNL-17389). Pacific Northwest National Laboratory, Richland, WA.

10. McCoy, S.T., Rubin, E.S., 2009. Variability and uncertainty in the cost of saline formation storage. Energy Procedia 1, 4151–4158.

11. Eccles, J.K., Pratson, L., Newell, R.G., Jackson, R.B., 2012. The impact of geologic variability on capacity and cost estimates for storing CO_2 in deep saline aquifers. Energy Economics 34, 1569 -1579.

12. McCoy, S.T., Rubin, E.S., 2008. An engineering-economic model of pipeline transport of CO_2 with application to carbon capture and storage. Int. J. Greenhouse Gas Control 2, 219–229.

13. Middleton, R.S., Bielicki, J.M., 2009. A scalable infrastructure model for carbon capture and storage: SimCCS. Energy Policy 37, 1052–1060.

14. Wildenborg, T., Gale, J., Hendriks, C., Holloway, S., Brandsma, R., Kreft, E., Lokhorst, A., 2004. Cost curves for CO_2 storage: European sector. Proceedings of the 7th International Conference on Greenhouse Gas Control Technologies (GHGT-7), September 2004, 5–9.

15. Dahowski, R.T., Li, X., Davidson, C.L., Wei, N., Dooley, J.J., Gentile, R.H., 2009. A preliminary cost curve assessment of carbon dioxide capture and storage potential in China. Energy Procedia 1, 2849–2856.

16. Gresham, R.L., McCoy, S.T., Apt, J., Morgan, M.G., 2010. Implications of compensating property owners for geologic sequestration of CO_2. Environ. Sci. Technol. 44, 2897–2903.

17. Rubin, E.S., Short, C., Booras, G., Davison, J., McCoy, S.T., 2013. A proposed methodology for CO_2 capture and storage cost estimate. Int. J. Greenhouse Gas Control 17, 488-503.

18. Environmental Protection Agency (EPA), 2010. Federal requirements Under the Underground Injection Control (UIC) program for carbon dioxide (CO_2) geologic sequestration (GS) wells; final rule.

19. Environmental Protection Agency (EPA), 2010. Geological CO_2 Sequestration Technology and Cost Analysis (Technical Support Document No. EPA 816-R10-008). EPA Office of Water, Washington, DC.

20. Environmental Protection Agency (EPA), 2010. Cost analysis for Federal requirements Under the Underground Injection Control Program for carbon dioxide (CO_2) geologic sequestration wells (Final GS rule).

21. Bureau of Economic Geology (BEG), 2000. Carbon-dioxide sequestration. Carbon dioxide sequestration - study areas URL http://www.beg. utexas.edu/environqlty/co2seq/co2data.htm2000.

Chapter 5. Conclusions

This Thesis focuses on development of a geostatistical model to estimate the storage resource and cost of CO_2 sequestration in sedimentary formations. In order to achieve this, a systematic approach is implemented, the first step of which is to document and compare existing methodologies for CO_2 resource assessment.

This study reveals that previous efforts to assess CO_2 storage resource used an array of approaches and methodologies, employing data sets of variable size and quality and resulting in a broad range of estimates with a high degree of uncertainty. Results of our comparative analyses indicate that methodologies developed by DOE, USGS, and CGSS are similar in terms of computational formulation. In particular, the compared methodologies use static volumetric methods to calculate CO_2 storage resource in open systems and are applicable at either regional or basin-scale levels. These methodologies, however, are not intended for site screening and selection. Siting of specific CCS facilities requires estimates of storage resource capacity for candidate formations based on field investigation and numerical modeling. We find that each of the explored methodologies is science- and engineering-based. As such, they are instrumental in identifying the geographical distribution of CO_2 storage resource and regional carbon sequestration potential at the national and basin-scale levels for use in energy-related government policy and business decisions.

Next, to estimate the magnitude of the CO_2 storage resource in saline formations we develop a geostatistical model. This model is applied here to a regional case study of the Oriskany Formation of the Appalachian sedimentary basin. Our spatial stochastic tool allows for the calculation of the CO_2 sequestration resource of a storage formation with subsequent uncertainty

analysis. We show that our model integrates basin-specific data with a probabilistic approach, is computationally efficient, and, as such is suitable for storage resource assessments in settings where data are limited. Since the model is flexible with respect to changing input parameters and assumptions it can be parameterized to calculate the CO_2 storage resource of any porous subsurface unit.

In this Thesis, we focus our modeling efforts on the calculation of the storage (prior to multiplication by E) as the first step in estimating the storage capacity of the Oriskany Formation; followed by discounting the value of the potential storage resource by applying an effective efficiency factor of 5 percent. Our results indicate that the CO_2 storage resource of the Oriskany Formation has substantial spatial variation due to heterogeneity of formation properties and basin geology leading to significant uncertainty in the total storage resource. The Oriskany Formation sequestration resource estimate ranges from 1.1 gigatonnes to 7.3 gigatonnes with a mean value of 4.08 gigatonnes of CO_2 ($E \cong 5\%$). Assuming that the average CO_2 emission of a 1 GW power plant is approximately 8 Mt per year, the Oriskany Formation can accommodate about 500 years of CO_2 emissions generated by the 1 GW power plant. However, these estimates are not actual realizable capacity estimates, and once other constraints are taken into account, the actual storage capacity that could be realized is likely to be much lower.

We propose that the estimation variances can be useful in the selection of optimum locations for additional exploratory wells to support the assessment of the CO_2 sequestration resource. The optimum locations of additional exploratory wells can be identified sequentially by substituting previously determined well locations into the interpolation equations, calculating new estimation variances, and identifying the grid location with the highest estimation variance (1). Thus, the information return measured by the reduction in CO_2 storage resource uncertainty would be

achieved. In other words, since a reduction in the uncertainty about the sequestration resource is desired, this subsequent analysis will suggest where reductions in uncertainty could be most valuable and what future studies and data collection (e.g. additional characterization wells) should be undertaken.

Finally, we evaluate the cost of CO_2 injection and storage for the Oriskany Formation utilizing storage resource estimates generated by our geostatistical model. Our modeling efforts produce outcomes with a large range of variability in the cost per tonne of CO_2 stored. Our study shows that the cost of sequestering CO_2 has significant spatial variation due to heterogeneity of formation properties and site geology. For injection at a rate of 1 Mt CO_2 per year, the cost of CO_2 sequestration (in terms of the present value using a discount rate of 10%) in the Oriskany Formation ranges from \$1.80 per tonne CO_2 to \$235.10 per tonne CO_2 with a mean value of \$30.60 per tonne CO_2.

We find that areas of the Oriskany Formation with the largest storage resource have the lowest sequestration cost. The depth and thickness of the Oriskany Formation, which are controlled by regional tectonics of the Appalachian basin, are positively correlated, so, generally, the deepest parts of Oriskany are also the thickest parts. The mass of CO_2 that can be stored in the formation increases with thickness, because the available volume is larger, and with depth, because the density of CO_2 (for a given depth range) increases with depth. Thus the thick, deep areas hold the majority of the potential formation sequestration resource. Estimated costs are lowest for these areas of the formation because the high fixed cost of sequestration is spread over larger masses of sequestered CO_2.

We show that the areas in the footprint of the Oriskany Formation with the lowest sequestration cost are located in the southeastern part of the play area, where the cells with highest storage resource are found. These areas correspond to the deepest region of the Appalachian basin and can hold about 51.5 Million tonnes at an average cost (in terms of the present value using a discount rate of 10%) of 5.45 $/tonne CO_2 stored (min = 1.84 $/tonne and max=6.98 $/tonne). These areas can be considered as potential CO_2 injection sites for initial CCS industrial scale projects.

The results for CO_2 storage resource and sequestration cost presented here are based on a case study for the Oriskany Formation. While inclusion of additional formations from 15 US sedimentary basins in our analysis would not enhance the current results for Oriskany Formation, it would give us a nationwide perspective.

As shown, our model does not account for the optimum injection rate; instead, we use a constant injection rate of 1 Mt/ year across the entire Oriskany Formation. This simplifying assumption affects the accuracy of results generated by our model. Undoubtedly, coupling the dynamic injection approach (2, 3) with a detailed formation geomodel will improve the accuracy of the cost projections.

Overall, we conclude that significant improvement can be made in the assessment of a potential reservoir by integrating basin geology and spatial heterogeneity of petrophysical formation properties into CCS cost assessments; and that should be a focus of future research efforts. This will allow for more accurate cost estimates for the entire CCS system and identify areas of sedimentary basins with optimal conditions for CO_2 injection and storage. To mitigate the effects of climate change, the U.S. will need a widespread deployment of low-carbon electricity generating technologies including natural gas and coal with CCS (4, 5). More precise CO_2 storage resource and CCS cost estimates will provide better recommendations for government

and industry leaders and inform their decisions on what greenhouse gas mitigation measures are the best fit for their regions.

References

(1) Journel, A.G.; Huijbregts, C.J., 1978. Mining Geostatistics. Academic Press Inc., London, UK, 580.

(2) McCoy, S.T., Rubin, E.S., 2009. Variability and uncertainty in the cost of saline formation storage. Energy Procedia 1, 4151–4158.

(3) Eccles, J.K., Pratson, L., Newell, R.G., Jackson, R.B., 2012. The impact of geologic variability on capacity and cost estimates for storing CO2 in deep saline aquifers. Energy Economics 34, 1569 -1579.

(4) Morgan, M.G., McCoy, S.T., 2012. Carbon Capture and Sequestration: Removing the legal and regulatory barriers, Taylor and Francis, 274.

(5) Rubin, E.S., Short, C., Booras, G., Davison, J., McCoy, S.T., 2013. A proposed methodology for CO2 capture and storage cost estimate. Int. J. Greenhouse Gas Control 17, 488-503.

Appendix A. Geological Setting of the Oriskany Formation

The Appalachian basin bounded by the Allegheny front to the southeast and the Cincinnati arch to the northwest was formed in response to the Alleghanian orogenic event (1, 2). A map showing the paleogeography of the Appalachian basin area during the Middle Devonian period is displayed in Figure A.1. Major causes of subsidence during the Paleozoic era were related to tectonic flexure of the lithosphere and sediment loading associated with the rejuvenation of the Appalachian foreland basin (3).

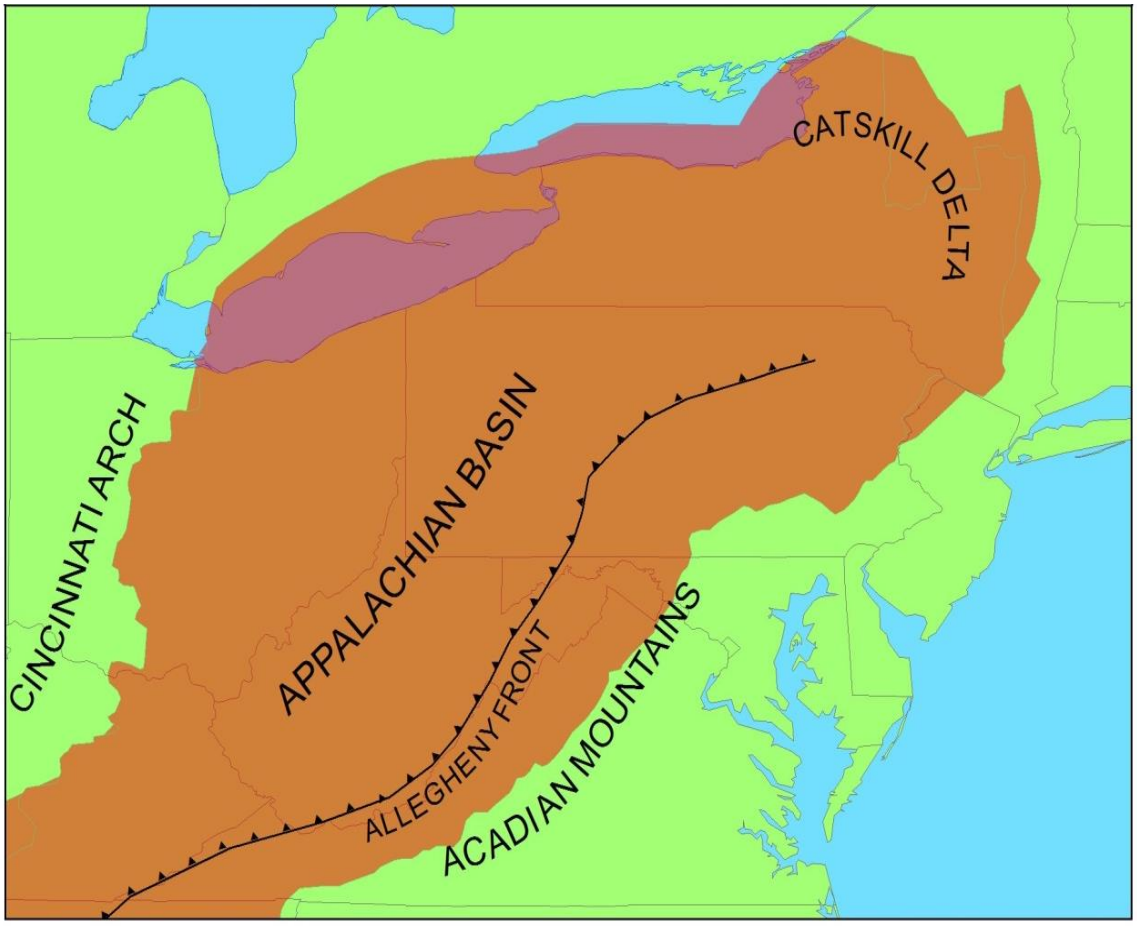

Figure A. 1. Paleogeography of the Appalachian Basin area during the Middle Devonian period.

The Appalachian basin encloses a platform-margin sedimentary succession that is dominated by siliciclastic and carbonate sequences of Early Cambrian through Early Permian age. The basin deepens toward its central parts, reaching more than 5 km depth at the thrust and fold belt of the Appalachian Mountains (4, 5). The Paleozoic strata of the basin are generally underpressured, being slightly sub-hydrostatic. The salinity of formation waters in the basin increases with depth from freshwater in shallow groundwater systems to more than 350,000 mg/l in deep Paleozoic (4, 5). The well-studied Lower Devonian Oriskany Formation is an eastward and southeastward thickening wedge of shallow marine sandstone and is exposed in northeast-trending folds in the Valley and Ridge province of the central Appalachians (4, 5).

Originally, the Oriskany Formation was described by Vanuxem from its outcrop near Oriskany Falls, Oneida County, New York, as white, fossiliferous quartz arenite (6). The Oriskany is typically a quartz arenite but varies from calcareous sandstone to sandy limestone depending on depositional environment and diagenetic controls (7-11). Previous research suggested that Oriskany was deposited in a shallow marine environment with a locally varying paleogeography (8, 10, 13). Figure A.2 presents a generalized regional cross section of the Middle Silurian to Middle Devonian interval in the Pennsylvania portion of the Appalachian basin. Contacts with underlying rocks are both conformable and unconformable, depending on location. Units immediately underlying the Oriskany varies with location and include Bois Blanc Formation, Onondaga Limestone, Huntersville Chert, or Needmore Shale (13, 14). Kostelnik and Carter (15) indicate that there exist primary intergranular, secondary dissolution, and fracture porosity within the Oriskany play.

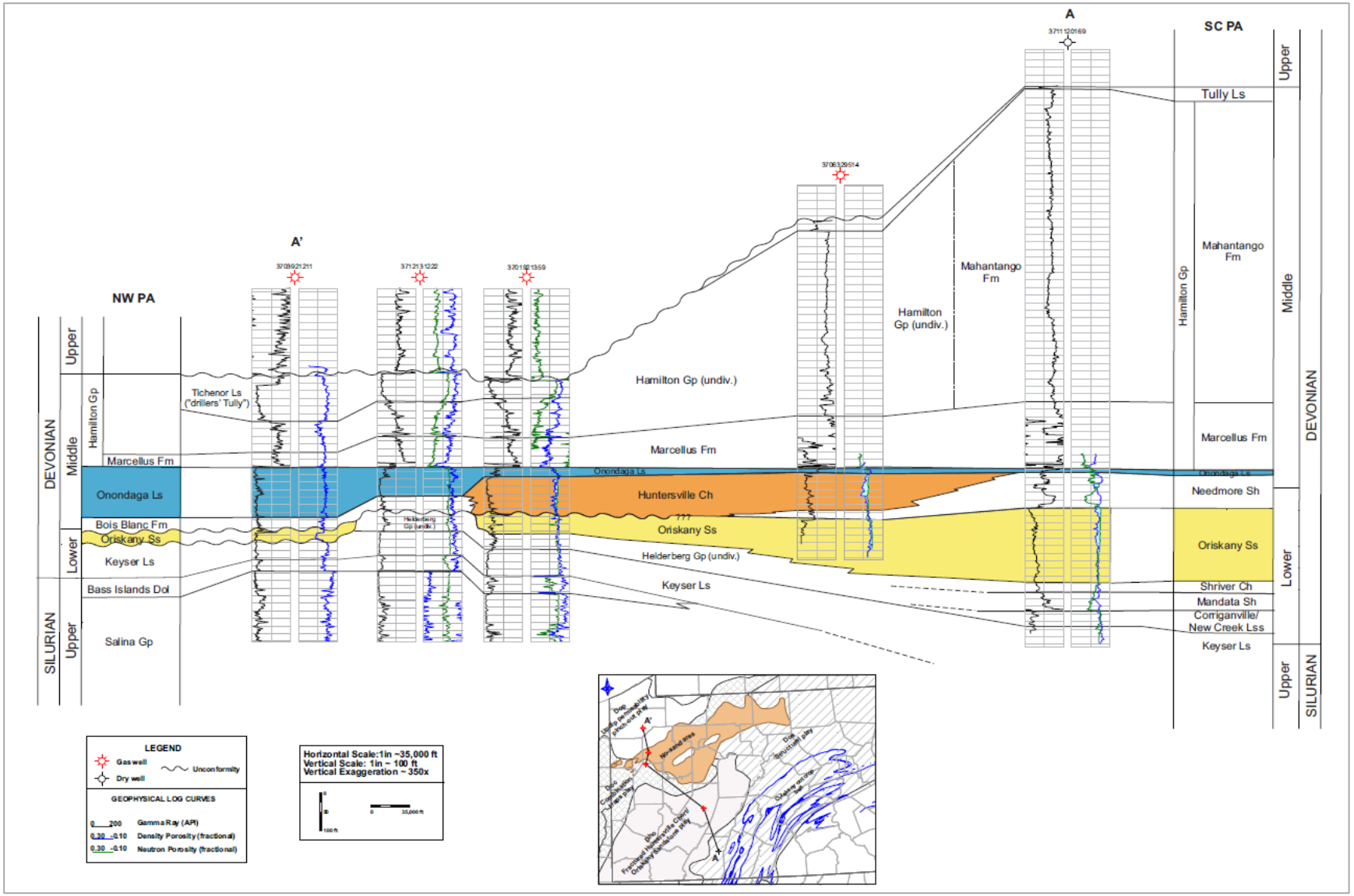

Figure A.2. Geological cross section through the Appalachian basin with the regional stratigraphic schema (Source: The Pennsylvania Bureau of Topographic and Geologic Survey).

References

(1) Quinlan, G.M. and C. Beaumont, 1984, Appalachian thrusting, lithospheric flexure, and the Paleozoic stratigraphy of the Eastern Interior of North America, Canadian Journal of Earth Sciences, 21(9), p. 973-996,

(2) Castle, J. W., 2001, Appalachian basin stratigraphic response to convergent-margin structural evolution, Basin Research, v. 13, Issue 4, p. 397–418.

(3) Schultz, C.H. ed., The Geology of Pennsylvania. Pittsburgh, PA, Pennsylvania Geologic Survey and Pittsburgh Geological Society special publication, 2002, 888.

(4) Roen, J. B.; Walker, B. J. (eds.), The atlas of major Appalachian gas plays. Morgantown, WV, West Virginia Geological and Economic Survey Publication 25, 1996, 201.

(5) Harper, I.A.; Laughrey, C.D., Geology of oil and gas fields of southwestern Pennsylvania. In Mineral Resource Report, Harrisburg, PA, Pennsylvania Geological Survey publication, 4th ser., 1987, 148-166.

(6) Vanuxem, L., Third annual report of the Geological Survey of the third district. New York, NY, New York State Geological Survey publication, 1839, 273.

(7) Diecchio, R. J., Regional controls of gas accumulation in the Oriskany Sandstone, central Appalachian Basin. AAPG Bulletin, 1985, 69, 722–732.

(8) Basan, P. B., D. L. Kissling, K. D. Hemsley, D. G. Kersey, W. G. Dow, M. S. Chaiffetz, P. Isaacson, S. Barrett, and L. Carne, 1980, Geological study and reservoir evaluation of Early Devonian formations of the Appalachians: Houston, Texas, Robertson Research Inc., 263 p.

(9) Bruner, K. R., 1988, Sedimentary facies of the Lower Devonian Oriskany Sandstone, Greenbrier County, West Virginia, in R. Smosna, organizer, A walk through the Paleozoic of the Appalachian Basin: AAPG Eastern Section Meeting, Core Workshop, Charleston, West Virginia, p. 38–47.

(10) Barrett, S. F., and P. E. Isaacson, 1977, Faunal assemblages developed in a coarse clastic sequence, in J. Gray, A. J. Boucot, and W. B. Berry, eds., Communities of the past: Stroudsburg, Pennsylvaniania, Dowden, Hutchinson and Ross, p. 165–183.

(11) Opritza, S. T., Play Dop: the Lower Devonian Oriskany Sandstone updip permeability pinchout. In Roen, J. B.; Walker, B.J. (eds.), Atlas of major Appalachian gas plays, Morgantown, WV, West Virginia Geological Survey publication, 1996, 25, 126–129.

(12) Patchen, D. G., and J. A. Harper, 1996, The Lower Devonian Oriskany combination traps play, in J. B. Roen, and B. J. Walker, eds., The atlas of major Appalachian gas plays: West Virginia Geological and Economic Survey Publication 25, p. 118–125.

(13) Stowe, M. H., Conditions of sedimentation and sources of the Oriskany Sandstone as indicated by petrology. AAPG Bulletin, 1938, 22, 541–564.

(14) Abel, K. D.; Heyman, L., The Oriskany Sandstone in the subsurface of Pennsylvania. In Mineral Resources Report, Harrisburg, PA, Pennsylvania Geological Survey publication 4th ser., 1981, 3-9.

(15) Kostelnik, J.; Carter, K. M., Unraveling the stratigraphy of the Oriskany Sandstone: A necessity in assessing its site-specific carbon sequestration potential. Environmental Geosciences Journal, 2009, 16, 4, 187-200.

Appendix B. Efficiency Factor

For storage efficiency estimation we use the approach developed in the DOE methodology by Goodman et al. [1]. For saline formations, the CO_2 storage efficiency factor is a function of geologic parameters such as area ($E_{An/At}$), gross thickness ($E_{hn/hg}$), and total porosity ($E_{\phi e/E\phi tot}$), which reflect the percentage of volume that is suitable for CO_2 storage and displacement efficiency components like macro displacement (E_V), which is the combined fraction of immediate volume surrounding an injection well that can be contacted by CO_2 and the fraction of net thickness that is contacted by CO_2 as a consequence of the density difference between CO_2 and *in situ* water, and microscopic displacement (E_d):

$$\mathbf{E_{saline} = E_{An/At}\, E_{hn/hg}\, E_{\phi e/E\phi tot}\, E_V\, E_d} \quad (1)$$

In DOE methodology, the efficiency for saline formations is based on the percentile values (P10 and P90) for the correspondent efficiency components as reported by IEA GHG [2]. The authors assumed all parameters to be independent as no significant correlation has been reported for these parameters at the basin scale or national level.

To estimate storage efficiency, DOE used the logistic (log-odds) normal distribution based on a transform for a fraction, p, as follows:

$$\mathbf{X = \ln\left(\frac{p}{1-p}\right)} \quad (2)$$

The transformed variable, X, is then normally distributed and sampled with appropriate Monte Carlo techniques for a normal random variable. Then, the X value is transformed back to the corresponding p value by inverse Equation (3):

$$\mathbf{p = \frac{1}{1+e^{-X}}} \quad (3)$$

Since the relationship between p and X is monotonic, X10 and X90 percentile values of geologic and displacement efficiencies provided by IEA GHG [2] can be estimated directly from P10 and P90 ranges. The mean and standard deviation of X can be computed, and these fully define its normal distribution. These moments are then used as input parameters into the spatial stochastic storage resource model. The mean (μ_X) and standard deviation (σ_X) are calculated from the X10 and X90 values using standard relationships between the percentiles and moments of a normal distribution as follows:

$$\boldsymbol{\mu_X = X_{10} - \sigma_X Z_{10}} \quad (4)$$

$$\boldsymbol{\sigma_X = \frac{(X_{90} - X_{10})}{(Z_{90} - Z_{10})}} \quad (5)$$

where Z10 and Z90 are the respective 10th and 90th percentile value of a standardized normal variable Z. We use values of μ_X and σ_X calculated by Goodman at al. [1] for clastic lithologies as shown in Table B.1.

Table B. 1. Values Calculated from X10 and X90 values for clastic lithologies provided by Goodman at al. [1].

Efficiency	Normal distribution parameters	
	μ_X	σ_X
$E_{An/At}$	0	1.1
$E_{hn/hg}$	-0.09	0.97
$E_{\phi e/\phi tot}$	0.89	0.25
E_V	-1.05	0.47
E_d	0.27	0.69

A SGS technique is implemented using the mean (μ_X) and standard deviation (σ_X) values presented in Table 2 as input parameters. The respective X values are sampled using normal distributions with a sample size of 1000 iterations for each. The corresponding values of p are computed using Equation 3, and the individual p values are multiplied together to determine the storage efficiency factor E as shown in Equation 6:

$$\mathbf{E = p(E_{An/At})p(E_{hn/hg})p(E_{\varphi e/\sigma tot})p(E_v)p(E_d)} \qquad (6)$$

or equivalently,

$$\mathbf{E = \left(1/1 + e^{-X(E_{An/At})}\right)\left(1/1 + e^{-X(E_{hn/hg})}\right)\left(1/1 + e^{-X(E_{\varphi e/\varphi tot})}\right)\left(1/1 + e^{-X(E_v)}\right)\left(1/1 + e^{-X(E_d)}\right)} \quad (7)$$

Using the regression models and the spatial stochastic tool implemented in Matlab with n=1000 SGS generalizations, we calculate the CO_2 volumetric storage resource of the Oriskany Formation over 5 by 5 km grid cells for the following scenarios: (a) with the efficiency factor in each cell assumed to be independent and sampled separately for each grid cell (SGS, n=100); and (b) with the efficiency factor assumed to be fully correlated across all cells in the model and sampled together for the entire Oriskany Formation (SGS, n=100). The results are summarized in Table B.2.

The mean CO_2 storage value ranges from 3.88 Gt to 4.53 Gt with the two methods. These values are approximately a factor of 20 below the potential storage mean of 81.53 Gt computed for the Oriskany using n=1000 SGS realizations and E=100%. An effective value of E for the formation is thus approximately 0.05 (=1/20).

Table B. 2. Summary statistics for the simulated CO_2 storage resource of the Oriskany Formation (over 7930 grid cells (5 by 5 km), n=1000 SGS realizations calculated with (a) independent E for each grid cell; and (b) fully correlated E for the entire formation.

Statistics	Independent E for each grid cell (Gt)	Fully correlated E across the entire Oriskany formation (Gt)
Mean	**3.88**	**4.53**
Median	**3.86**	**4.41**
10% Percentile	**1.83**	**2.09**
90% Percentile	**5.83**	**6.96**
Standard deviation	**1.60**	**1.90**
Minimum	**0.01**	**0.02**
Maximum	**9.84**	**11.68**
Range width	**9.83**	**11.66**

The results (fully correlated) also indicate that the storage resource simulated with the efficiency factor sampled for the entire formation is distributed over the wider range (11.66 Gt) compared with the range of simulated storage resource with the independent efficiency factor (9.83 Gt). Similarly, the fully correlated case yields a larger standard deviation (1.90 vs. 1.60).

The results of applying two different approaches to add the efficiency factor to the storage model are shown in the corresponding CDF charts in Figure B.1. Again, the storage resource displays greater variability when the efficiency factor is sampled for the entire formation.

However, the degree to which the uncertainty in an individual formation property parameter contributes to the uncertainty in the outputs is not clear from these results. Knowing which input

parameters contribute most to the variability of the storage resource suggests where the greatest reduction in the storage resource estimate variability can be gained through a reduction in input uncertainty.

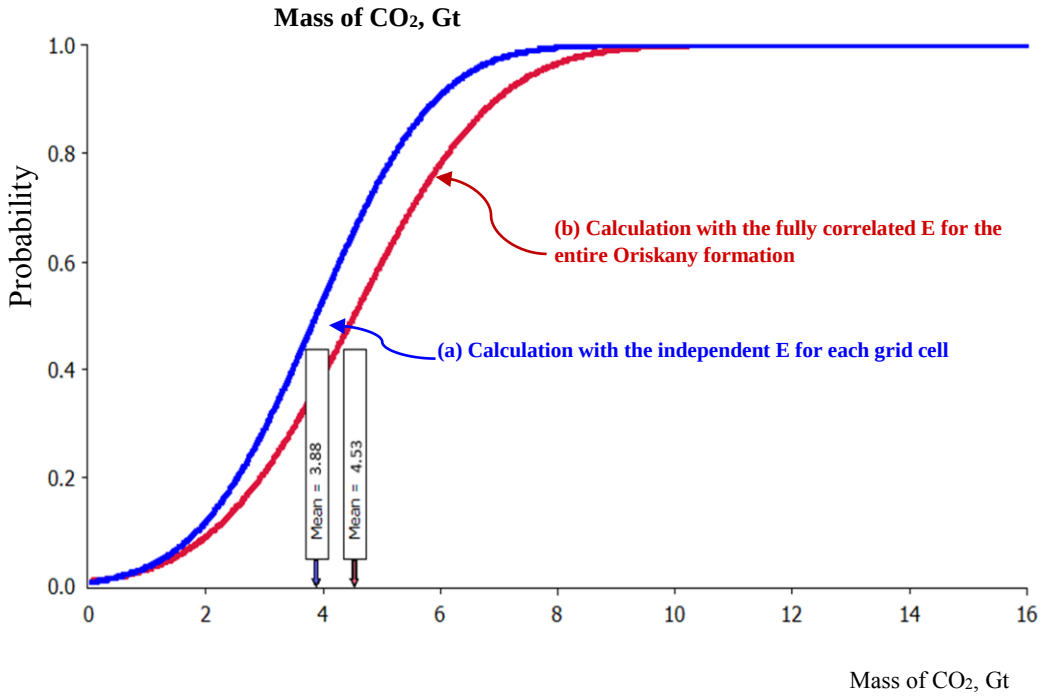

Figure B.1. CDFs of the simulated CO_2 storage resource of the Oriskany Formation (over 7930 grid cells, 5 by 5 km, n=1000 SGS realizations) calculated with (a) the independent E for each grid cell; and (b) the fully correlated E for the entire formation.

We use ArcGis 10.1 to prepare semivariogram specifications. We use Matlab to build a geostatistical model and perform SGS employing mGstat 0.991 (a geostatistical Matlab toolbox). MGstat provides an interface to gStat 2.4.5, which is an open source computer code for multivariate geostatistical modelling.

References

(1) Goodman, A.; Hakala, A.; Bromhal, G.; Deel, D.; Rodosta, T.; Frailey, S.; Small, M. J.; Allen, D.; Romanov, V.; Fazio, J.; Huerta, N.; McIntyre, D.; Kutchko, B.; Guthrie, G., U.S.

DOE methodology for development of geologic storage potential for carbon dioxide at the national and regional scale. *International Journal of Greenhouse Gas Control*, 2011, 5, 4, 952–965, http://www.sciencedirect.com/science/article/pii/S1750583611000405 (accessed February 24, 2013).

(2) IEA GHG (International Energy Agency Greenhouse Gas R&D Programme), *Development of Storage Coefficients for CO_2 Storage in Deep Saline Formations 2009/13*, 2009**,** http://www.ieaghg.org/, (accessed February 24, 2013).

Appendix C. EPA Cost Breakdowns for Geological CO_2 Sequestration Technology (Final rule)[9]

Table C. 1. Major Sources of GS Cost Information.

API Joint Association Survey of Drilling Costs	Drilling costs in the U.S. for oil, gas, and dry holes by depth interval
EIA Oil and Gas Lease Equipment and Operating	Surface equipment costs, annual operating costs, pump costs
Pipeline Prime Mover and Compressor Costs	Pumps
2009 Petroleum Services of Canada Well Cost Study	Canada drilling costs, plugging costs, logging costs
Oil and Gas Journal Report on Pipeline Cost Data	Pipeline costs per inch-mile
Land Rig Newsletter	Onshore day rates/ well cost algorithms
New Orleans Sequestration Technology Meeting, January, 2008	Monitor station costs in several categories; seismic costs
FutureGen Sequestration Site Materials	Monitoring station layout/number of stations
Preston Pipe Report	Casing and tubing costs
U.S. Bureau of Labor Statistics, American	Hourly labor rates
Selected presentations and papers (see below)	Sensor costs, monitoring costs, number of stations, seismic costs

[9] Environmental Protection Agency (EPA), 2010. Geological CO_2 Sequestration Technology and Cost Analysis (Technical Support Document No. EPA 816-R10-008). EPA Office of Water, Washington, DC.

Table C. 2. Geologic Site Characterization Unit Costs.

Tracking Number	Cost Item	Cost Algorithm	Data Sources
A-1	Develop maps and cross sections of local geologic structure	60 hours of geologists @$107.23/hr = $6,434 per site	AAPG 2009 salary survey of petroleum geologists
A-2	Conduct 3D seismic survey to identify faults and fractures in primary and secondary containment units	$104,000/square mile for good resolution	Several published reports are in range of this cost. Cost depends on resolution (number of lines shot) of survey.
A-3	Obtain and analyze seismic (earthquake) history.	60 hours of geologists @$107.23/hr = $6,434 per site	AAPG 2009 salary survey of petroleum geologists
A-4	Remote (aerial) survey of land, land uses, structures etc.. Should assume survey is twice the project's actual CO2 footprint due to uncertainty during site characterization phase of exact location of facilities and plume.	$3,100/site + $415/square mile surveyed. (Should assume survey is twice project's actual footprint.)	Advertised cost of an aerial survey company for high-resolution (1/2 meter).
A-5	Obtain data on areal extent, thickness, capacity, porosity and permeability of receiving formations and confining systems	24 hours of geologists @$107.23/hr = $2,574 per site	AAPG 2009 salary survey of petroleum geologists
A-6	Obtain geomechanical information on fractures, stress, rock strength, in situ fluid pressures (from existing data and literature)	120 hours of geologists @$107.23/hr = $12,868 per site	AAPG 2009 salary survey of petroleum geologists
A-7	Obtain geomechanical information on fractures, stress, rock strength, in situ fluid pressures (new cores and tests)	$78/foot for stratigraphic test well + $3,100/core	Drilling cost is estimated from drilling cost equations developed from JAS and PSAC data. Core analysis cost is best professional judgement.
A-8	List names and depth of all potentially affected USDWs	24 hours of geologists @$107.23/hr = $2,574 per site	AAPG 2009 salary survey of petroleum geologists
A-9	Provide geochemical information and maps/cross section on subsurface aquifers.	60 hours of geologists @$107.23/hr = $6,434 per site	AAPG 2009 salary survey of petroleum geologists

Tracking Number	Cost Item	Cost Algorithm	Data Sources
A-10	Provide information on water-rock-CO2 geochemistry and mineral reactions.	240 hours of geologists @$107.23/hr +$10,300 lab fees = $36,035 per site	Best professional judgement of time required and lab fee.
A-11	Develop list of penetrations into injection zone within AoR (from well history data bases)	12 hours @$107.23/hr = $1,287 per square mile	Best professional judgement of time required. Hourly rate derived from AAPG 2009 salary survey of petroleum geologists. Cost expected to vary widely
A-12	Develop list of penetrations into containment systems within AoR (from well history data bases)	12 hours @$107.23/hr = $1,287 per square mile	Best professional judgement of time required. Hourly rate derived from AAPG 2009 salary survey of petroleum geologists. Cost expected to vary widely based on well ages and quality of record keeping.
A-13	Develop list of water wells within AoR (from public data)	36 hours @$107.23/hr = $3,860 per square mile	Best professional judgement of time required. Hourly rate derived from AAPG 2009 salary survey of petroleum geologists. Cost expected to vary widely based on well ages and quality of record keeping.
A-14	Prepare geologic characterization report demonstrating: suitability of receiving zone, storage capacity and injectivity, trapping mechanism free of nonsealing faults, competent confining system, etc.	240 hours of geologists @$107.23/hr = $25,735 per site	Best professional judgement of time required. Hourly rate derived from AAPG 2009 salary survey of petroleum geologists.
A-15	Operating G&A	20% of annual operating costs	Best professional judgement based on oil and gas industry factors.

Table C. 3. Monitoring Unit Costs.

Tracking Number	Cost Item	Cost Algorithm	Data Sources
B-1	Develop geochemical baseline for injection zones and confining zone.	$207 per sample. Assume 4 samples per injection well = $828 per injection well	Lab analysis fee of $100 to $200 discussed in N.O. meeting.
B-2	Develop baseline of surface air CO2 flux for Eddy Covariance leakage monitoring.	$36,200 per station	Range of costs discussed at N.O. meeting Jan 2008 was $20,000 to $50,000 per station.
B-3a	Conduct front-end engineering and design (monitoring wells ABOVE injection zone)	$20,700 + $5,200/shallow monitoring well	Best professional judgement.
B-3b	Conduct front-end engineering and design (monitoring wells INTO injection zone)	$5,200/deep monitoring well	Best professional judgement.
B-4a	Obtain rights-of-way for surface uses. (monitoring wells ABOVE injection zone)	$10,400 per monitoring well site	Best judgement. Cost of land rights are highly variable.
B-4b	Obtain rights-of-way for surface uses. (monitoring wells INTO injection zone)	$10,400 per monitoring well site	Best judgement. Cost of land rights are highly variable.
B-5	Obtain rights-of-way for surface uses. (monitoring sites)	$5,200 per air monitoring station site (microseismic is done inside monitoring well and has no extra land costs)	Best judgement. Cost of land rights are highly variable.
B-6a	Downhole safety shut-off valve	$15,500 + $2.10/ft depth. Would be placed 100 or more feet above packer	Best professional judgement.
B-6b	Downhole check valve	$500	Best professional judgement.
B-7	Standard monitoring well stopping above the injection zone (used lookup table). Standard monitoring wells for ER projects stop below the injection zone.	Use look-up table. $/foot = $155 to $207 per foot typical down to 9,000 ft.	Drilling cost is estimated from drilling cost equations developed from JAS and PSAC data.
B-8	Standard monitoring well drilled into the injection zone (used lookup table); applies to RA 3-4 only).	Use look-up table. $/foot = $155 to $207 per foot typical down to 9,000 ft.	Drilling cost is estimated from drilling cost equations developed from JAS and PSAC data.

Tracking Number	Cost Item	Cost Algorithm	Data Sources
B-9a	Pressure, temperature, and resistivity gauges and related equipment for monitoring wells ABOVE injection zone	$10,400/well	Best professional judgement.
B-9b	Pressure, temperature, and resistivity gauges and related equipment for monitoring wells INTO injection zone	$10,400/well	Best professional judgement.
B-10a	Salinity, CO_2, tracer, etc. monitoring equipment for wells ABOVE injection zone (portion of equipment may be at surface such as for in situ sampling using U-tubes)	$10,400/well	Best professional judgement.
B-10b	Salinity, CO_2, tracer, etc. monitoring equipment for wells INTO injection zone (portion of equipment may be at surface such as for in situ sampling using U-tubes)	$10,400/well	Best professional judgement.
B-10c	ER Only. U-tube for sensing oil movement away from bottom of formation. Applies to 2 of 8 EOR wells.	$16/ft + $30,000 per well	Best professional judgement.
B-11a	Develop plan and implement Eddy Covariance air monitoring.	40 hours @$107.23/hr = $4,289 for plan plus $75,000/monitoring site	Best professional judgment of time required. Hourly rate derived from SPE 2009 salary survey of petroleum geologists. Monitoring station cost estimate from Benson 2004.
B-11b	Develop plan and implement Digital Color Infrared Orthoimagery (CIR) or Hyperspectral Imaging to detect changes to vegetation.	No construction costs, but planning and quality assurance costs would add $10,000 per square mile.	Best professional judgement.
B-11c	Develop plan and implement LIDAR airborne survey to detect surface leaks. Works best where vegetation is sparse.	No construction costs, but planning and quality assurance costs would add $10,000 per square mile.	Best professional judgement.

Tracking Number	Cost Item	Cost Algorithm	Data Sources
B-11d	Develop plan and implement soil zone monitoring	40 hours @$107.23/hr = $4,289 for plan plus $6,000/monitoring site	Best professional judgement.
B-11e	Develop plan and implement vadose zone monitoring wells to sample gas above water table.	40 hours @$107.23/hr = $4,289 for plan plus $8,000/monitoring site	Best professional judgement.
B-11f	Develop plan and implement monitoring wells for samples from water table.	40 hours @$107.23/hr = $4,289 for plan plus $80,000/monitoring site	Best professional judgement.
B-12	Conduct periodic monitoring of groundwater quality and geochemistry. (146.90(d) of GS Rule).	$200/sample and 4 samples per well = $800 per well plus 0.5 hours of engineer labor for sampling per well per month.	Lab analysis fee of $100 to $200 discussed in New Orleans mtg.
B-13	Surface microseismic detection equipment	$52,000/ site (geophone arrays go into monitoring wells)	Best professional judgement.
B-14a	Monitoring well O&M (ABOVE injection zone)	Annual O&M costs are $25,900 + $3.10/ft per well per year	Operating and maintenance costs adapted from EIA Oil and Gas Lease Equipment and Operating Cost estimates.
B-14b	Monitoring well O&M (INTO injection zone)	Annual O&M costs are $25,900 + $3.10/ft per well per year	Operating and maintenance costs adapted from EIA Oil and Gas Lease Equipment and Operating Cost estimates.
B-14c	ER Only; U-tube O&M; for 2 of 8 wells drilled 200 feet below injection zone	$10,000 per year base O&M costs plus monthly sampling (=12*8 hrs/sample * $110.62/hr + 12* $200 (chromatograph cost) per sample = $10,000 plus $13,019 for 12 samples annually per well.	Best professional judgement with reference to Benson, 2004
B-15a	Annual cost of air and soil surveys: Eddy Covariance	$10,000 per station per year	Best professional judgement with reference to Benson, 2004
B-15b	Annual cost of air and soil surveys: Digital Color Infrared Orthoimagery (CIR) or Hyperspectral Imaging to detect changes to vegetation.	Airborne survey costs of $6,250 per square mile plus mobilization costs of $5,000 per site.	Best professional judgement with reference to Benson, 2004

Tracking Number	Cost Item	Cost Algorithm	Data Sources
B-15c	Annual cost of air and soil surveys: LIDAR airborne survey to detect surface leaks. Works best where vegetation is sparse.	Airborne survey costs of $6,250 per square mile plus mobilization costs of $5,000 per site.	Best professional judgement with reference to Benson, 2004
B-15d	Annual cost of air and soil surveys: Soil zone monitoring	$200 lab fee per sample plus $100 to collect.	Best professional judgement with reference to Benson, 2004
B-15e	Annual cost of air and soil surveys: Vadose zone monitoring wells to sample gas above water table.	$200 lab fee per sample plus $100 to collect.	Best professional judgement with reference to Benson, 2004
B-15f	Annual cost of air and soil surveys: Monitoring wells for samples from water table.	$200 lab fee per sample plus $1,000 to collect.	Best professional judgement with reference to Benson, 2004
B-16	Annual cost of passive seismic equipment	$10,500 per station per year	Best professional judgement with reference to cited Mattoon site report
B-17	Periodic seismic surveys: 3D	$104,000/square mile for good resolution	Several published reports are in range of this cost. Cost depends on resolution (number of lines shot) of
B-18	Complex modeling of fluid flows and migration (reservoir simulations) over 100 years (RA0-3) or 10,000 years (RA4).	180 hours of engineers @$110.62/hr = $19,912 per site + 64 hours of engineers @$110.62/hr = $7,080 per injection well	Best judgement of time required. Hourly rate derived from SPE 2009 salary survey of petroleum geologists.
B-19	Annual reports to regulators and recordkeeping for all data gathering activities.	20 hours of engineers @$110.62/hr = $2,212 per report plus 24 hours annually of engineer labor @110.62 per hour = $2,655 for recordkeeping	Best judgement of time required. Hourly rate derived from SPE 2009 salary survey of petroleum geologists.
B-20	Semi-Annual (RA3) or quartery (RA4) reports to regulators and recordkeeping for all data gathering activities and recordkeeping.	15 hours of engineers @$110.62/hr = $1,659 per report plus 36 hours of engineer labor @$110.62/hr for recordkeeping = $3,982	Best judgement of time required. Hourly rate derived from SPE 2009 salary survey of petroleum geologists.

Tracking Number	Cost Item	Cost Algorithm	Data Sources
B-21	Monthly reports to regulators and recordkeeping for all data gathering activities and recordkeeping.	8 hours of engineers @$110.62/hr = $885 per report	Best judgement of time required. Hourly rate derived from SPE 2009 salary survey of petroleum geologists.
B-22	Operating G&A	20% of annual operating costs	Best professional judgement based on oil and gas industry factors.

Table C. 4. Injection Well Construction Unit Costs.

Tracking Number	Cost Item	Cost Algorithm	Data Sources
C-1	Conduct front-end engineering and design (general and	$207,000/site + $41,400/injection well	Best professional judgement.
C-2	Obtain rights-of-way for surface uses. (equipment, injection wells)	$20,700 per injection (pipeline right of ways included in pipeline costs) Half of cost is legal fees for developer, other half is bonus to landowner.	Best professional judgement. Cost of land rights are highly variable.
C-3	Lease rights for subsurface (pore space) use.	Upfront payment of $52/acre (additional injection fees under O&M costs)	Best professional judgement. Cost of land rights are highly variable.
C-4	Land use, air emissions, water discharge permits	$103,400/site + $20,700/square mile	Best professional judgement.
C-5	UIC permit filing, including preparation of attachments	$10,400/site + $6,000/injection well for first 5 wells at a site, then $2,000 thereafter	Best professional judgement.
C-6a	Standard injection well cost	Use look-up table. $/foot = $220 to $290 per foot typically down to 9,000 ft.	Drilling cost is estimated from drilling cost equations developed from JAS and PSAC data.
C-6b	Well stimulation	Total cost of stimulation based on cost per pound of proppant injected (coated sand); $1.25 /lb. of sand; 25,000 to 200,000 lbs per frac	Modified from PSAC cost study
C-7	Corrosion resistant tubing	Additional $1.15/foot length - inch diameter for glass reinforced epoxy (GRE) lining	Based on SPE article on economics o GRE tubing.

Tracking Number	Cost Item	Cost Algorithm	Data Sources
C-8	Corrosion resistant casing	Additional $1.81/foot length inch diameter (low alloy) or $2.70/ft (higher alloy) - for corrosion resistant casing	PSAC and Preston Pipe Report
C-9	Cement well from surface through base of lowermost USDW and throughout injection zone.	$1.20/foot length - inch diameter	Cementing cost based on 2008 PSAC Well Cost Study.
C-10	Use CO2-resistant cement	Adds 25% to total cementing costs	Best professional judgement.
C-13	Injection pressure limited to 90% of fracture pressure of injection formation	Affects maximum flow of well, number of wells needed	Due to uncertainty of injectability, this pressure impact is ignored.
C-14	Pumps	$1550/HP. Installation of electrical service adds $20,700 per well site.	Electrification cost based on EIA Oil and Gas Lease Equipment and Operating Cost estimates. Pump costs based on pipeline prime mover and compressor cost reported to FERC.
C-15	Wellhead and Control Equipment	Cost per well is $520*(maximum tons per day injected per well)^0.6	Based on 2008 PSAC Well Cost Study.
C-16	All elements of pipeline costs	$83,000/inch-mile	From pipeline cost data reported to FERC. Published annually in Oil and Gas Journal.
C-17	Operating G&A	20% of annual operating costs	Best professional judgement based on oil and gas industry factors.

Table C. 5. Area of Review and Corrective Action Unit Costs.

Tracking Number	Cost Item	Cost Algorithm	Data Sources
D-1	Simple fluid flow calculations to predict CO_2 fluid flow.	36 hours of engineers @$110.62/hr = $3982 per site + 12 hours of engineers @$110.62/hr = $1327 per injection well	Best professional judgement of time required. Hourly rate may change based on labor survey data.

Tracking Number	Cost Item	Cost Algorithm	Data Sources
D-2	Complex modeling of CO_2 fluid flows and migration (reservoir simulations) over 100 years	180 hours of engineers @$110.62/hr = $19,912 per site + 24 hours of engineers @$110.62/hr = $2,655 per injection well	Best professional judgement of time required. Hourly rate derived from SPE 2009 salary survey of petroleum geologists.
D-3	Complex modeling of CO_2 fluid flows and migration (reservoir simulations) over 10,000 years	180 hours of engineers @$110.62/hr = $19,912 per site + 36 hours of engineers @$110.62/hr = $3,982 per injection well	Best professional judgement of time required. Hourly rate derived from SPE 2009 salary survey of petroleum geologists.
D-4	Areal search for old wells (artificial penetrations)	helicopter magnetic survey requires about 9 hours/square mile @$1,240 per hour. Cost = $5,200 mobilization + $11,160 per square mile. Follow-up ground surveys will add another $2,070 per square mile. (helicopter survey interline spacing is about 80 feet with speed of 10 ft/sec)	Based on DOE sponsored research at Salt Creek WY . Helicopter hourly rate is in range of several published estimates, adjusted for fuel costs.
D-5	Evaluate integrity of construction and record of completion and/or plugging of existing wells that penetrate containment system.	24 hours @$107.23/hr = $2,574 per site + 6 hours @$110.62/hr = $664 per well	Best judgement of time required. Hourly rate derived from AAPG 2009 salary survey of petroleum geologists.
D-6	Evaluate integrity of construction and record of completion and/or plugging of existing shallow wells that pose a treat to USDWs.	6 hours @$110.62/hr = $664 per well	Best professional judgement of time required. Hourly rate derived from SPE 2009 salary survey of petroleum geologists.
D-7	Remediate old wells in AoR that pose a risk to USDWs	$31,200 for clean out, $13,500 to replug and $11,400 to log (two cement plugs - one in producing formation and one for surface to bottom of USDWs, remainder of borehole filled with mud). Water well remediation is $20,700.	Plugging and logging cost based on 2008 and 2009 PSAC Well Cost Studies. Clean out cost will vary widely. Cost here is 3 days of rig use @ $10,400 per day. Rig cost from Land Rig Newsletter US Land Rig Rates

Tracking Number	Cost Item	Cost Algorithm	Data Sources
D-8	Remediate old wells in AoR that lack high quality cementing information	$31,200 for clean out, $13,500 to replug and $11,400 to log (two cement plugs - one in producing formation and one for surface to bottom of USDWs, remainder of borehole filled with mud). Water well remediation is $20,700.	Plugging and logging cost based on 2008 and 2009 PSAC Well Cost Studies. Clean out cost will vary widely. Cost here is 3 days of rig use @ $10,400 per day. Rig cost from Land Rig Newsletter US Land Rig Rates
D-9	Operating G&A	20% of annual operating costs	Best professional judgement based on oil and gas industry factors.

Table C.6. Well Operation Unit Costs.

Tracking Number	Cost Item	Cost Algorithm	Data Sources
E-1	Develop a corrosion monitoring and prevention program	24 hours of engineers @$110.62/hr = $2655 per site	Best professional judgement of time required. Hourly rate derived from SPE
E-2	Corrosion monitoring; quarterly analysis of injectate stream and measurement of corrosion of well material coupons.	6 hours a@ $110.62/hr= $663.72/well plus $25/well (quarterly) plus $300 per sample (4 samples per injection well)	Best professional judgement.
E-3	Continuous measurement / monitoring equipment: injected volumes, pressure, flow rates and annulus	$15,500/well	Best professional judgement.
E-4	Equipment to add tracers	$10,400/well	Best professional judgement.
E-5	Electricity cost for pump, equipment	$0.066/kWh	2007 average industrial sector electricity price reported by EIA.
E-6	Injection well O&M	Annual O&M costs are $77,500 + $3.10/ft per well per year	Operating and maintenance cost based on EIA Oil and Gas Lease Equipment and Operating Cost estimates.

Tracking Number	Cost Item	Cost Algorithm	Data Sources
E-7	Land use rent, rights-of-way	$5.20/acre/year	Best professional judgement based on oil & gas industry costs. Cost of land rights are highly variable.
E-8	Pore space use costs	$0.052/barrel or about $0.36 per metric ton	Best professional judgement based on oil & gas industry costs. Cost of land rights are highly variable.
E-9	Property Taxes & Insurance	$0.03/$1CAPEX	Best professional judgement.
E-10	Tracers in injected fluid	$0.05/ton of CO2 injected	Best professional judgement. Cost will depend of type of tracer.
E-12	Repair, replace wells and equipment	Assume 1%/year of initial well and eequipment cost	Best professional judgement
E-13	General failure of containment at site: cost to remove and relocate CO_2	Assuming a 1% chance of failure over injection life, then approximately 0.083% of total capital costs each year would cover such a contingency	Best professional judgement
E-14	Operating G&A	20% of annual operating costs	Best professional judgement based on oil and gas industry factors.

Table C. 7. Mechanical Integrity Tests Unit Costs.

Tracking Number	Cost Item	Cost Algorithm	Data Sources
F-1	Internal mechanical integrity pressure tests	$2,070/test	Best professional judgement.
F-2	Casing inspection log	$2,070 plus $4.15/foot	Studies for wireline log suite. Cost of MIT log could be lower.

Tracking Number	Cost Item	Cost Algorithm	Data Sources
F-3	Conduct a tracer survey of the bottom-hole cement using a CO2-soluble isotope	$5,200/test	Best professional judgement.
F-5	External mechanical integrity tests to detect flow adjacent to well using temperature or noise log	$2,070 plus $4.15/foot	Based on 2008 PSAC Well Cost Study for wireline log suite. Cost of external MIT log could be lower.
F-6	External mechanical integrity tests to detect flow adjacent to well using temperature or noise log	$2,070 plus $4.15/foot	Based on 2008 PSAC Well Cost Study for wireline log suite. Cost of external MIT log could be lower.
F-7	Conduct pressure fall-off test	$2,070/test	Best professional judgement.
F-9	Operating G&A	0% of annual operating costs	Best professional judgement based on oil and gas industry factors.

Table C. 8. Well Plugging, Equipment Removal, and PISC Costs.

Tracking Number	Cost Item	Cost Algorithm	Data Sources
G-1	Flush wells with a buffer fluid before closing	$1000 + $0.085/inch-foot casing diameter	Best professional judgement.
G-2	Plug injection wells (done to all wells)	$13,500 to plug and $11,400 to log (two cement plugs - one in injection formation and one for surface to bottom of USDWs, remainder of borehole filled with mud)	Plugging and logging cost based on 2008 PSAC Well Cost Study.
G-3	Perform a mechanical integrity test prior to plugging to evaluate integrity of casing and cement to remain in ground	$2,070 plus $4.15/foot	Based on 2008 PSAC Well Cost Study for wireline log suite.

Tracking Number	Cost Item	Cost Algorithm	Data Sources
G-4a	Plug monitoring wells ABOVE injection zone	$6,700 to plug and $5,700 to log (one cement plugs - surface to bottom of USDWs, remainder of borehole filled with mud)	Plugging and logging cost based on 2008 PSAC Well Cost Study.
G-4b	Plug monitoring wells INTO injection zone	$6,700 to plug and $5,700 to log (one cement plugs - surface to bottom of USDWs, remainder of borehole filled with mud)	Plugging and logging cost based on 2008 PSAC Well Cost Study.
G-5	Remove surface equipment, structures, restore vegetation (injection wells)	$25,900/injection well	Best professional judgement.
G-6a	Remove surface equipment, structures, restore vegetation (monitoring wells ABOVE injection zone)	$10,400/monitoring well, $5,200 for monitoring stations	Best professional judgement.
G-6b	Remove surface equipment, structures, restore vegetation (monitoring wells INTO injection zone)	$10,400/monitoring well, $5,200 for monitoring stations	Best professional judgement.
G-7	Document plugging and closure process (well plugging, post- injection plans, notification of intent to close, post-closure report)	120 hours of engineers @$110.62/hr = $13,274 per site	Best professional judgement of time required. Hourly rate derived from SPE 2009 salary survey of petroleum geologists.
G-8a	Post-closure monitoring well O&M (ABOVE injection zone)	Annual O&M costs are $25,900 + $3.10/ft per well per year	Operating and maintenance costs adapted from EIA Oil and Gas Lease Equipment and Operating Cost estimates.
G-8b	Post-closure monitoring well O&M (INTO injection zone)	Annual O&M costs are $25,900 + $3.10/ft per well per year	Operating and maintenance costs adapted from EIA Oil and Gas Lease Equipment and Operating Cost estimates.
G-9	Post-injection air and soil surveys	$10,400 per station per year	Best professional judgement.
G-10	Post-closure seismic survey	$104,000/square mile for good resolution	Several published reports are in range of this cost. Cost depends on resolution (number of lines shot) of survey.

Tracking Number	Cost Item	Cost Algorithm	Data Sources
G-11	Periodic post-injection monitoring reports to regulators	40 hours @$110.62/hr = $4,425 per report	Best professional judgement of time required. Hourly rate derived from SPE 2009 salary survey of petroleum geologists.
G-12	Operating G&A	20% of annual operating costs	Best professional judgement based on oil and gas industry factors.

References

(1) Carbon Capture and Storage: A Regulatory Framework for States – Summary of Recommendations,, by Kevin Bliss, Interstate Oil and Gas Compact Commission, January, 2005.

(2) Carbon Dioxide Storage: Geological Security and Environmental Issues – Case Study on the Sleipner Field, Norway, S. Soloman, Bellona Foundation, May, 2007.

(3) Carbon Sequestration Technology Roadmap and Program Plan 2007, Ensuring the Future of Fossil Energy Systems through the Successful Deployment of Carbon Capture and Storage Technologies, U.S. Department of Energy, Office of Fossil Energy, National Energy Technology Laboratory, 2007.

(4) CO_2 Storage in Saline Aquifers, by M. Bentham and G. Kirby, Oil and Gas Science and Technology, vol. 60, no. 3, 2005.

(5) Determination of the Mechanical Integrity of Injection Wells, EPA Region 5 website, www.epa.gov/region5/water/uic/r5guid/r5_05.htm

(6) Discussion Paper: Identifying Gaps in CO_2 Monitoring and Verification of Storage, by B. Reynen, M. Wilson, N. Riley, T. Manai, O. M. Mathiassen, and S. Holloway, A Task Force under the Technical Group of the Carbon Sequestration Leadership Foru, (CSLF), Paper No. CSLF-T-2005-3, Presented at the Technical Group Meeting, April 30, 2005.

(7) Economic Evaluation of CO_2 Storage and Sink Options, by B. R. Bock, R. Rhudy, H. Herzog, M. Klett, J. Davison, D. De la Torre Ugarte, and D. Simbeck, DOE Research Report DE-FC26-

(8) 00NT40937, February, 2003.

(9) GEO-SEQ Best Practices Manual, Geologic Carbon Dioxide Sequestration: Site Evaluation to Implementation, by the GEO-SEQ Project Team, Earth Sciences Division, Lawrence Berkeley National Laboratory, Berkeley, California, September 30, 2004.

(10) Investigation of Novel Geophysical Techniques for Monitoring CO_2

Movement during Sequestration, Final Report No. 822176, by G. M. Hoversten and E. Gasperikova, Lawrence Berkeley National Laboratory, Berkeley California, October 2003.

(11) IPCC, 2005: IPCC Special Report on Carbon Dioxide Capture and Storage, by Working Group III of the Intergovernmental Panel on Climate Change [B. Metz, O. Davidson, H. C. de Coninck, M. Loos, and L. A. Meyer (eds.)], Cambridge University Press, Cambridge, United Kingdom and New York, NY, USA, 442 pp.

(12) Joint Association Survey of Drilling Costs, American Petroleum Institute, Washington, DC. http://www.api.org/statistics/accessapi/api-reports.cfm

(13) Matoon Site Environmental Information Volume, FutureGen Alliance,www.futuregenalliance.org, December 1, 2006.

(14) Measurement, Monitoring, and Verification, L. H. Spangler, Zero Emission Research and

(15) Technology Center, Carbon Sequestration Leadership Forum, date unknown.

(16) Measuring and Modeling for Site Characterization: A Global Approach, D. Vu-Hoang, L. Jammes, O. Faivre, and T.S. Ramakrishnan, Schlumberger Carbon Services, March, 2006.

(17) Monitoring Carbon Dioxide Sequestration in Deep Geological Formations for Inventory Verification and Carbon Credits, Paper SPE102833, by S. M. Benson, Earth Sciences Division, Lawrence Berkeley National Laboratory, for SPE ATCE, San Antonio, Texas, September 26, 2006.

(18) Monitoring Geologically Sequestered CO_2 during the Frio Brine Pilot Test using Perfluorocarbon Tracers, by S. D. McCallum, D. E. Reistenberg, D. R. Cole, B. M. Freifeld, R. C. Trautz, S. D. Hovorka, and T. J. Phelps, Conference Proceedings, Fourth Annual Conference on Carbon Capture and Sequestration, DOE/NETL, May 2-5, 2005.

(19) Monitoring of Aquifer Disposal of CO_2: Experience from Underground Gas Storage and Enhanced

(20) Oil Recovery, by W. D. Gunter, Alberta Research Council, R. J. Chalaturnyk, University of

(21) Alberta, and J. D. Scott, University of Alberta, for Alberta Research Council, Edmonton, Alberta, Canada.

(22) Monitoring of Sequestered CO_2: Meeting the Challenge with Emerging Geophysical Technologies, S.N. Dasgupta, Saudi Aramco, 2005.

(23) Monitoring Protocols and Life-Cycle Costs for Geologic Storage of Carbon Dioxide, by S. M. Benson, Lawrence Berkeley National Laboratory, for Carbon Sequestration Leadership Forum, Melbourne, Australia, September 13-15, 2004.

(24) Monitoring Protocols and Life-Cycle Costs for Geologic Storage of Carbon Dioxide, by S. M. Benson, M. Hoversten, and E. Gasperikova of Lawrence Berkeley National Laboratory, and M. Haines of EA Greenhouse Gas R&D Programme, Proceedings of the 7th International Conference on Greenhouse Gas Control Technologies (GHGT-7), September 5–9, 2004, Vancouver, Canada, v. II, 1259-1266, 2005.

(25) Monitoring to Ensure Safe and Effective Geological Sequestration of Carbon Dioxide, S. Benson and L. Myer, Lawrence Berkeley Laboratory, Berkeley, California, 2002.

(26) Oil and Gas Lease Equipment and Operating Costs, U.S. Energy Information Administration,

(27) 2006, http://www.eia.doe.gov/pub/oil_gas/natural_gas/data_publications/cost_indices_equipment_produc tion/current/coststudy.html

(28) Oil and Gas Journal Pipeline Cost Survey, Oil and Gas Journal Magazine, September 3, 2007.

(29) Overview of Monitoring Requirements for Geologic Storage Projects, IEA Greenhouse Gas

(30) Programme, Report No. PH4/29, November, 2004.

(31) Overview of Monitoring Techniques and Protocols for Geological Storage Projects, S. M. Benson, E. Gasperikova, and G. M. Hoversten, IEA Greenhouse Gas R&D Program report, 2004.

(32) PSAC Well Cost Study – 2008, Petroleum Services Association of Canada, October 30, 2007.

(33) Report on Monitoring Workshop, organized by IEA Greenhouse Gas R&D Programme and BP with the support of EPRI and the U.S. DOE/NETL, at University of California at Santa Cruz, November 8-9, 2004.

(34) Reservoir Monitoring Methods and Installation Practices, by G. V. Chalifoux and R. M. Taylor, Petrospec Engineering Ltd., CADE eNews, February 2007.

(35) SACS – 2, Work Package 4, Monitoring Well Scenarios, by I. M. Carlsen, S. Mjaaland, and F. Nyhavn, SINTEF Petroleum Research, Trondheim, Norway, for SACS group, April 6, 2001.

(36) Sensitivity and Cost of Monitoring Geologic Sequestration Using Geophysics, by L. R. Myer, G. M. Hoversten, and E. Gasperikova, Lawrence Berkeley National Laboratory, Berkeley California, Proceedings of the 6th International Conference on Greenhouse Gas Control Technologies (GHGT-6), J. Gale and Y. Kaya (eds.), 1-4 October 2002, Kyoto, Japan, Pergamon, Vol. 1, pp. 377-382, 2003.

(37) Summary of Carbon Dioxide Enhanced Oil Recovery (CO_2EOR) Injection Well Technology, supporting information provided by J. P. Meyer, Contek Solutions, for

the American Petroleum Institute, 2007.

(38) Surface Environmental Monitoring at the Frio CO_2 Sequestration Test Site, Texas, H.S. Nance, Texas Bureau of Economic Geology, Austin, Texas, DOE/NETL Conference on Carbon Capture and Storage, May, 2005.

(39) Technology Status Review – Monitoring Technologies for the Geological Storage of CO_2, Report No. COAL R285 DTI/Pub URN 05/1033, by J. Pearce, A. Chadwick, M. Bentham, S. Holloway, and G. Kirby, British Geological Survey, Coordinator of the European Network of Excellence on Underground CO_2 Storage (CO_2GeoNet), Keyworth, Nottingham, UK, March 2005.

(40) The Economics of CO_2 Storage, Gemma Heddle, Howard Herzog, and Michael Klett, Laboratory for Energy and the Environment, Massachusetts Institute of Technology, August, 2003.

(41) The Future of Coal, Options for a Carbon-constrained World, An Interdisciplinary MIT Study, Massachusetts Institute of Technology, 2007.

(42) The U-Tube – Novel System for Sampling and Analyzing Mult-Phase Borehole Fluid Samples, by Barry M. Freifeld, et al, Lawrence Berkely National Laboratory, Berkely, CA. (publication date unknown).

(43) UIC Pressure Falloff Requirements, USEPA Region 9, August, 2002.

(44) UIC Program Mechanical Integrity Testing: Lessons for Carbon Capture and Storage, Jonathan Koplos, Bruce Kobelski, Anhar Karimjee, and Chi Ho Sham, Fifth Annual Conference on Carbon Capture and Sequestration, DOE/NETL, May, 2006.

(45) Underground Injection Control Rules, www.bogc.dnrc.state.mt.us/uicrules.htm.

Appendix D. Summary of Cost Calculation for CO_2 Sequestration and Storage in the Oriskany Formation

Table D. 1. Summary of capital and O&M expenditures including fixed and cost-on depth components over the CO_2 sequestration project lifetime.

Timeline	Project Phase	Expenditure, $		Summary of steps Expenditure, $		
0 year				*steps 1-4*	*steps 1-4 and 8*	steps 1-7
Capital cost	**1. Site Characterization**	**1,505,370**	*fixed*	**5,922,925**	**5,994,752**	**6,912,149**
		274	*on-depth*	**2,936**	**2,968**	**3,056**
	2. Review	**247,346**	*fixed*			
	3. Inj well construction					
		3,187,162	*fixed*			
		2,019	*on-depth*			
	4. Monitor well, survey station construction					
		983,046	*fixed*			
		643	*on-depth*			
Injection 1-3 years	**5. Inj well O&M**	**702,910**	*fixed*	*steps 5-6*		
		22	*on-depth*	**989,224**		
	6. MIT	**39,932**	*fixed*	**120**		
		87	*on-depth*			
	7. Monitoring O&M	**246,382**	*fixed*			
		11	*on-depth*			
	seismic surveys: 3D every 5 years	**1,003,600**	*fixed*			
				step 8		
	8. Inj well plugging	**71,827**	*fixed*	**71,827**		
				32		
		32	*on-depth*			

Timeline	Project Phase	Expenditure, $		Summary of steps Expenditure, $
Post-injection monitoring 50 years	**9. Post inj monitoring O&M**	**145,765**	*fixed*	*steps 9 and 10* **1,534,121**
Closure	**10. Monitor well plugging final seismic survey**	**1,388,356**	*fixed*	

Table D. 2. Total costs by cost component (fixed and cost-on depth), Period of injection 0 year using 10%, 15%, and 20% discount rates.

Dis-count rate	0.10			0.15			0.20		
Year	Cash flow $	fixed Present value $	On-depth Current value $	Current value $	fixed Present value $	On-depth Current value $	Current value $	fixed Present value $	On-depth Current value $
0	6,912,149	6,912,149	3,055	6,912,149	6,912,149	3,055	6,912,149	6,912,149	3,055
1	217,592	197,811	31	217,592	189,210	31	217,592	181,326	31
2	145,765	120,467		145,765	110,219		145,765	101,226	
3	145,765	109,515		145,765	95,843		145,765	84,355	
4	145,765	99,559		145,765	83,342		145,765	70,296	
5	145,765	90,508		145,765	72,471		145,765	58,580	
6	145,765	82,280		145,765	63,018		145,765	48,816	
7	145,765	74,800		145,765	54,798		145,765	40,680	
8	145,765	68,000		145,765	47,651		145,765	33,900	
9	145,765	61,819		145,765	41,435		145,765	28,250	
10	145,765	56,199		145,765	36,031		145,765	23,542	
11	145,765	51,090		145,765	31,331		145,765	19,618	
12	145,765	46,445		145,765	27,244		145,765	16,348	
13	145,765	42,223		145,765	23,691		145,765	13,624	
14	145,765	38,384		145,765	20,601		145,765	11,353	
15	145,765	34,895		145,765	17,914		145,765	9,461	

Dis-count rate	0.10			0.15			0.20		
Year	Cash flow $	fixed Present value $	On-depth Current value $	Current value $	fixed Present value $	On-depth Current value $	Current value $	fixed Present value $	On-depth Current value $
16	145,765	31,723		145,765	15,577		145,765	7,884	
17	145,765	28,839		145,765	13,545		145,765	6,570	
18	145,765	26,217		145,765	11,779		145,765	5,475	
19	145,765	23,834		145,765	10,242		145,765	4,563	
20	145,765	21,667		145,765	8,906		145,765	3,802	
21	145,765	19,697		145,765	7,745		145,765	3,168	
22	145,765	17,907		145,765	6,734		145,765	2,640	
23	145,765	16,279		145,765	5,856		145,765	2,200	
24	145,765	14,799		145,765	5,092		145,765	1,834	
25	145,765	13,454		145,765	4,428		145,765	1,528	
26	145,765	12,230		145,765	3,850		145,765	1,273	
27	145,765	11,119		145,765	3,348		145,765	1,061	
28	145,765	10,108		145,765	2,911		145,765	884	
29	145,765	9,189		145,765	2,532		145,765	737	
30	145,765	8,354		145,765	2,201		145,765	614	
31	145,765	7,594		145,765	1,914		145,765	512	
32	145,765	6,904		145,765	1,665		145,765	426	
33	145,765	6,276		145,765	1,448		145,765	355	
34	145,765	5,706		145,765	1,259		145,765	296	
35	145,765	5,187		145,765	1,095		145,765	247	
36	145,765	4,715		145,765	952		145,765	206	
37	145,765	4,287		145,765	828		145,765	171	
38	145,765	3,897		145,765	720		145,765	143	
39	145,765	3,543		145,765	626		145,765	119	
40	145,765	3,221		145,765	544		145,765	99	
41	145,765	2,928		145,765	473		145,765	83	

Dis-count rate	0.10			0.15			0.20		
Year	Cash flow $	fixed Present value $	On-depth Current value $	Current value $	fixed Present value $	On-depth Current value $	Current value $	fixed Present value $	On-depth Current value $
42	145,765	2,662		145,765	411		145,765	69	
43	145,765	2,420		145,765	358		145,765	57	
44	145,765	2,200		145,765	311		145,765	48	
45	145,765	2,000		145,765	271		145,765	40	
46	145,765	1,818		145,765	235		145,765	33	
47	145,765	1,653		145,765	205		145,765	28	
48	145,765	1,502		145,765	178		145,765	23	
49	145,765	1,366		145,765	155		145,765	19	
50	1,388,356	10,752		1,388,356	1,114		1,388,356	127	
	NPV	**8,433,429** fixed	**3,085** On-depth		**7,946,590** fixed	**3,084** On-depth		**7,700,876** fixed	**3,083** On-depth

Table D. 3. Total costs by cost component (fixed and cost-on depth), Period of injection 1 year using 10%, 15%, and 20% discount rates.

Dis-count rate	0.10			0.15			0.20		
Year	Cash flow $	fixed Present value $	On-depth Current value $	Current value $	fixed Present value $	On-depth Current value $	Current value $	fixed Present value $	On-depth Current value $
0	5,922,925	5,922,925	2,936	5,922,925	5,922,925	2,936	5,922,925	5,922,925	2,936
1	989,224	899,295	120	989,224	860,195	120	989,224	824,354	120
2	217,592	179,828	32	217,592	164,531	32	217,592	151,105	32
3	145,765	109,515		145,765	95,843		145,765	84,355	
4	145,765	99,559		145,765	83,342		145,765	70,296	
5	145,765	90,508		145,765	72,471		145,765	58,580	
6	145,765	82,280		145,765	63,018		145,765	48,816	
7	145,765	74,800		145,765	54,798		145,765	40,680	

Dis-count rate	0.10			0.15			0.20		
Year	Cash flow $	fixed Present value $	On-depth Current value $	Current value $	fixed Present value $	On-depth Current value $	Current value $	fixed Present value $	On-depth Current value $
8	145,765	68,000		145,765	47,651		145,765	33,900	
9	145,765	61,819		145,765	41,435		145,765	28,250	
10	145,765	56,199		145,765	36,031		145,765	23,542	
11	145,765	51,090		145,765	31,331		145,765	19,618	
12	145,765	46,445		145,765	27,244		145,765	16,348	
13	145,765	42,223		145,765	23,691		145,765	13,624	
14	145,765	38,384		145,765	20,601		145,765	11,353	
15	145,765	34,895		145,765	17,914		145,765	9,461	
16	145,765	31,723		145,765	15,577		145,765	7,884	
17	145,765	28,839		145,765	13,545		145,765	6,570	
18	145,765	26,217		145,765	11,779		145,765	5,475	
19	145,765	23,834		145,765	10,242		145,765	4,563	
20	145,765	21,667		145,765	8,906		145,765	3,802	
21	145,765	19,697		145,765	7,745		145,765	3,168	
22	145,765	17,907		145,765	6,734		145,765	2,640	
23	145,765	16,279		145,765	5,856		145,765	2,200	
24	145,765	14,799		145,765	5,092		145,765	1,834	
25	145,765	13,454		145,765	4,428		145,765	1,528	
26	145,765	12,230		145,765	3,850		145,765	1,273	
27	145,765	11,119		145,765	3,348		145,765	1,061	
28	145,765	10,108		145,765	2,911		145,765	884	
29	145,765	9,189		145,765	2,532		145,765	737	
30	145,765	8,354		145,765	2,201		145,765	614	
31	145,765	7,594		145,765	1,914		145,765	512	
32	145,765	6,904		145,765	1,665		145,765	426	
33	145,765	6,276		145,765	1,448		145,765	355	

Dis-count rate	**0.10**			**0.15**			**0.20**		
Year	Cash flow $	fixed Present value $	On-depth Current value $	Current value $	fixed Present value $	On-depth Current value $	Current value $	fixed Present value $	On-depth Current value $
34	145,765	5,706		145,765	1,259		145,765	296	
35	145,765	5,187		145,765	1,095		145,765	247	
36	145,765	4,715		145,765	952		145,765	206	
37	145,765	4,287		145,765	828		145,765	171	
38	145,765	3,897		145,765	720		145,765	143	
39	145,765	3,543		145,765	626		145,765	119	
40	145,765	3,221		145,765	544		145,765	99	
41	145,765	2,928		145,765	473		145,765	83	
42	145,765	2,662		145,765	411		145,765	69	
43	145,765	2,420		145,765	358		145,765	57	
44	145,765	2,200		145,765	311		145,765	48	
45	145,765	2,000		145,765	271		145,765	40	
46	145,765	1,818		145,765	235		145,765	33	
47	145,765	1,653		145,765	205		145,765	28	
48	145,765	1,502		145,765	178		145,765	23	
49	145,765	1,366		145,765	155		145,765	19	
50	145,765	1,242		145,765	135		145,765	16	
51	1,388,356	10,752		1,388,356	1,114		1,388,356	127	
	NPV	**8,205,050** fixed	**3,072** On-depth		**7,682,662** fixed	**3,065** On-depth		**7,404,559** fixed	**3,058** On-depth

Table D. 4. Total costs by cost component (fixed and cost-on depth), Period of injection 2 years using 10%, 15%, and 20% discount rates.

Dis-count rate	0.10			0.15			0.20		
Year	Cash flow $	fixed Present value $	On-depth Current value $	Current value $	fixed Present value $	On-depth Current value $	Current value $	fixed Present value $	On-depth Current value $
0	5,922,925	5,922,925	2,936	5,922,925	5,922,925	2,936	5,922,925	5,922,925	2,936
1	989,224	899,295	120	989,224	860,195	120	989,224	824,354	120
2	989,224	817,541	120	989,224	747,996	120	989,224	686,961	120
3	217,592	163,480	32	217,592	143,070	32	217,592	125,921	32
4	145,765	99,559		145,765	83,342		145,765	70,296	
5	145,765	90,508		145,765	72,471		145,765	58,580	
6	145,765	82,280		145,765	63,018		145,765	48,816	
7	145,765	74,800		145,765	54,798		145,765	40,680	
8	145,765	68,000		145,765	47,651		145,765	33,900	
9	145,765	61,819		145,765	41,435		145,765	28,250	
10	145,765	56,199		145,765	36,031		145,765	23,542	
11	145,765	51,090		145,765	31,331		145,765	19,618	
12	145,765	46,445		145,765	27,244		145,765	16,348	
13	145,765	42,223		145,765	23,691		145,765	13,624	
14	145,765	38,384		145,765	20,601		145,765	11,353	
15	145,765	34,895		145,765	17,914		145,765	9,461	
16	145,765	31,723		145,765	15,577		145,765	7,884	
17	145,765	28,839		145,765	13,545		145,765	6,570	
18	145,765	26,217		145,765	11,779		145,765	5,475	
19	145,765	23,834		145,765	10,242		145,765	4,563	
20	145,765	21,667		145,765	8,906		145,765	3,802	
21	145,765	19,697		145,765	7,745		145,765	3,168	
22	145,765	17,907		145,765	6,734		145,765	2,640	
23	145,765	16,279		145,765	5,856		145,765	2,200	
24	145,765	14,799		145,765	5,092		145,765	1,834	
25	145,765	13,454		145,765	4,428		145,765	1,528	
26	145,765	12,230		145,765	3,850		145,765	1,273	
27	145,765	11,119		145,765	3,348		145,765	1,061	
28	145,765	10,108		145,765	2,911		145,765	884	
29	145,765	9,189		145,765	2,532		145,765	737	
30	145,765	8,354		145,765	2,201		145,765	614	
31	145,765	7,594		145,765	1,914		145,765	512	
32	145,765	6,904		145,765	1,665		145,765	426	
33	145,765	6,276		145,765	1,448		145,765	355	
34	145,765	5,706		145,765	1,259		145,765	296	
35	145,765	5,187		145,765	1,095		145,765	247	
36	145,765	4,715		145,765	952		145,765	206	
37	145,765	4,287		145,765	828		145,765	171	

Dis-count rate	0.10			0.15			0.20		
Year	Cash flow $	fixed Present value $	On-depth Current value $	Current value $	fixed Present value $	On-depth Current value $	Current value $	fixed Present value $	On-depth Current value $
38	145,765	3,897		145,765	720		145,765	143	
39	145,765	3,543		145,765	626		145,765	119	
40	145,765	3,221		145,765	544		145,765	99	
41	145,765	2,928		145,765	473		145,765	83	
42	145,765	2,662		145,765	411		145,765	69	
43	145,765	2,420		145,765	358		145,765	57	
44	145,765	2,200		145,765	311		145,765	48	
45	145,765	2,000		145,765	271		145,765	40	
46	145,765	1,818		145,765	235		145,765	33	
47	145,765	1,653		145,765	205		145,765	28	
48	145,765	1,502		145,765	178		145,765	23	
49	145,765	1,366		145,765	155		145,765	19	
50	145,765	1,242		145,765	135		145,765	16	
51	145,765	1,242		145,765	135		145,765	16	
52	1,388,356	10,752		1,388,356	1,114		1,388,356	127	
	NPV	**8,896,728** fixed	**3,169** On-depth		**8,313,355** fixed	**3,152** On-depth		**7,981,981** fixed	**3,138** On-depth

Table D. 5. Total costs by cost component (fixed and cost-on depth), Period of injection 3 years using 10%, 15%, and 20% discount rates.

Dis-count rate	0.10			0.15			0.20		
Year	Cash flow $	fixed Present value $	On-depth Current value $	Cash flow $	fixed Present value $	On-depth Current value $	Cash flow $	fixed Present value $	On-depth Current value $
0	5,922,925	5,922,925	2,936	5,922,925	5,922,925	2,936	5,922,925	5,922,925	2,936
1	989,224	989,224	120	989,224	989,224	120	989,224	989,224	120
2	989,224	989,224	120	989,224	989,224	120	989,224	989,224	120
3	989,224	989,224	120	989,224	989,224	120	989,224	989,224	120
4	217,592	217,592	32	217,592	217,592	32	217,592	217,592	32
5	145,765	145,765		145,765	145,765		145,765	145,765	
6	145,765	145,765		145,765	145,765		145,765	145,765	
7	145,765	145,765		145,765	145,765		145,765	145,765	

Dis-count rate	0.10			0.15			0.20		
		fixed	On-depth		fixed	On-depth		fixed	On-depth
Year	Cash flow	Present value	Current value	Cash flow	Present value	Current value	Cash flow	Present value	Current value
	$	$	$	$	$	$	$	$	$
8	145,765	145,765		145,765	145,765		145,765	145,765	
9	145,765	145,765		145,765	145,765		145,765	145,765	
10	145,765	145,765		145,765	145,765		145,765	145,765	
11	145,765	145,765		145,765	145,765		145,765	145,765	
12	145,765	145,765		145,765	145,765		145,765	145,765	
13	145,765	145,765		145,765	145,765		145,765	145,765	
14	145,765	145,765		145,765	145,765		145,765	145,765	
15	145,765	145,765		145,765	145,765		145,765	145,765	
16	145,765	145,765		145,765	145,765		145,765	145,765	
17	145,765	145,765		145,765	145,765		145,765	145,765	
18	145,765	145,765		145,765	145,765		145,765	145,765	
19	145,765	145,765		145,765	145,765		145,765	145,765	
20	145,765	145,765		145,765	145,765		145,765	145,765	
21	145,765	145,765		145,765	145,765		145,765	145,765	
22	145,765	145,765		145,765	145,765		145,765	145,765	
23	145,765	145,765		145,765	145,765		145,765	145,765	
24	145,765	145,765		145,765	145,765		145,765	145,765	
25	145,765	145,765		145,765	145,765		145,765	145,765	
26	145,765	145,765		145,765	145,765		145,765	145,765	
27	145,765	145,765		145,765	145,765		145,765	145,765	
28	145,765	145,765		145,765	145,765		145,765	145,765	
29	145,765	145,765		145,765	145,765		145,765	145,765	
30	145,765	145,765		145,765	145,765		145,765	145,765	
31	145,765	145,765		145,765	145,765		145,765	145,765	
32	145,765	145,765		145,765	145,765		145,765	145,765	
33	145,765	145,765		145,765	145,765		145,765	145,765	
34	145,765	145,765		145,765	145,765		145,765	145,765	
35	145,765	145,765		145,765	145,765		145,765	145,765	
36	145,765	145,765		145,765	145,765		145,765	145,765	
37	145,765	145,765		145,765	145,765		145,765	145,765	
38	145,765	145,765		145,765	145,765		145,765	145,765	
39	145,765	145,765		145,765	145,765		145,765	145,765	
40	145,765	145,765		145,765	145,765		145,765	145,765	
41	145,765	145,765		145,765	145,765		145,765	145,765	
42	145,765	145,765		145,765	145,765		145,765	145,765	

Dis-count rate	**0.10**			**0.15**			**0.20**		
		fixed	On-depth		fixed	On-depth		fixed	On-depth
Year	Cash flow	Present value	Current value	Cash flow	Present value	Current value	Cash flow	Present value	Current value
	$	$	$	$	$	$	$	$	$
43	145,765	145,765		145,765	145,765		145,765	145,765	
44	145,765	145,765		145,765	145,765		145,765	145,765	
45	145,765	145,765		145,765	145,765		145,765	145,765	
46	145,765	145,765		145,765	145,765		145,765	145,765	
47	145,765	145,765		145,765	145,765		145,765	145,765	
48	145,765	145,765		145,765	145,765		145,765	145,765	
49	145,765	145,765		145,765	145,765		145,765	145,765	
50	145,765	145,765		145,765	145,765		145,765	145,765	
51	145,766	145,766		145,766	145,766		145,766	145,766	
52	145,767	145,767		145,767	145,767		145,767	145,767	
53	1,388,358	1,388,358		145,768	145,768		145,768	145,768	
	NPV	**9,525,525**	**3,257**		**8,861,783**	**3,229**		**8,463,167**	**3,204**
		fixed	On-depth		fixed	On-depth		fixed	On-depth

Appendix E. Matlab code script: calculation of CO_2 storage resource for a porous sedimentary formation

```
%% Versions v4b

% Code writing: Stephen Rose, Carnegie Mellon University, 2013
% Geostatistical modeling: Olga Popova, Carnegie Mellon University, 2013
% Note: before running this code in Matlab two additional tools should be
% downloaded: mGstat: a geostatistical Matlab toolbox, available at
% http://sourceforge.net/projects/mgstat/files/mGstat/
% and Gstat, an open source computer code for multivariate geostatistical
% modelling, available at: http://www.gstat.org/index.html
% See Matlab instructions at: http://mgstat.sourceforge.net/htmldoc/ch03.html


clear all


%%%%%%%%%%%%%%%%%%%%%%%%%
show_diagnostic = false;
norm_transform = true;

% Input file layout
lat_col = 2;  % What column of the input data is that latitude in?
lon_col = 3;  % What column of the input data is that latitude in?
raw_data_col = 4; % What column contains the raw data of interest?
transformed_data_col = 5; % What column contains the tranformed data of interest

% Output file information
output_filename = 'Oriskany_GSS_output';
xvalid_filename = 'Oriskany_cross_validation';

% Ask user to under some simulation parameters
prompt = {'Enter number of realizations:','Enter grid size [km]:','Enter efficiency
factor(s):','Enter minimum depth [m]:','Enter random number seed:'};
dlg_title = 'Inputs for Sequential Gaussian Simulation';
num_lines = 1;
def = {'20','5','[0.01, 0.02, 0.05]', '800', num2str(round(1e5*rand))}; % Default random
seed is random
answer = inputdlg(prompt,dlg_title,num_lines,def);

validateattributes(str2num(answer{1}), {'numeric'}, {'positive', 'integer','scalar'})
k_num_realizations = str2num(answer{1}); % Number of Sequential Gaussian Simulations
sim_params.num_sims = k_num_realizations;
```

```
validateattributes(str2num(answer{2}), {'numeric'}, {'positive','scalar'})
k_grid_size = km2deg(str2num(answer{2})); % grid size (input is km, output is deg.)

validateattributes(str2num(answer{3}), {'numeric'}, {'>', 0, '<=', 1})
E = str2num(answer{3}); % efficiency factor for CO2 in pore space

validateattributes(str2num(answer{4}), {'numeric'}, {'>=', 0, 'scalar'})
k_min_depth = str2num(answer{4}); % Minimum depth to calculate CO2 storage capacity

validateattributes(str2num(answer{5}), {'numeric'}, {'scalar'})
my_rand_seed = str2num(answer{5});


% Other Simulation parameters
k_max_neighbors = 12; % max number of neighboring locations to use in calculation
sim_params.max_neighbors = k_max_neighbors;
k_min_neighbors = 3; % max number of neighboring locations to use in calculation
sim_params.min_neighbors = k_min_neighbors;
k_min_distance = 0.5; % Minimum allowable distance between sampling locations. If they
are closer, they will be averaged together and one thrown out [km]

% Gstat parameters
k_no_data_val = -9999;

% Filenames
k_filename_base = 'Oriskany_GSS_';

% Constants for CO2 properties
T_crit = 304.1282; % [K]parishioner.
P_crit = 7.3773e6; % [Pa]

klatlimit=[35, 50];
klonglimit=[-90, -70];

%% Select a working directory to store all the generated files
working_dir = uigetdir('', 'Select the working directory to store all the generated files.');


%% Import the data
% Assumptions:
% Latitude in "lat_col"
% Longitude in "lon_col"
% Transformed data in "transformed_data_col"
% Raw data in "raw_data_col"

    % 1. Import depth [meters]
```

```
   [FileName,PathName,~] = uigetfile('*.xlsx','Select the Depth data'); % Write a comment
here
   [num, txt, ~] = xlsread(fullfile(PathName, FileName));
   temp.lat = num(:,lat_col);
   temp.lon = num(:,lon_col);
   temp.values = num(:,raw_data_col);
   out_data = avgNearby( temp, km2deg(k_min_distance) );

   depth_data.lat = out_data.lat;
   depth_data.lon = out_data.lon;
   if norm_transform
      [depth_data.values,depth_data.nscore_obj]=nscore( out_data.values);
   else
      depth_data.values =  out_data.values;
   end

   clear FileName PathName num txt temp out_data

   % 2. Import thinkness [meters]
   [FileName,PathName,~] = uigetfile('*.xlsx','Select the Thickness data'); % Write a
comment here
   [num, txt, ~] = xlsread(fullfile(PathName, FileName));
   temp.lat = num(:,lat_col);
   temp.lon = num(:,lon_col);
   temp.values = num(:,raw_data_col);
   out_data = avgNearby( temp, km2deg(k_min_distance) );

   thickness_data.lat = out_data.lat;
   thickness_data.lon = out_data.lon;
   if norm_transform
      [thickness_data.values,thickness_data.nscore_obj]=nscore(log(out_data.values));
   else
      thickness_data.values = out_data.values;
   end
   clear FileName PathName num txt temp out_data

   % 3. Import logit-porosity residuals [unitless]
   [FileName,PathName,~] = uigetfile('*.xlsx','Select the Porosity data'); % Write a
comment here
   [num, txt, ~] = xlsread(fullfile(PathName, FileName));
   temp.lat = num(:,lat_col);
   temp.lon = num(:,lon_col);
   temp.values = num(:,transformed_data_col);
   out_data = avgNearby( temp, km2deg(k_min_distance) );

   logit_porosity_resid_data.lat = out_data.lon;
```

```
   logit_porosity_resid_data.lon = out_data.lat;
   if norm_transform
      [logit_porosity_resid_data.values,
logit_porosity_resid_data.nscore_obj]=nscore(out_data.values);
   else
      logit_porosity_resid_data.values = out_data.values;
   end

%     porosity_data.lat = num(:,lat_col);
%     porosity_data.lon = num(:,lon_col);
%     porosity_data.values = num(:,raw_data_col);

   % Not necessary to do norm transform here because these aren't unsed in Seq. Gaussian
Sim.

   clear FileName PathName num txt temp out_data

%     if show_diagnostic
%        figure
%        dx = usamap(klatlimit, klonglimit);
%        states = shaperead('usastatehi','UseGeoCoords', true, 'BoundingBox', [klonglimit',
klatlimit']);
%        geoshow(states, 'FaceColor', [1, 1, 1])
%        textm(states.LabelLat, states.LabelLon, states.Name,'HorizontalAlignment',
'center')
%        scatterm(dx, porosity_data.lat, porosity_data.lon, 8, porosity_data.values, 'filled')
%        colorbar
%        title('Measured Porosity')
%     end


   % 4. Import temperature residuals [K]
   [FileName,PathName,~] = uigetfile('*.xlsx','Select the Temperature residuals'); % Write
a comment here
   [num, txt, ~] = xlsread(fullfile(PathName, FileName));
   temp.lat = num(:,lat_col);
   temp.lon = num(:,lon_col);
   temp.values = num(:,transformed_data_col);
   out_data = avgNearby( temp, km2deg(k_min_distance) );

   temp_resid_data.lat = out_data.lat;
   temp_resid_data.lon = out_data.lon;
   if norm_transform
      [temp_resid_data.values, temp_resid_data.nscore_obj]=nscore(out_data.values);
   else
      temp_resid_data.values = out_data.values;
```

```
    end
    clear FileName PathName num txt temp out_data

    % 5. Import pressure residuals [MPa]
    [FileName,PathName,~] = uigetfile('*.xlsx','Select the Pressure data'); % Write a
comment here
    [num, txt, ~] = xlsread(fullfile(PathName, FileName));
    temp.lat = num(:,lat_col);
    temp.lon = num(:,lon_col);
    temp.values = num(:,transformed_data_col);
    out_data = avgNearby( temp, km2deg(k_min_distance) );

    press_resid_data.lat = out_data.lat;
    press_resid_data.lon = out_data.lon;
    if norm_transform
       [press_resid_data.values, press_resid_data.nscore_obj]=nscore(out_data.values);
    else
       press_resid_data.values = out_data.values;
    end

%     press_data.lat = num(:,lat_col); % Not necessary to do norm transform here because
these aren't unsed in Seq. Gaussian Sim.
%     press_data.lon = num(:,lon_col);
%     press_data.values = num(:,raw_data_col);
    clear FileName PathName num txt temp out_data


%% Plot the measurement locations
% figure
% ax = usamap(klatlimit, klonglimit);
%  states = shaperead('usastatehi','UseGeoCoords', true, 'BoundingBox', [klonglimit',
klatlimit']);
% geoshow(states, 'FaceColor', [1, 1, 1])
% textm(states.LabelLat, states.LabelLon, states.Name,'HorizontalAlignment', 'center')
%
% scatterm(ax, depth_data.lat, depth_data.lon, 8, depth_data.values, 'filled')
% colorbar

%% Calculate and plot semivar
% k_num_bins = 50;
% x_dist=deg2km(depth_data.lon-min(depth_data.lon))*1000; % convert long to meters,
we use south-west corner
% y_dist=deg2km(depth_data.lat-min(depth_data.lat))*1000; % convert lat to meters
% pos=[x_dist,y_dist]; % create position matrix
% [gamma,h,ang_center,gamma_cloud,h_cloud]=semivar_exp(pos,depth_data.values,
k_num_bins); %calculate semivar
```

```
% figure
% plot(h,gamma, 'b.-'); %plot semivar
% xlabel('distance in meters')
% ylabel('semivariance')
% title ('Semivariogram of Depth, [m]')
%
% % Group points
% bin_edges = linspace(0, max(h_cloud), k_num_bins+1);
% bin_centers = bin_edges(1:end-1) + 0.5*(bin_edges(2:end) - bin_edges(1:end-1));
% bin_num = zeros(size(h_cloud));
% for k = 1:k_num_bins
%     in_bin = (h_cloud > bin_edges(k)) & (h_cloud <= bin_edges(k+1));
%     bin_num(in_bin) = k;
% end
% % figure, boxplot(gamma_cloud, bin_num)
% bin_mean = grpstats(gamma_cloud, bin_num);
% figure, plot(bin_centers ,bin_mean, 'b.-')



%% create grid for kriging
temp_grid_vertex.lat =
min(depth_data.lat):k_grid_size:max(depth_data.lat)+2*k_grid_size; %create vector of lat
with "k_grid_size" step. Add constant at end to ensure grid is bigger
temp_grid_vertex.lon =
min(depth_data.lon):k_grid_size:max(depth_data.lon)+2*k_grid_size; %create vector of
lon with 1km step
[vertex_grid.deg.lon,vertex_grid.deg.lat] = meshgrid(temp_grid_vertex.lon,
temp_grid_vertex.lat); %create 2 matrices with lat for each point and with lon for each
point d

%% Determine which points are in Oriskany formation
[FileName, PathName, ~] = uigetfile('*.shp', 'Select the Oriskany extent shapefile');
[S, A] = shaperead(fullfile(PathName, FileName));
      figure

      states = shaperead('usastatehi','UseGeoCoords', true, 'BoundingBox', [klonglimit',
klatlimit']);
      ax = usamap(klatlimit, klonglimit);
      geoshow(states, 'FaceColor', [1, 1, 1])
      for k=1:numel(S)
         geoshow(ax, S(k).Y, S(k).X, 'DisplayType', 'polygon')
      end
      clear ax states

in_Oriskany = zeros(size(vertex_grid.deg.lon));
```

```
for k = 1:length(S)
   IN = inpolygon(vertex_grid.deg.lon, vertex_grid.deg.lat, S(k).X, S(k).Y);
   in_Oriskany = in_Oriskany | IN;
end

grid_in_Oriskany = k_no_data_val*ones(size(vertex_grid.deg.lon));
grid_in_Oriskany(in_Oriskany) = 1;
   mask_Oriskany = grid_in_Oriskany(end:-1:1, :); % Reverse order of rows for Gstat.

in_Oriskany_flipped = in_Oriskany(end:-1:1, :); % Reverse order of rows for the output
files

mask.lat = vertex_grid.deg.lat;
mask.lon = vertex_grid.deg.lon;
mask.pred_OK = grid_in_Oriskany;
mask.grid_size = k_grid_size;

clear grid_in_Oriskany

%% 1. Run GSS for depth
   % Specify the Semivariogram model structure and parameters (from ArcGIS)
   depth_semivar_model.V(1).par1 = 0; % Calculated by ArcGIS for depth
   depth_semivar_model.V(1).par2 = 0;
   depth_semivar_model.V(1).type = 'Nug';
   depth_semivar_model.V(1).itype = 0;
   depth_semivar_model.V(2).par1 = 407850; % Calculated by ArcGIS for depth, based on
ordinary kriging
%     depth_semivar_model.V(2).par1 = 1.6327; % Calculated by ArcGIS for depth
   depth_semivar_model.V(2).par2 = 370610;
   depth_semivar_model.V(2).type = 'Exp';
   depth_semivar_model.V(2).itype = 1;

    % Cross-validation
   [ depth_xvalid ] = crossValid(depth_data, depth_semivar_model, sim_params,
'depth_xvalid', working_dir);
   xlswrite(xvalid_filename, [depth_xvalid.lat, depth_xvalid.lon, depth_xvalid.obs,
depth_xvalid.pred], 'Depth');
   if show_diagnostic
      figure, plot(depth_xvalid.obs, depth_xvalid.pred, 'b.')
      xlabel('Observed (m)'), ylabel('Predicted (m)')
      title('Depth Cross-validation')
      max_x = max(depth_xvalid.obs);
      min_x = min(depth_xvalid.obs);
      max_y = max(depth_xvalid.pred);
      min_y = min(depth_xvalid.pred);
      my_max = max(max_x, max_y);
```

```
        my_min = min(min_x, min_y);
        xlim([my_min my_max]), ylim([my_min my_max])
        hold on, plot([my_min, my_max], [my_min, my_max], 'm-'), hold off
    end

    % Run the Gaussian Sequential Simulation
    if norm_transform
        [ depth_pred_norm ] = GaussianSequentialSimulation(depth_data, mask,
depth_semivar_model, sim_params, 'depth', working_dir, my_rand_seed);
        depth_pred.lat = depth_pred_norm.lat;
        depth_pred.lon = depth_pred_norm.lon;
        depth_pred.values = inscore(depth_pred_norm.values , depth_data.nscore_obj); %
Inverse of normal score transform
    else
        [ depth_pred ] = GaussianSequentialSimulation(depth_data, mask,
depth_semivar_model, sim_params, 'depth', working_dir, my_rand_seed);
    end

    % Calculate mask to exclude grid cells with depth < k_min_depth
    depth_mask_2D = (mean(depth_pred.values, 3) >= k_min_depth);
    depth_mask_3D = zeros(size(depth_pred.values));
    for k = 1:size(depth_pred.values, 3)
        depth_mask_3D(:,:,k) = depth_mask_2D;
    end

%% 2. Run GSS for thickness
    % Specify the Semivariogram model structure and parameters (from ArcGIS)
    thick_semivar_model.V(1).par1 = 7.4323;  % Calculated by ArcGIS for depth
    thick_semivar_model.V(1).par2 = 0;
    thick_semivar_model.V(1).type = 'Nug';
    thick_semivar_model.V(1).itype = 0;
    thick_semivar_model.V(2).par1 = 11.328; % Calculated by ArcGIS for thickness
    thick_semivar_model.V(2).par2 = 32159;
    thick_semivar_model.V(2).type = 'Exp';
    thick_semivar_model.V(2).itype = 1;

    % Cross-validation
    [ thick_xvalid ] = crossValid(thickness_data, thick_semivar_model, sim_params,
'thick_xvalid', working_dir);
    xlswrite(xvalid_filename, [thick_xvalid.lat, thick_xvalid.lon, thick_xvalid.obs,
thick_xvalid.pred], 'Thickness');
    if show_diagnostic
        figure, plot(thick_xvalid.obs, thick_xvalid.pred, 'b.')
        xlabel('Observed (m)'), ylabel('Predicted (m)')
        title('Thickness Cross-validation')
        max_x = max(thick_xvalid.obs);
```

```
    min_x = min(thick_xvalid.obs);
    max_y = max(thick_xvalid.pred);
    min_y = min(thick_xvalid.pred)
    my_max = max(max_x, max_y);
    my_min = min(min_x, min_y);
    xlim([my_min my_max]), ylim([my_min my_max])
    hold on, plot([my_min, my_max], [my_min, my_max], 'm-'), hold off
  end


  % Run the Gaussian Sequential Simulation
  if norm_transform
    [ thickness_pred_norm ] = GaussianSequentialSimulation(thickness_data, mask,
thick_semivar_model, sim_params, 'thick', working_dir, my_rand_seed);
    thickness_pred.lat = thickness_pred_norm.lat;
    thickness_pred.lon = thickness_pred_norm.lon;
    thickness_pred.values = exp(thickness_inscore(thickness_pred_norm.values ,
thickness_data.nscore_obj)); % Inverse of normal score transform
  else
    [ thickness_pred ] = GaussianSequentialSimulation(thickness_data, mask,
thick_semivar_model, sim_params, 'thick', working_dir, my_rand_seed);
  end

%% 3. Porosity
%   3a. Run GSS for logit porosity residuals
  % Specify the Semivariogram model structure and parameters (from ArcGIS)
  poros_semivar_model.V(1).par1 = 0.27472; % Calculated by ArcGIS for residuals of
logit-transformed porosity
  poros_semivar_model.V(1).par2 = 0;
  poros_semivar_model.V(1).type = 'Nug';
  poros_semivar_model.V(1).itype = 0;
  poros_semivar_model.V(2).par1 = 0.19515; % Calculated by ArcGIS for residuals of
logit-transformed porosity
  poros_semivar_model.V(2).par2 = 51462;
  poros_semivar_model.V(2).type = 'Exp';
  poros_semivar_model.V(2).itype = 1;


% Cross-validation
  % It appears that there is no spatial pattern in the residuals of the
  % logit-transformed porosity, so doing kriging to interpolate those
  % values probably doesn't add anything. It's probably sufficient just
  % to calculate porosity from the regression and add a random error
  % term. However, it shouldn't change anthing to leave in the kriging of
  % residuals. 2013 June 5
```

```
   [ poros_xvalid ] = crossValid(logit_porosity_resid_data, poros_semivar_model,
sim_params, 'poros_xvalid', working_dir);
   xlswrite(xvalid_filename, [poros_xvalid.lat, poros_xvalid.lon, poros_xvalid.obs,
poros_xvalid.pred], 'LT Porosity Residuals');
   if show_diagnostic
      figure, plot(poros_xvalid.obs, poros_xvalid.pred, 'b.')
      xlabel('Observed'), ylabel('Predicted')
      title('LT Porosity Residuals Cross-validation')
      max_x = max(poros_xvalid.obs);
      min_x = min(poros_xvalid.obs);
      max_y = max(poros_xvalid.pred);
      min_y = min(poros_xvalid.pred)
      my_max = max(max_x, max_y);
      my_min = min(min_x, min_y);
      xlim([my_min my_max]), ylim([my_min my_max])
      hold on, plot([my_min, my_max], [my_min, my_max], 'm-'), hold off
   end

   % Run the Gaussian Sequential Simulation
   if norm_transform
      [ pred_logit_porosity_resid_norm ] =
GaussianSequentialSimulation(logit_porosity_resid_data, mask, poros_semivar_model,
sim_params, 'poros', working_dir, my_rand_seed);
      pred_logit_porosity_resid.lat = pred_logit_porosity_resid_norm.lat;
      pred_logit_porosity_resid.lon = pred_logit_porosity_resid_norm.lon;
      pred_logit_porosity_resid.values = inscore(pred_logit_porosity_resid_norm.values ,
logit_porosity_resid_data.nscore_obj); % Inverse of normal score transform
   else
      [ pred_logit_porosity_resid ] =
GaussianSequentialSimulation(logit_porosity_resid_data, mask, poros_semivar_model,
sim_params, 'poros', working_dir, my_rand_seed);
   end

%   3b. Combine regrssion model with GSS residuals (Appalachia)
   reg_model_logit_porosity = -2.182215-0.000198*depth_pred.values; % Olga calculated
this model by regressing logit-tranformed porosity vs depth.
   if show_diagnostic
      reg_model_porosity.lat = pred_logit_porosity_resid.lat;
      reg_model_porosity.lon = pred_logit_porosity_resid.lon;
      reg_model_porosity.values = 1./(exp(-reg_model_logit_porosity));   % Undo the logit
transform

      figure
      dx = usamap(klatlimit, klonglimit);
      states = shaperead('usastatehi','UseGeoCoords', true, 'BoundingBox', [klonglimit',
klatlimit']);
```

```
        geoshow(states, 'FaceColor', [1, 1, 1])
%       textm(states.LabelLat, states.LabelLon, states.Name,'HorizontalAlignment',
'center')
        scatterm(dx, reshape(reg_model_porosity.lat, [], 1), reshape(reg_model_porosity.lon,
[], 1), 8, reshape(mean(reg_model_porosity.values,3), [] , 1), 'filled')
        colorbar
        title('Porosity, calculated from logit-porisity as linear function of depth')
    end



    logit_porosity = reg_model_logit_porosity + pred_logit_porosity_resid.values; % Add
the residuals from the Gaussian Sequential Simulations

    porosity_pred.lat = pred_logit_porosity_resid.lat;
    porosity_pred.lon = pred_logit_porosity_resid.lon;
    porosity_pred.values = 1./(exp(-logit_porosity)); % Un-do the logit transformation to get
porosity

    clear reg_model_logit_porosity  logit_porosity

%% 4. Temperature
%   4a. Run GSS for temperature residuals
    % Specify the Semivariogram model structure and parameters (from ArcGIS)
    temp_semivar_model.V(1).par1 = 0; % Calculated by ArcGIS for depth
    temp_semivar_model.V(1).par2 = 0;
    temp_semivar_model.V(1).type = 'Nug';
    temp_semivar_model.V(1).itype = 0;
    temp_semivar_model.V(2).par1 = 10.97; % Calculated by ArcGIS for temperature
residuals
    temp_semivar_model.V(2).par2 = 386.5861;
    temp_semivar_model.V(2).type = 'Exp';
    temp_semivar_model.V(2).itype = 1;

    % Cross-validation
    [ temp_xvalid ] = crossValid( temp_resid_data, temp_semivar_model, sim_params,
'temp_xvalid', working_dir);
    xlswrite(xvalid_filename, [temp_xvalid.lat, temp_xvalid.lon, temp_xvalid.obs,
temp_xvalid.pred], 'Temperature Residuals');
    if show_diagnostic
        figure, plot(temp_xvalid.obs, temp_xvalid.pred, 'b.')
        xlabel('Observed (K)'), ylabel('Predicted (K)')
        title(' Temperature Residuals Cross-validation')
        max_x = max(temp_xvalid.obs);
        min_x = min(temp_xvalid.obs);
        max_y = max(temp_xvalid.pred);
```

```
    min_y = min(temp_xvalid.pred)
    my_max = max(max_x, max_y);
    my_min = min(min_x, min_y);
    xlim([my_min my_max]), ylim([my_min my_max])
    hold on, plot([my_min, my_max], [my_min, my_max], 'm-'), hold off
  end

  % Run the Gaussian Sequential Simulation
  if norm_transform
    [ pred_temperature_resid_norm ] = GaussianSequentialSimulation(temp_resid_data,
mask, temp_semivar_model, sim_params, 'temp', working_dir, my_rand_seed);
    pred_temperature_resid.lat = pred_temperature_resid_norm.lat;
    pred_temperature_resid.lon = pred_temperature_resid_norm.lon;
    pred_temperature_resid.values = inscore(pred_temperature_resid_norm.values ,
temp_resid_data.nscore_obj); % Inverse of normal score transform
  else
    [ pred_temperature_resid ] = GaussianSequentialSimulation(temp_resid_data, mask,
temp_semivar_model, sim_params, 'temp', working_dir, my_rand_seed);
  end

%   4b. Combine regression model with GSS residuals (Appalachia)
  reg_model_temp.values = 282.47+0.021309595*depth_pred.values; % Olga calculated
this model by regressing temperature vs depth.
  if show_diagnostic
    reg_model_temp.lat = pred_temperature_resid.lat;
    reg_model_temp.lon = pred_temperature_resid.lon;

    figure
    dx = usamap(klatlimit, klonglimit);
    states = shaperead('usastatehi','UseGeoCoords', true, 'BoundingBox', [klonglimit',
klatlimit']);
    geoshow(states, 'FaceColor', [1, 1, 1])
%       textm(states.LabelLat, states.LabelLon, states.Name,'HorizontalAlignment',
'center')
    scatterm(dx, reshape(reg_model_temp.lat, [], 1), reshape(reg_model_temp.lon, [], 1), 8,
reshape(mean(reg_model_temp.values,3), [] , 1), 'filled')
    colorbar
    title('Temperature, calculated as linear function of depth [K]')
  end

  temperature_pred.values = reg_model_temp.values + pred_temperature_resid.values; %
Add the residuals from the Gaussian Sequential Simulations

  temperature_pred.lat = pred_temperature_resid.lat;
  temperature_pred.lon = pred_temperature_resid.lon;
```

```
clear reg_model_temp


%% 5. Pressure
%   5a. Run GSS for pressure residuals
   % Specify the Semivariogram model structure and parameters (from ArcGIS)
   press_semivar_model.V(1).par1 = 0.0087054; % Calculated by ArcGIS for depth
   press_semivar_model.V(1).par2 = 0;
   press_semivar_model.V(1).type = 'Nug';
   press_semivar_model.V(1).itype = 0;
   press_semivar_model.V(2).par1 = 1.794; % Calculated by ArcGIS for pressure residuals
   press_semivar_model.V(2).par2 = 223370;
   press_semivar_model.V(2).type = 'Exp';
   press_semivar_model.V(2).itype = 1;

     % Cross-validation
   [ press_xvalid ] = crossValid(press_resid_data, press_semivar_model, sim_params,
'press_xvalid', working_dir);
   xlswrite(xvalid_filename, [press_xvalid.lat, press_xvalid.lon, press_xvalid.obs,
press_xvalid.pred], 'Pressure Residuals');
   if show_diagnostic
      figure, plot(press_xvalid.obs, press_xvalid.pred, 'b.')
      xlabel('Observed (MPa)'), ylabel('Predicted (MPa)')
      title('Pressure Residuals Cross-validation')
      max_x = max(press_xvalid.obs);
      min_x = min(press_xvalid.obs);
      max_y = max(press_xvalid.pred);
      min_y = min(press_xvalid.pred)
      my_max = max(max_x, max_y);
      my_min = min(min_x, min_y);
      xlim([my_min my_max]), ylim([my_min my_max])
      hold on, plot([my_min, my_max], [my_min, my_max], 'm-'), hold off
   end

   % Run the Gaussian Sequential Simulation
   if norm_transform
      [ pred_pressure_resid_norm ] = GaussianSequentialSimulation(press_resid_data,
mask, press_semivar_model, sim_params, 'press', working_dir, my_rand_seed);
      pred_pressure_resid.lat = pred_pressure_resid_norm.lat;
      pred_pressure_resid.lon = pred_pressure_resid_norm.lon;
      pred_pressure_resid.values = inscore(pred_pressure_resid_norm.values ,
press_resid_data.nscore_obj); % Inverse of normal score transform
   else
      [ pred_pressure_resid ] = GaussianSequentialSimulation(press_resid_data, mask,
press_semivar_model, sim_params, 'press', working_dir, my_rand_seed);
   end
```

```
%   5b. Combine regrssion model with GSS residuals (Appalachia)
   reg_model_press.values = 2.028251097 +0.003343143*depth_pred.values; % Olga
calculated this model by regressing pressure vs depth. [MPa]
   if show_diagnostic
      reg_model_press.lat = pred_pressure_resid.lat;
      reg_model_press.lon = pred_pressure_resid.lon;

      figure
      dx = usamap(klatlimit, klonglimit);
      states = shaperead('usastatehi','UseGeoCoords', true, 'BoundingBox', [klonglimit',
klatlimit']);
      geoshow(states, 'FaceColor', [1, 1, 1])
%       textm(states.LabelLat, states.LabelLon, states.Name,'HorizontalAlignment',
'center')
      scatterm(dx, reshape(reg_model_press.lat, [], 1), reshape(reg_model_press.lon, [], 1),
8, reshape(mean(reg_model_press.values,3), [] , 1), 'filled')
      colorbar
      title('Pressure, calculated as linear function of depth [Mpa]')
   end

   pressure_pred.values = reg_model_press.values + pred_pressure_resid.values; % Add
the residuals from the Gaussian Sequential Simulations

   pressure_pred.lat = pred_pressure_resid.lat;
   pressure_pred.lon = pred_pressure_resid.lon;

   clear reg_model_temp

%% Plot some example results
   % 1. Depth
   figure
   subplot(3,1,1)
   ax(1) = usamap(klatlimit, klonglimit);
   states = shaperead('usastatehi','UseGeoCoords', true, 'BoundingBox', [klonglimit',
klatlimit']);
   geoshow(states, 'FaceColor', [1, 1, 1])
%    textm(states.LabelLat, states.LabelLon, states.Name,'HorizontalAlignment', 'center')
   scatterm(ax(1), depth_data.lat, depth_data.lon, 8, depth_data.values, 'filled')
   tightmap
   colorbar
   title('Measured Depth, [m]')


%% Export simulation results to Excel spreadsheet
% Each worksheet is a variable,
```

```
% each row is a location
% each column is a simulation

   % 1. Depth [m]
   temp_depth = reshape(depth_pred.values, size(depth_pred.values,
1)*size(depth_pred.values, 2), size(depth_pred.values, 3)); % reshape
%     in_Oriskany = ~any(isnan(temp_depth), 2);
   temp_coords = [reshape(depth_pred.lat, [],1) reshape(depth_pred.lon, [],1)];
   if (size(temp_depth, 1) > 65000) | (size(temp_depth, 2) > 250)  % Too many rows or
columns for Excel 2003
      csvwrite([output_filename '_Depth'], [temp_coords(in_Oriskany_flipped, :),
temp_depth(in_Oriskany_flipped, :)]);
   else
      xlswrite(output_filename, [temp_coords(in_Oriskany_flipped, :),
temp_depth(in_Oriskany_flipped, :)], 'Depth');
   end

   clear temp_depth temp_coords

   % 2. Thickness [m]
   temp_thick = reshape(thickness_pred.values, size(thickness_pred.values,
1)*size(thickness_pred.values, 2), size(thickness_pred.values, 3)); % reshape
%     in_Oriskany = ~any(isnan(temp_thick), 2);
   temp_coords = [reshape(thickness_pred.lat, [],1) reshape(thickness_pred.lon, [],1)];
   if (size(temp_thick, 1) > 65000) | (size(temp_thick, 2) > 250)  % Too many rows or
columns for Excel 2003
      csvwrite([output_filename '_Thickness'], [temp_coords(in_Oriskany_flipped, :),
temp_thick(in_Oriskany_flipped, :)]);
   else
      xlswrite(output_filename, [temp_coords(in_Oriskany_flipped, :),
temp_thick(in_Oriskany_flipped, :)], 'Thickness');
   end
   clear temp_thick temp_coords

   % 3. Porosity
   temp_poros = reshape(porosity_pred.values, size(porosity_pred.values,
1)*size(porosity_pred.values, 2), size(porosity_pred.values, 3)); % reshape
%     in_Oriskany = ~any(isnan(temp_poros), 2);
   temp_coords = [reshape(porosity_pred.lat, [],1) reshape(porosity_pred.lon, [],1)];
   if (size(temp_poros, 1) > 65000) | (size(temp_poros, 2) > 250)  % Too many rows or
columns for Excel 2003
      csvwrite([output_filename '_Porosity'], [temp_coords(in_Oriskany_flipped, :),
temp_poros(in_Oriskany_flipped, :)]);
   else
      xlswrite(output_filename, [temp_coords(in_Oriskany_flipped, :),
temp_poros(in_Oriskany_flipped, :)], 'Porosity');
```

```
   end
   clear temp_poros temp_coords

   % 4. Temperature [K]
   temp_temp = reshape(temperature_pred.values, size(temperature_pred.values,
1)*size(temperature_pred.values, 2), size(temperature_pred.values, 3)); % reshape
%     in_Oriskany = ~any(isnan(temp_temp), 2);
   temp_coords = [reshape(temperature_pred.lat, [],1) reshape(temperature_pred.lon,
[],1)];
   if (size(temp_temp, 1) > 65000) | (size(temp_temp, 2) > 250)  % Too many rows or
columns for Excel 2003
      csvwrite([output_filename '_Temperature'], [temp_coords(in_Oriskany_flipped, :),
temp_temp(in_Oriskany_flipped, :)]);
   else
      xlswrite(output_filename, [temp_coords(in_Oriskany_flipped, :),
temp_temp(in_Oriskany_flipped, :)], 'Temperature');
   end
   clear temp_temp  temp_coords

   % 5. Pressure [MPa]
   temp_press = reshape(pressure_pred.values, size(pressure_pred.values,
1)*size(pressure_pred.values, 2), size(pressure_pred.values, 3)); % reshape
%     in_Oriskany = ~any(isnan(temp_press), 2);
   temp_coords = [reshape(pressure_pred.lat, [],1) reshape(pressure_pred.lon, [],1)];
   if (size(temp_press, 1) > 65000) | (size(temp_press, 2) > 250)  % Too many rows or
columns for Excel 2003
      csvwrite([output_filename '_Pressure'], [temp_coords(in_Oriskany_flipped, :),
temp_press(in_Oriskany_flipped, :)]);
   else
      xlswrite(output_filename, [temp_coords(in_Oriskany_flipped, :),
temp_press(in_Oriskany_flipped, :)], 'Pressure');
   end
   clear temp_press  temp_coords

%% Calculate CO2 density
is_liquid = 1;

Z = zeros(size(temperature_pred.values));
fhi = zeros(size(temperature_pred.values));
density = zeros(size(temperature_pred.values));
for i = 1:size(temperature_pred.values,1)
   for j = 1:size(temperature_pred.values,2)
      for k = 1:size(temperature_pred.values,3)
         if ~isnan(temperature_pred.values(i,j,k))
            [Z(i,j,k), fhi(i,j,k), density(i,j,k)] = PengRobinson(temperature_pred.values(i,j,k),
1e6*pressure_pred.values(i,j,k), T_crit, P_crit,  0.228, 0.04401, is_liquid); % [kg/m^3]
```

```
        else
            Z(i,j,k) = NaN;
            fhi(i,j,k) = NaN;
            density(i,j,k) = NaN;
        end
      end
   end
end

% Save the calculated densities in a spreadsheet after removing NaNs
   temp_density = reshape(density, size(density, 1)*size(density, 2), size(density, 3)); %
reshape
%     in_Oriskany = ~any(isnan(temp_density), 2);
   temp_coords = [reshape(pressure_pred.lat, [],1) reshape(pressure_pred.lon, [],1)];
   if (size(temp_density, 1) > 65000) | (size(temp_density, 2) > 250)  % Too many rows or
columns for Excel 2003
      csvwrite([output_filename '_Peng-Robinson_Density'],
[temp_coords(in_Oriskany_flipped, :), temp_density(in_Oriskany_flipped, :)]);
   else
      xlswrite(output_filename, [temp_coords(in_Oriskany_flipped, :),
temp_density(in_Oriskany_flipped, :)], 'Peng-Robinson Density');
   end
   clear temp_density  temp_coords

% Plot mean and COV of density for each locations
   figure
   subplot(2,1,1)
   ax(16) = usamap(klatlimit, klonglimit);
   states = shaperead('usastatehi','UseGeoCoords', true, 'BoundingBox', [klonglimit',
klatlimit']);
   geoshow(states, 'FaceColor', [1, 1, 1])
%     textm(states.LabelLat, states.LabelLon, states.Name,'HorizontalAlignment', 'center')
   scatterm(ax(16), reshape(pressure_pred.lat, [], 1), reshape(pressure_pred.lon, [], 1), 8,
reshape(mean(density,3), [], 1), 'filled')
   colorbar
   title('Estimated CO_2 Density [kg/m^3]')

   subplot(2,1,2)
   ax(17) = usamap(klatlimit, klonglimit);
   states = shaperead('usastatehi','UseGeoCoords', true, 'BoundingBox', [klonglimit',
klatlimit']);
   geoshow(states, 'FaceColor', [1, 1, 1])
%     textm(states.LabelLat, states.LabelLon, states.Name,'HorizontalAlignment', 'center')
   scatterm(ax(17), reshape(pressure_pred.lat, [], 1), reshape(pressure_pred.lon, [], 1), 8,
reshape(std(density, 1, 3)./mean(density,3), [], 1), 'filled')
   colorbar
```

```
    title('Estimated CO_2 Density, Coefficient of Variation')


%% Calculate CO2 mass
total_mass_CO2 = zeros(size(density,3), numel(E));   % Initialize varialbe to store results.
Each row is a simulation, each column an efficiency factor value

sq_area = (deg2km(k_grid_size)*1000)^2; % Area of each grid square, assuming they're
all the same [m^2]
mass_per_square_max_efficiency =
sq_area.*thickness_pred.values.*porosity_pred.values.*density.*depth_mask_3D; % %
Mass per grid square assuming 100% effiency (must multiply by E for realistic numbers)
[kg]. Multiplying by "depth_mask_3D" excludes grid squares shallower than k_min_depth
mass_per_squarekm_max_efficiency = mass_per_square_max_efficiency/k_grid_size^2;
for k=1:numel(E)
    total_mass_CO2(:,k) =
squeeze(nansum(nansum(mass_per_square_max_efficiency*E(k),2),1));
end

% Save the calculated mass in each grid square in a spreadsheet after
%   removing NaNs (each column is a realization, each row a grid quare)
    temp_mass = reshape(mass_per_square_max_efficiency,
size(mass_per_square_max_efficiency, 1)*size(mass_per_square_max_efficiency, 2),
size(mass_per_square_max_efficiency, 3)); % reshape
    temp_depth_OK = reshape(depth_mask_2D, size(depth_mask_2D,
1)*size(depth_mask_2D, 2), 1); % reshape

    %%%%%%%%%%%%%%%%%%%%%%%%%%%%%%%%%%%%%%
    % Note: this disables minimum depth %
    %%%%%%%%%%%%%%%%%%%%%%%%%%%%%%%%%%%%%%
    grid_cell_OK = reshape(in_Oriskany_flipped, [],1);
%     grid_cell_OK = temp_depth_OK & reshape(in_Oriskany_flipped, [],1);
    temp_coords = [reshape(pressure_pred.lat, [],1) reshape(pressure_pred.lon, [],1)];
    if (size(temp_mass, 1) > 65000) | (size(temp_mass, 2) > 250)  % Too many rows or
columns for Excel 2003
        csvwrite([output_filename '_Mass_kg_100_eff'], [temp_coords(in_Oriskany_flipped,
:), temp_mass(in_Oriskany_flipped, :)]);
    else
        xlswrite(output_filename, [temp_coords(grid_cell_OK, :), temp_mass(grid_cell_OK,
:)], 'Mass_kg (100% efficiency)');
    end
    clear temp_mass  temp_coords

% Save the calculated total mass in a spreadsheet after removing NaNs (each column is an
efficiency factor, each row a realization)
    tab_name = ['TotMassKg (' sprintf('%0.2f, ', E) ')'];
```

```
   if (size(total_mass_CO2, 1) > 65000) | (size(total_mass_CO2, 2) > 250)  % Too many rows
or columns for Excel 2003
      csvwrite([output_filename '_TotMassKg'], [temp_coords(grid_cell_OK, :),
total_mass_CO2]);
   else
      xlswrite(output_filename, total_mass_CO2, tab_name);
   end
   clear temp_mass temp_coords

figure
for k=1:numel(E)
   subplot(numel(E),1, k)
   hist(total_mass_CO2(:,k)/1e12, 20)
   xlabel('Mass of CO_2 [Gigatonnes]')
   title(['E = ' num2str(E(k))])
end

% Plot mean and COV of mass per square
   figure
   subplot(2,1,1)
   ax(18) = usamap(klatlimit, klonglimit);
   states = shaperead('usastatehi','UseGeoCoords', true, 'BoundingBox', [klonglimit',
klatlimit']);
   geoshow(states, 'FaceColor', [1, 1, 1])
%     textm(states.LabelLat, states.LabelLon, states.Name,'HorizontalAlignment', 'center')
   scatterm(ax(18), reshape(pressure_pred.lat, [], 1), reshape(pressure_pred.lon, [], 1), 8,
reshape(mean(mass_per_square_max_efficiency*E(2)/1e6, 3), [], 1), 'filled')
   colorbar
   title('Estimated CO_2 Mass [Kilotonnes]')

   subplot(2,1,2)
   ax(19) = usamap(klatlimit, klonglimit);
   states = shaperead('usastatehi','UseGeoCoords', true, 'BoundingBox', [klonglimit',
klatlimit']);
   geoshow(states, 'FaceColor', [1, 1, 1])
%     textm(states.LabelLat, states.LabelLon, states.Name,'HorizontalAlignment', 'center')
   scatterm(ax(19), reshape(pressure_pred.lat, [], 1), reshape(pressure_pred.lon, [], 1), 8,
reshape(std(mass_per_square_max_efficiency*E(2)/1e6, 1,
3)./mean(mass_per_square_max_efficiency*E(2)/1e6, 3), [], 1), 'filled')
   colorbar
   title('Estimated CO_2 Mass, Coefficient of Variation')

%     % Plot mean and COV of mass per square km
   figure
   subplot(2,1,1)
   ax(20) = usamap(klatlimit, klonglimit);
```

```
   states = shaperead('usastatehi','UseGeoCoords', true, 'BoundingBox', [klonglimit',
klatlimit']);
   geoshow(states, 'FaceColor', [1, 1, 1])
%     textm(states.LabelLat, states.LabelLon, states.Name,'HorizontalAlignment', 'center')
   scatterm(ax(20), reshape(pressure_pred.lat, [], 1), reshape(pressure_pred.lon, [], 1), 8,
reshape(mean(mass_per_squarekm_max_efficiency*E(2)/1e6, 3), [], 1), 'filled')
   colorbar
   title('Estimated CO_2 Mass per square kilometer [Kilotonnes]')

   subplot(2,1,2)
   ax(21) = usamap(klatlimit, klonglimit);
   states = shaperead('usastatehi','UseGeoCoords', true, 'BoundingBox', [klonglimit',
klatlimit']);
   geoshow(states, 'FaceColor', [1, 1, 1])
%     textm(states.LabelLat, states.LabelLon, states.Name,'HorizontalAlignment', 'center')
   scatterm(ax(21), reshape(pressure_pred.lat, [], 1), reshape(pressure_pred.lon, [], 1), 8,
reshape(std(mass_per_squarekm_max_efficiency*E(2)/1e6, 1,
3)./mean(mass_per_squarekm_max_efficiency*E(2)/1e6, 3), [], 1), 'filled')
   colorbar
   title('Estimated CO_2 Mass, Coefficient of Variation')
```